Role of REMOTE SENSING applications in MINERAL exploration and sustainable development in OMAN

Rajendran Sankaran* and **Sobhi Nasir****
*** Department of Earth Sciences, Sultan Qaboos University, Oman**
**** Earth Science Research Centre, Sultan Qaboos University, Oman.**
E-mail: rajendra@squ.edu.om

Spectra of minerals:

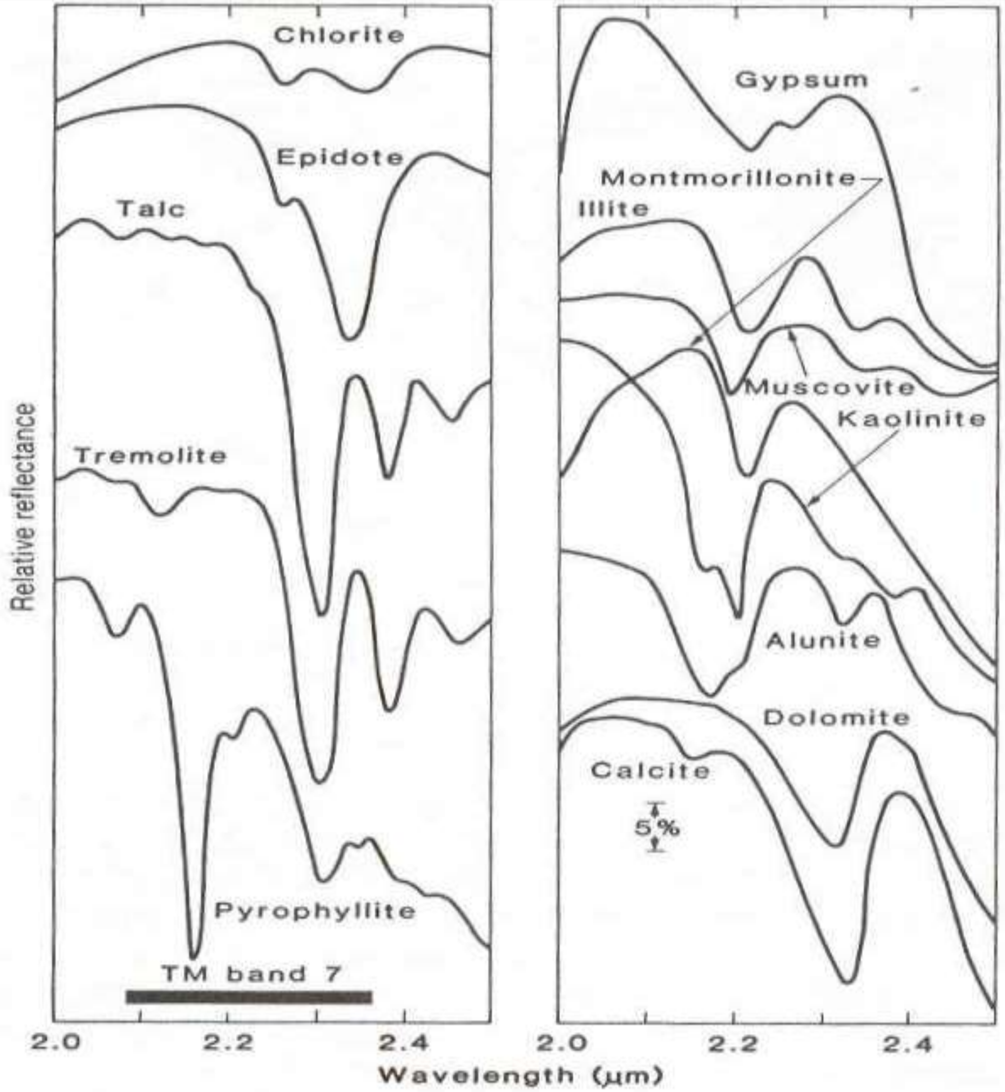

igure 5.40 Selected laboratory spectra of minerals showing liagnostic absorptance and reflectance characteristics. The pectra are displaced vertically to avoid overlap. The andwidth of band 7 of the Landsat TM (Chapter 6) is also hown. (From Goetz et al., 1985. Copyright 1985 by the AAAS. Courtesy NASA Jet Propulsion Laboratory.)

Remote Sensing capability to map minerals

- Hyperspectral images can be analyzed in ways that multispectral images cannot

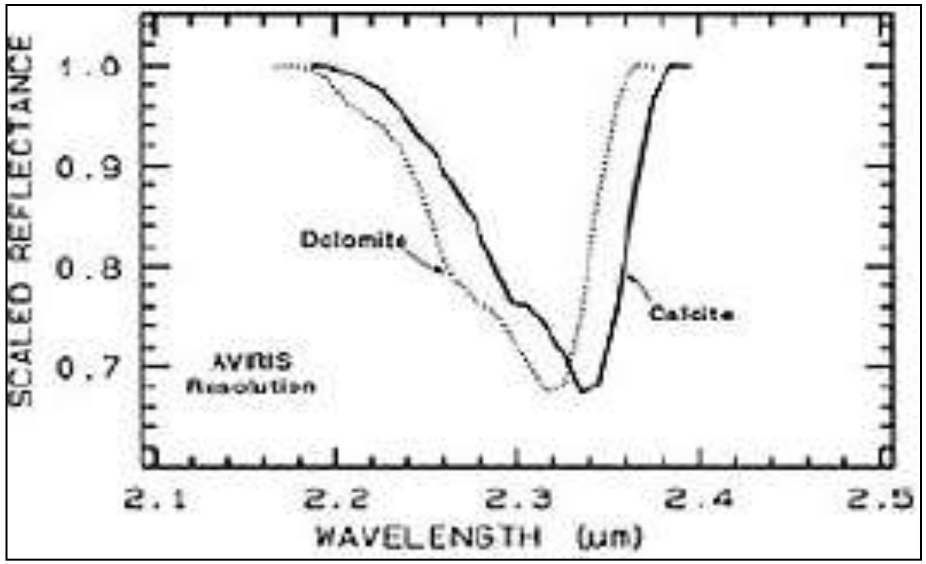

Table1 sensors character of Landsat 8 and ASTER instruments.

Sensors Characteristics	Landsat 8	ASTER		
		VNIR	SWIR	TIR
Spectral bands with range (μm)	OLI Band1 0.43 - 0.45 Coastal Band2 0.45 - 0.51 VNIR Band3 0.53 - 0.59 VNIR Band4 0.63 - 0.67 VNIR Band5 0.85 - 0.88 NIR Band6 1.57 - 1.65 SWIR 1 Band7 2.11 - 2.29 SWIR2 Band8 0.50 - 0.68 PAN - VNIR Band9 1.36 - 1.38 Cirrus TIRS Band 1010.6 - 11.19 TIRS1 Band 1111.5 - 12.51 TIRS2	Band 01 0.52–0.60 Nadir looking Band 02 0.63–0.69 Nadir looking Band 03N 0.76–0.86 Nadir looking Band 03B 0.76–0.86 Backward looking	Band 04 1.6–1.7 Band 05 2.145–2.185 Band 06 2.185–2.225 Band 07 2.235–2.285 Band 08 2.295–2.365 Band 09 2.36–2.43	Band 10 8.125–8.475 Band 11 8.475–8.825 Band 12 8.925–9.275 Band 13 10.25–10.95 Band 14 10.95–11.65
Spatial Resolution (m)	15 (PAN); 30 (VNIR/SWIR) 100 (TIR)	15	30	90
Swath width (km)	185	60	60	60
Radiometric Resolution (bits)	12	8	8	12
Cross Track Pointing		± 318km (± 24 deg)	± 116km (± 8.55 deg)	± 116km (± 8.55 deg)

ASTER spectral bands Absorptions

Figure Shows the spectral absorptions of major minerals rocks stacked from the USGS Spectral Library for minerals (Rajendran and Nasir, 2015).

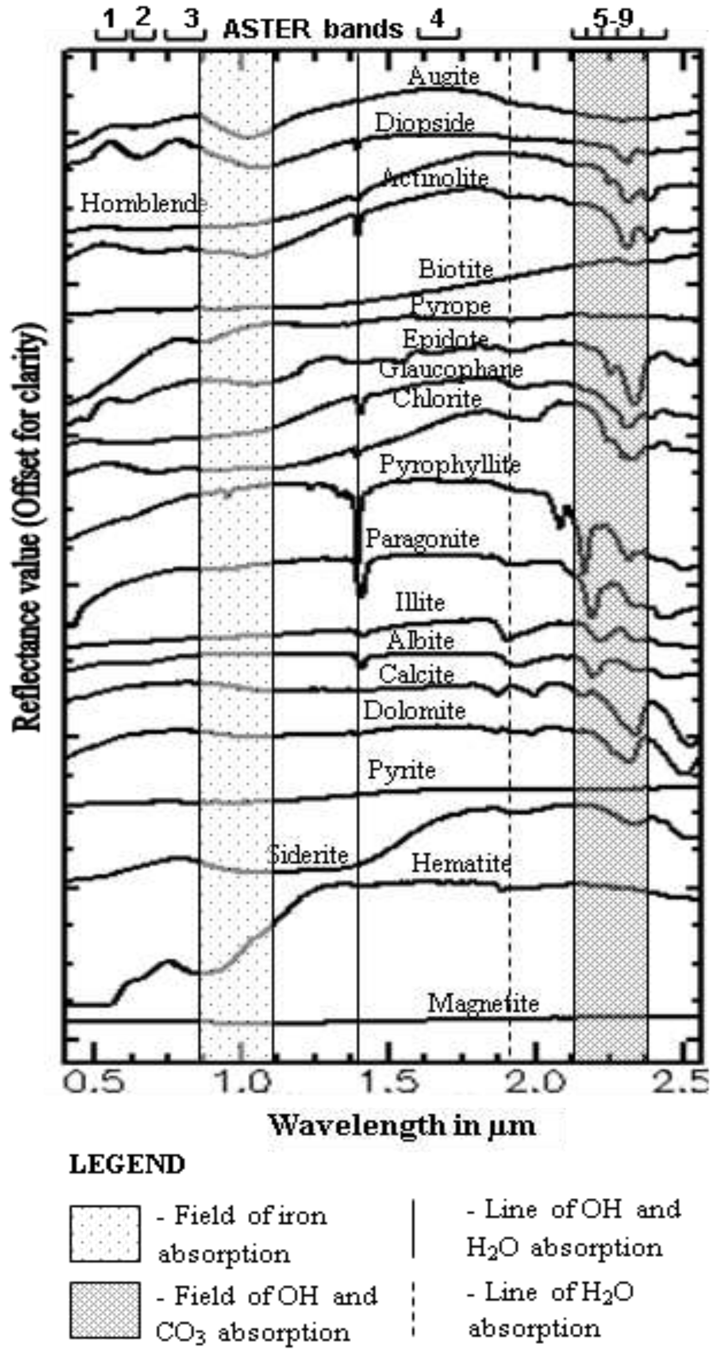

Economic Mineral Resources of the Sultanate of Oman

(Ministry of Commerce and Industry, Oman. 2012).

Fig. 1. Minerals occurrence map of the Sultanate of Oman

Significance: Satellite data and Mapping of minerals of the Sultanate of Oman

- Applications of remotely sensed satellite data are wide and unique in mapping of different lithologies, mineral resources and ore deposits.

- Oman has potential occurrence of the industrial minerals and ore deposits which are mostly occurred in inaccessible mountains and deserts regions where it is difficult to do conventional geological mapping.

- The technique is low-cost and save time in mapping and exploration of such resources and well suitable and applicable to Oman and arid region.

Spectral bands Absorption characters of ASTER and Image processing Methods

- **This work shows t he absorption characters of spectral bands of Advanced Space borne Thermal Emission and Reflection Radiometer (ASTER) and**

- **Selected imaging processing methods namely decorrelation stretching, band ratios, linear spectral unmixing (LSU) and Mixture Tuned Matched Filtering (MTMF)**

- **To understand the sensor has capability to map several mineral deposits and different rock lithologies in Oman**

- **It includes copper, chromite, awaruite, and manganese deposits, and limestone, listwaenites, carbonatites, metamorphic zones rock formations of different parts of the Sultanate of Oman.**

CASE STUY 1:

ASTER detection of chromite bearing mineralized zones in Semail Ophiolite Massifs of the northern Oman mountain

Rajendran et al. (2012) Ore geology reviews, 44, 121-135.

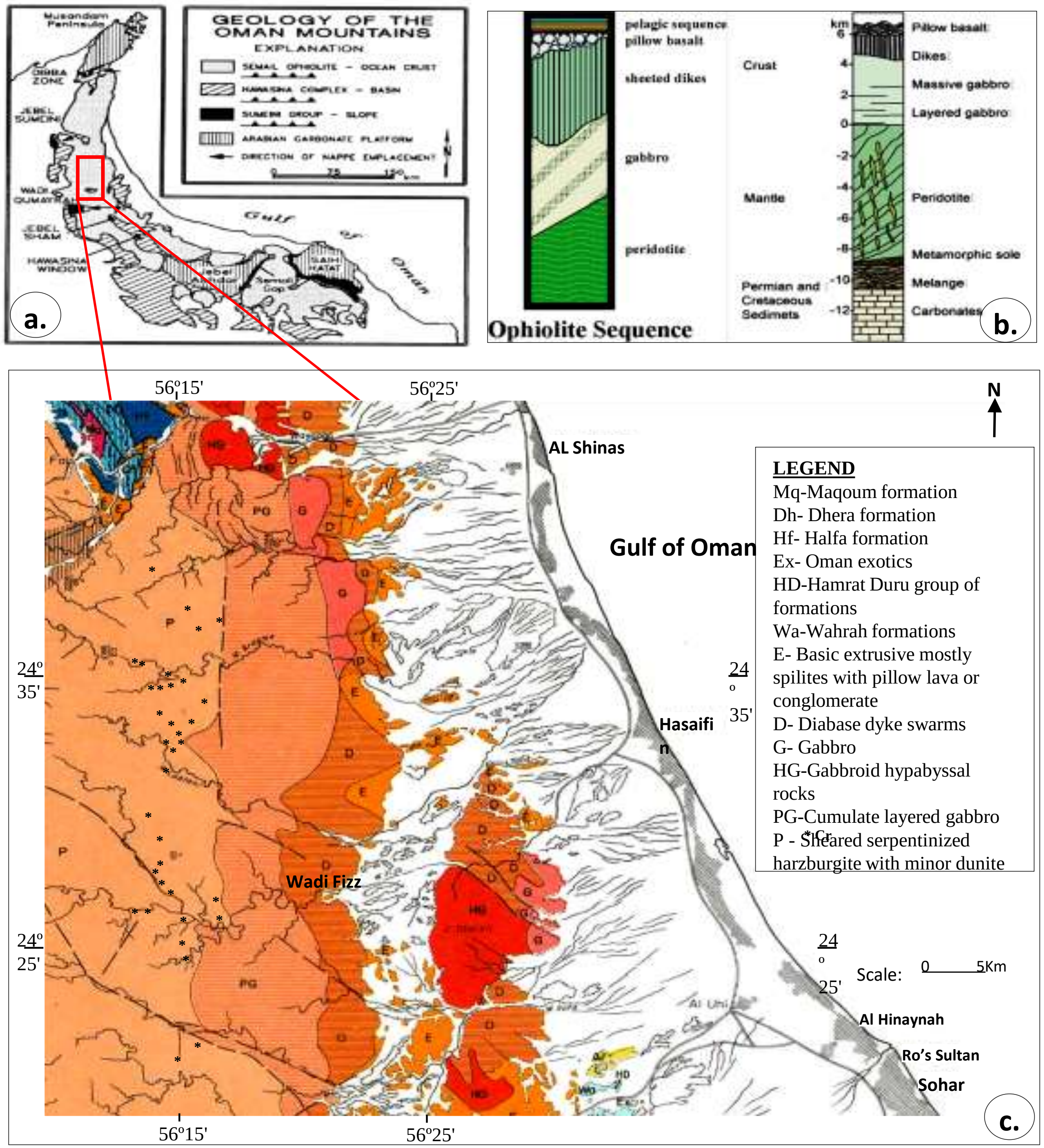

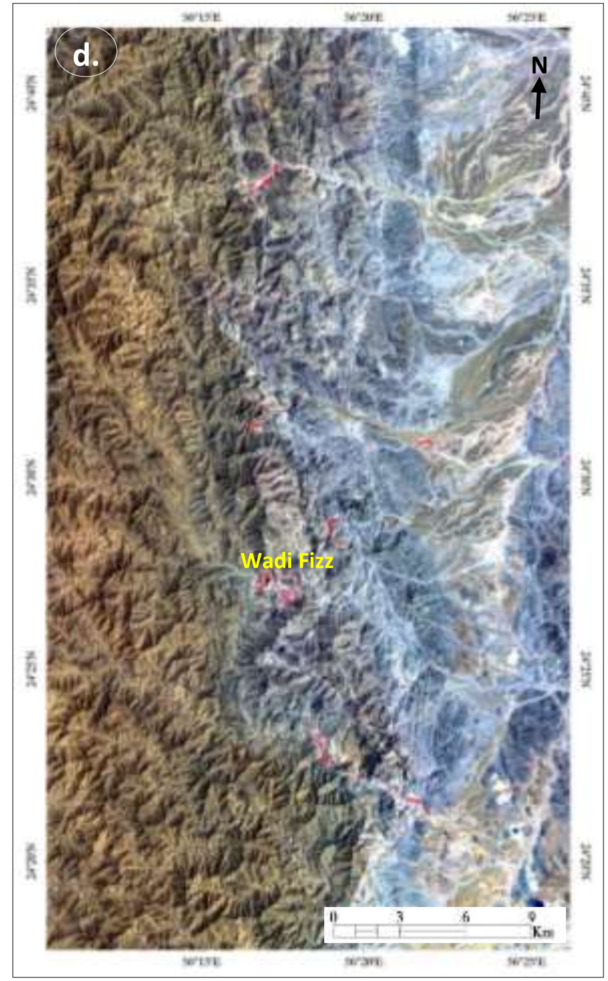

Geology of Oman Mountain (after Watts, 1990) showing the locations of b. Ophiolite Sequence, c. geology (Source: Ministry of Petroleum and Minerals, 1987) and d. ASTER RGB (3,2,1) image of study area

Landsat TM RGB (7, 5, 4 bands) decorrelated image of Study area (Abrams et al., 1988). The abbreviations of the image are E- Basic extrusives mostly spilites with pillow lava or conglomerate; D- Diabase dyke swarms; G- Gabbro; HG- Gabbroid hypabyssal rocks; PG- Cumulate layered gabbro; P and CD- Sheared serpentinized harzburgite.

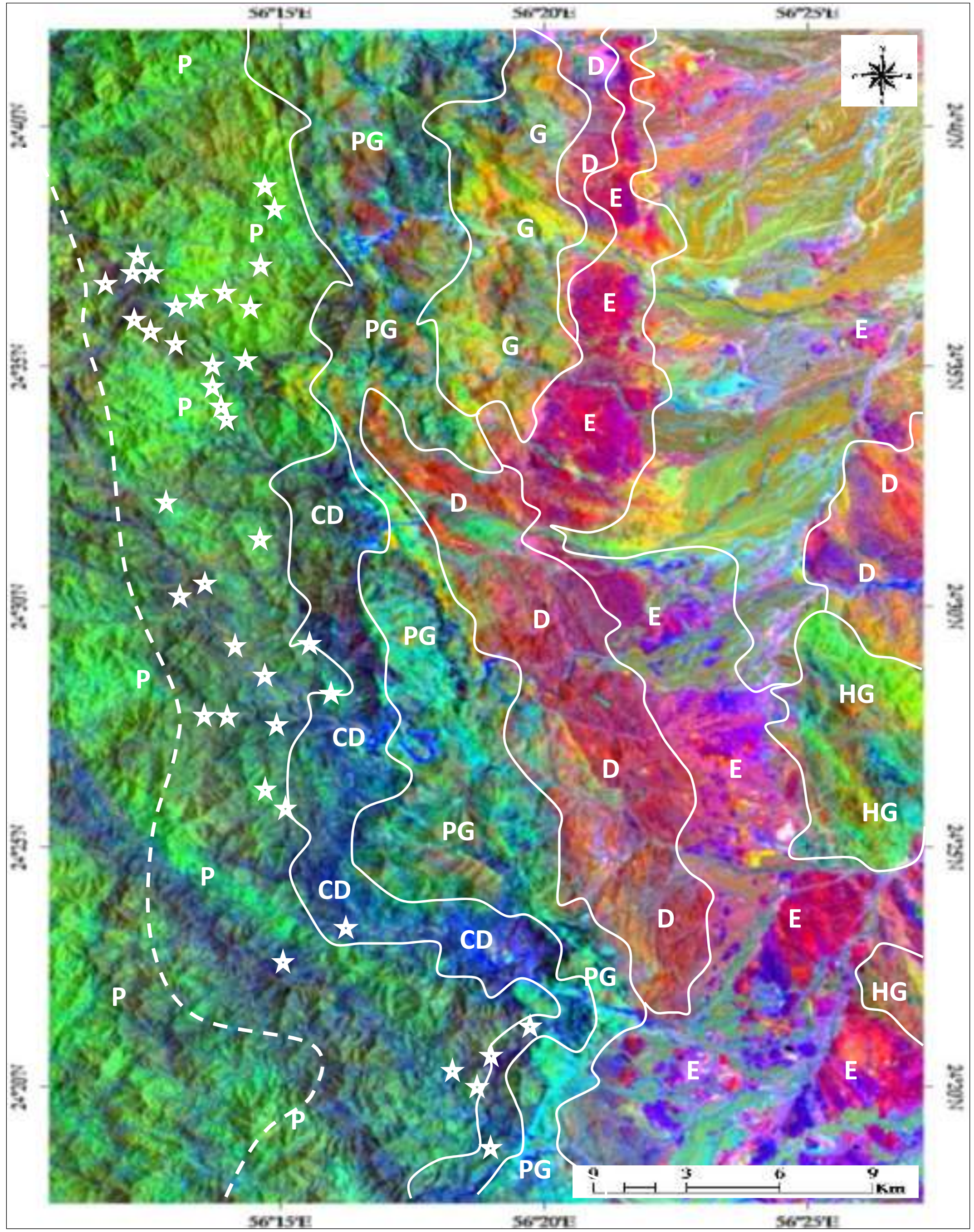

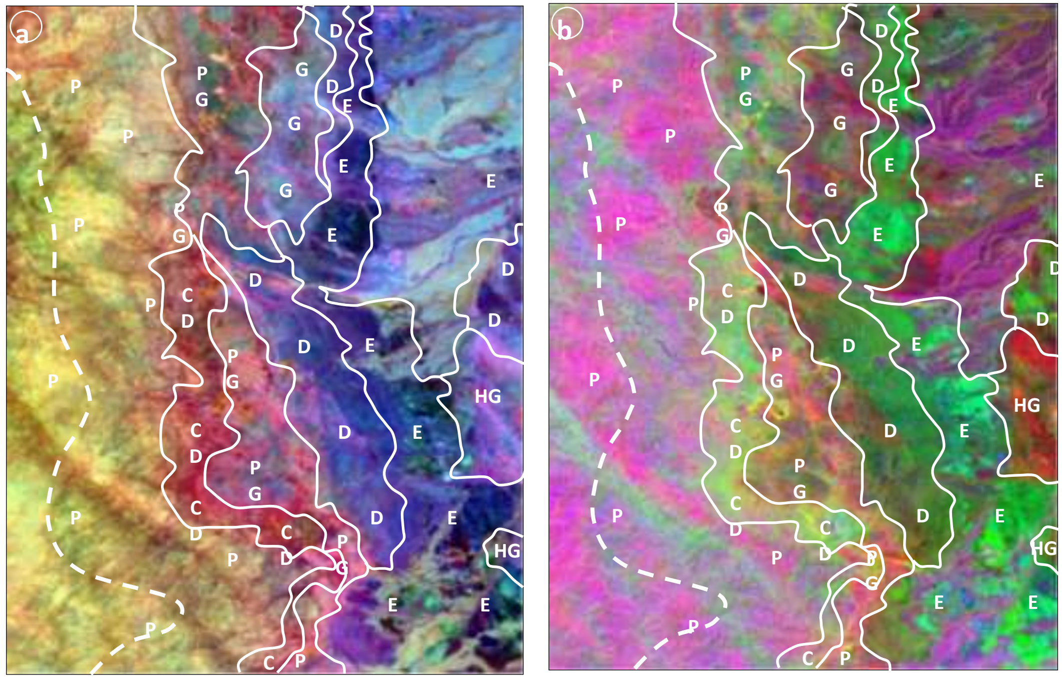

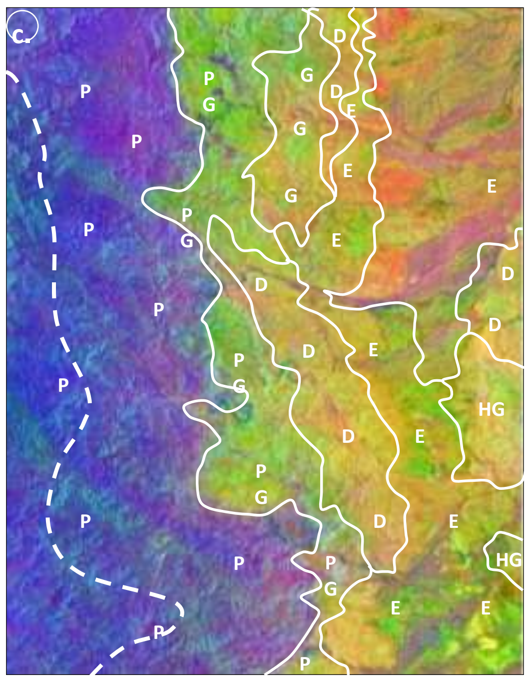

ASTER RGB band ratios image a. Abdeen et al., 2001 (4/7, 4/1, 2/3*4/3) b. (4/7, 3/4, 2/1) and c. Amer et al., 2009 ((2+4)/3, (5+7)/6, (7+9)/8) of the study area. The abbreviations of the image are E- Basic extrusives mostly spilites with pillow lava or conglomerate; D- Diabase dyke swarms; G- Gabbro; HG- Gabbroid hypabyssal rocks; PG- Cumulate layered gabbro; P and CD- Sheared serpentinized harzburgite.

RGB image of PC7, PC5 and PC4 of PCA bands of the study area. The abbreviations of the image are E- Basic extrusives mostly spilites with pillow lava or conglomerate; D- Diabase dyke swarms; G- Gabbro; HG- Gabbroid hypabyssal rocks; PG- Cumulate layered gabbro; P and CD- Sheared serpentinized harzburgite.

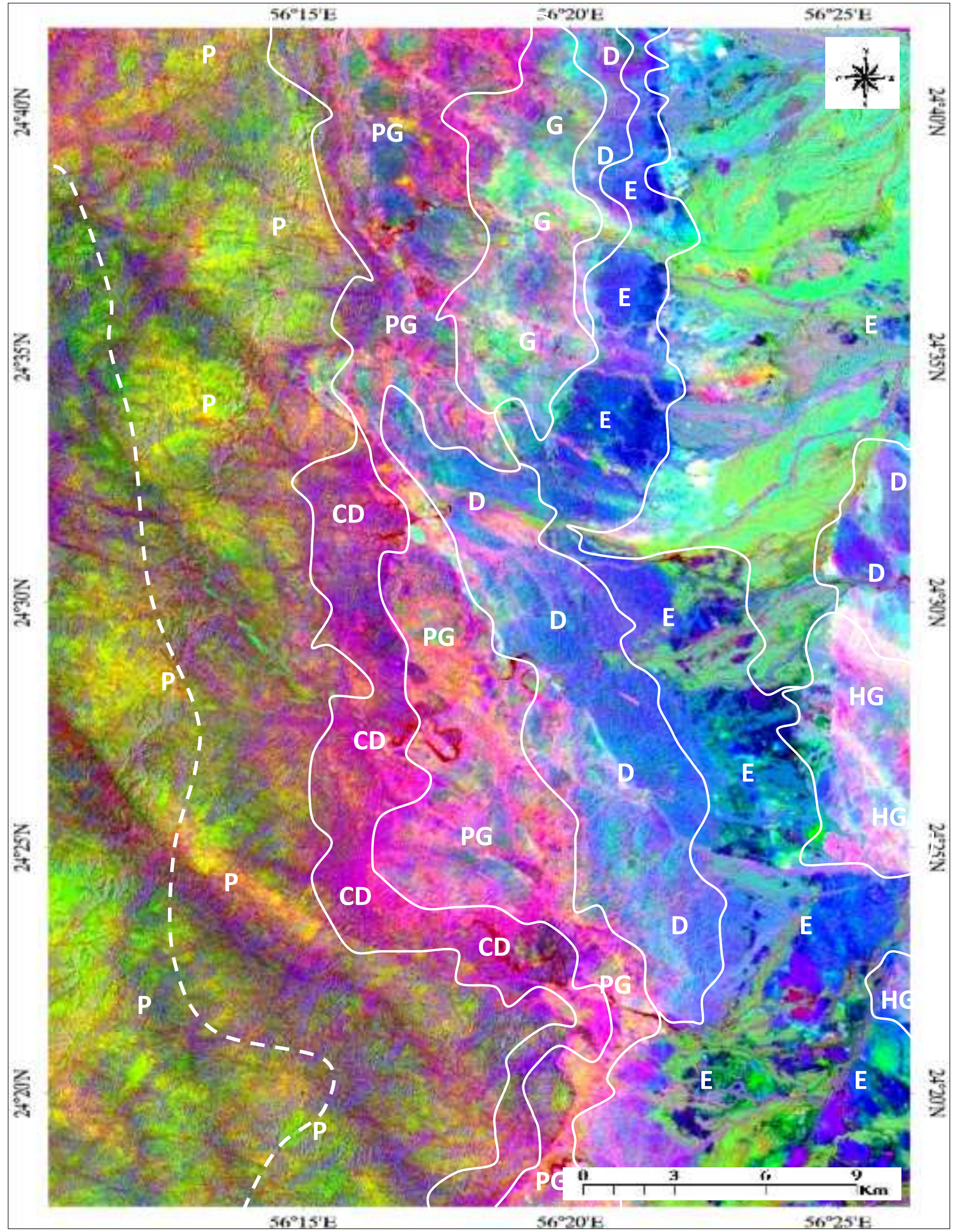

CASE STUY 2:

Characterization of ASTER spectral bands for mapping of alteration zones of volcanogenic massive sulphide deposits

Rajendran and Nasir (2017) reviewed paper submitted to Ore geology reviews.

Geology of study area shows the occurrence of Cu, Au and Ag mainly in the lower extrusive (Ministry of Petroleum and Minerals, 1987)

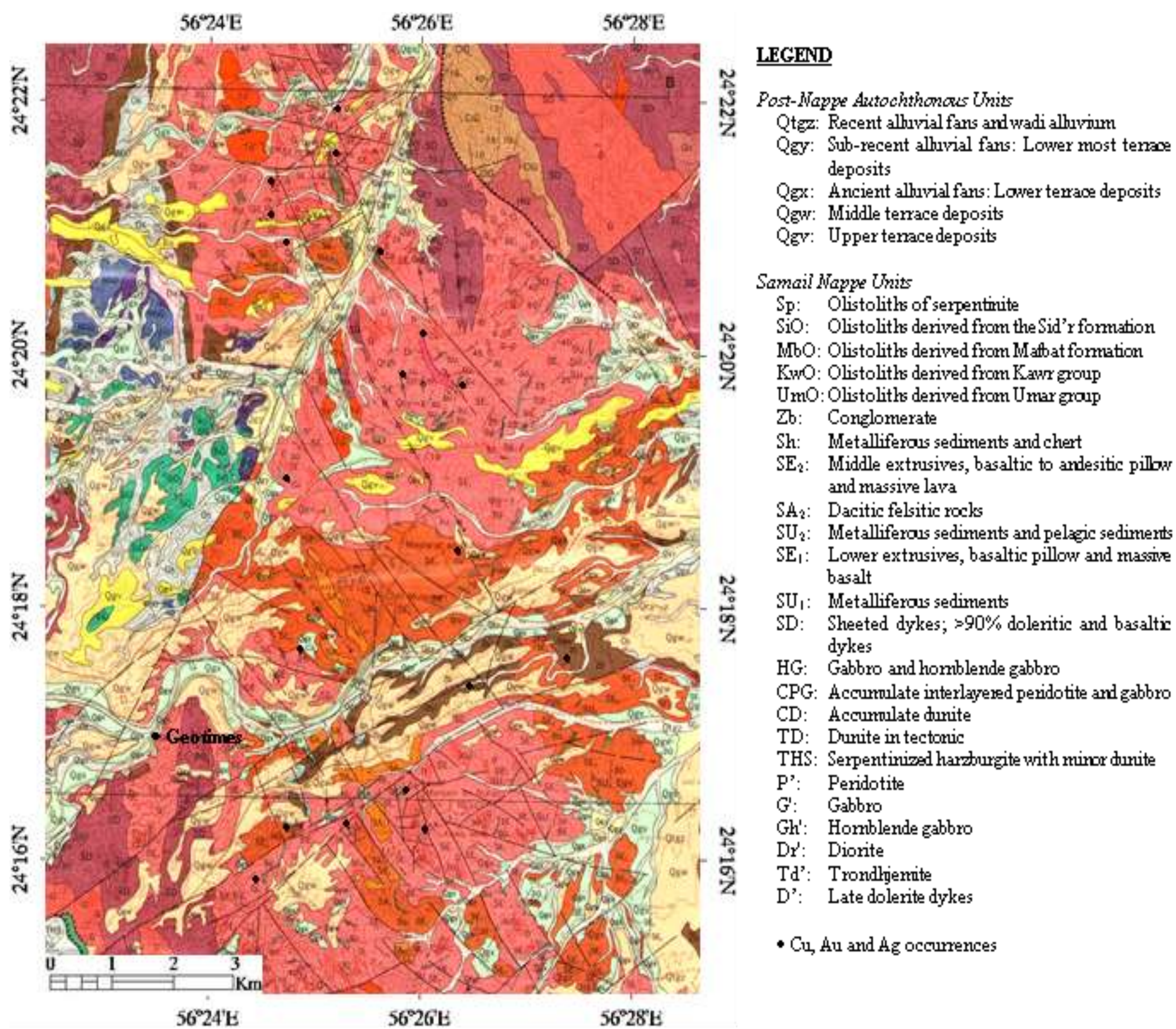

RGB image of ASTER band ratios (5/3+1/2), (4+6)/5 and (5+7)/6 shows the mineralized zones (spotted Cu occurrences) of the study area (Image is linear stretched with Red: 1.1 to 1.3; Green: 3.6 to 4.3; Blue: 1.8 to 2.0).

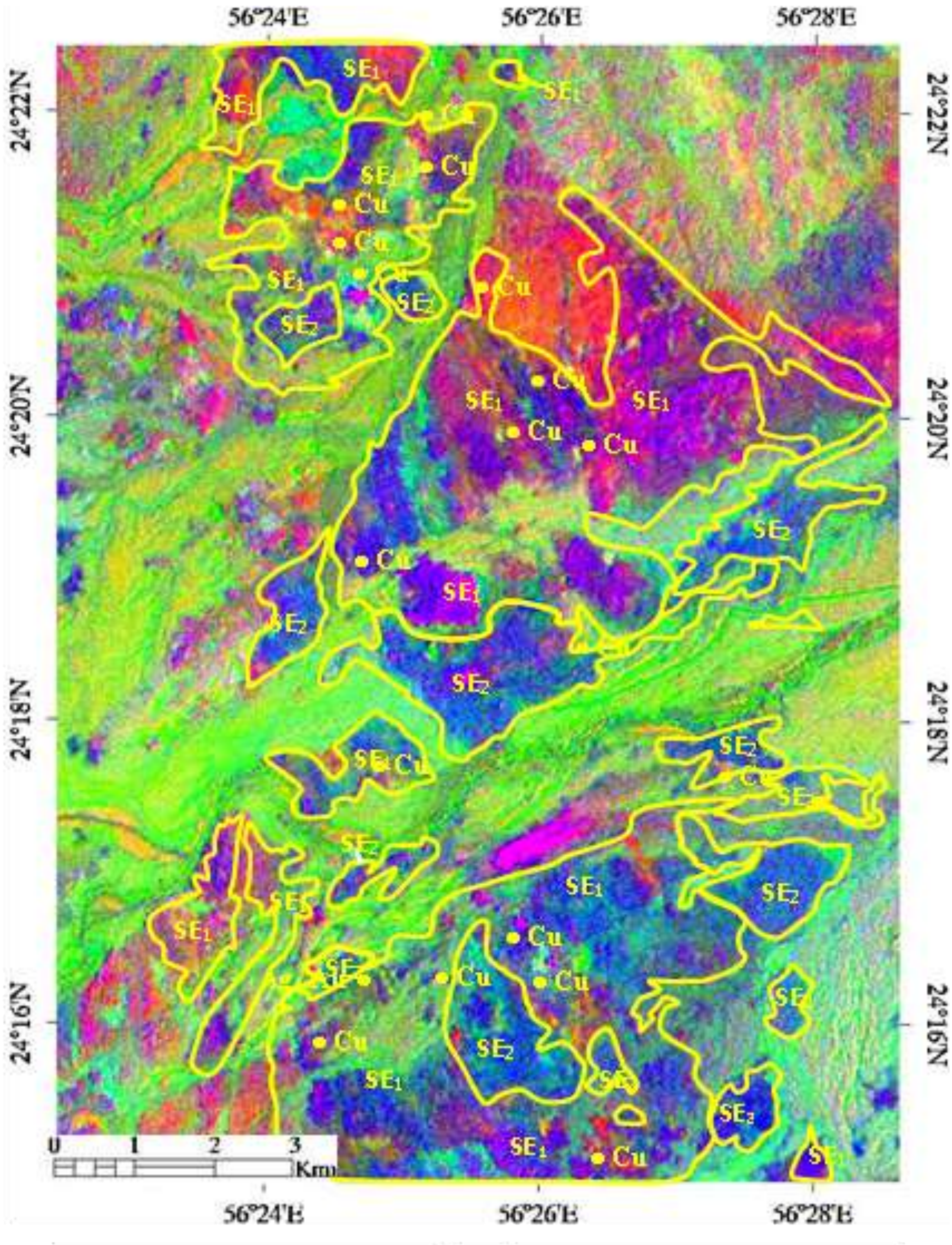

RGB image of ASTER indices (R: OH bearing altered minerals, G: kaolinite B: alunite minerals indices) shows the occurrence and spatial distribution of altered minerals in the study area (Red square is an area chosen for detailed study; the image is linear stretched with Red: 2.5 to 3.1; Green: 1.6 to 2.0; Blue: 1.0 to 1.4).

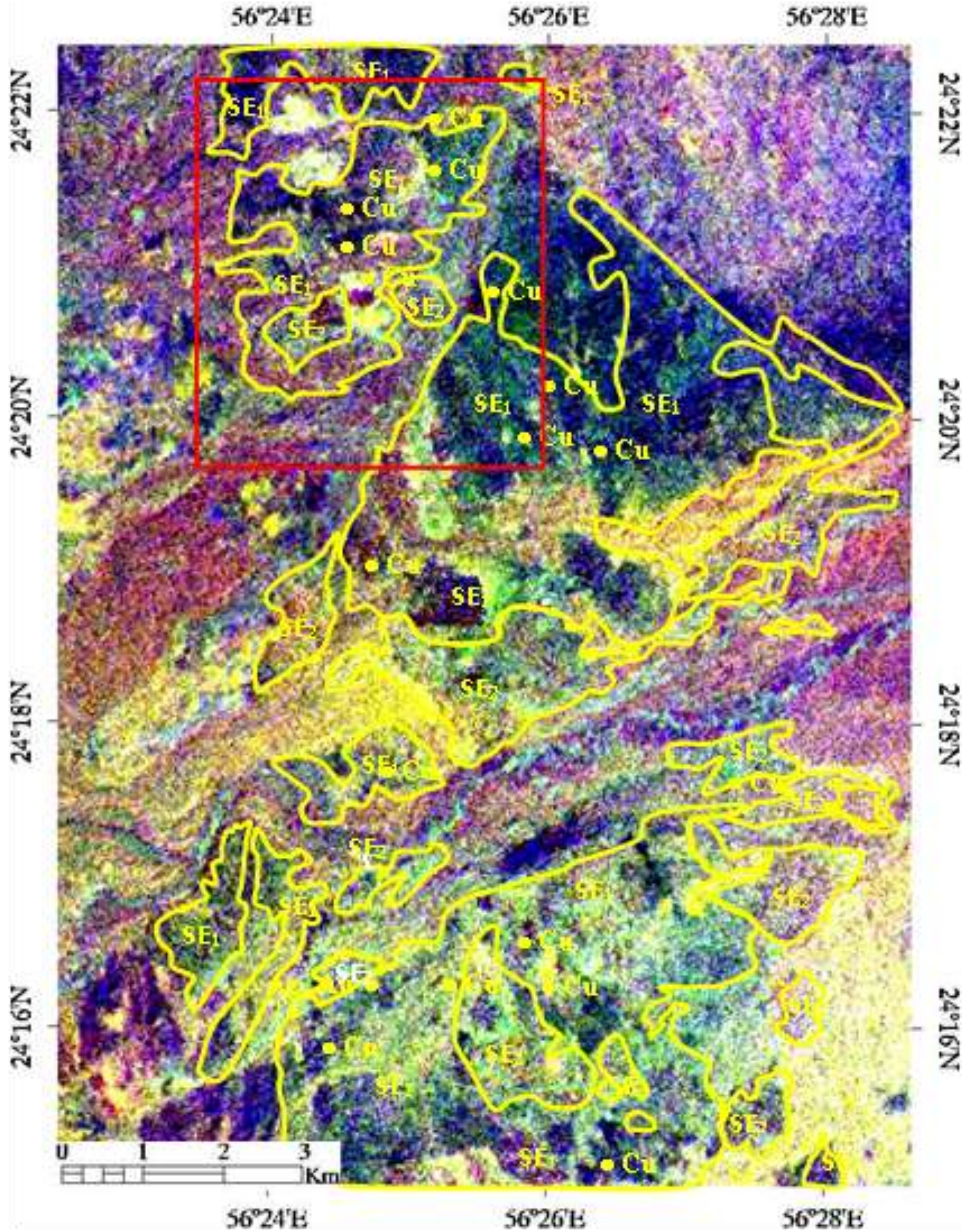

(a) ASTER RGB (3, 2, 1) image shows the occurrence of gossan (yellow squared, the area in Fig. 16) and old mine, and (b) the distribution of pixels of the oxidised (red), propylitic (green), argillaceous (cyan) and phyllic (pink) zones derived based on SAM endmembers (1, 3, 5 and 7) over MNF image (band 2) of the gossanized area.

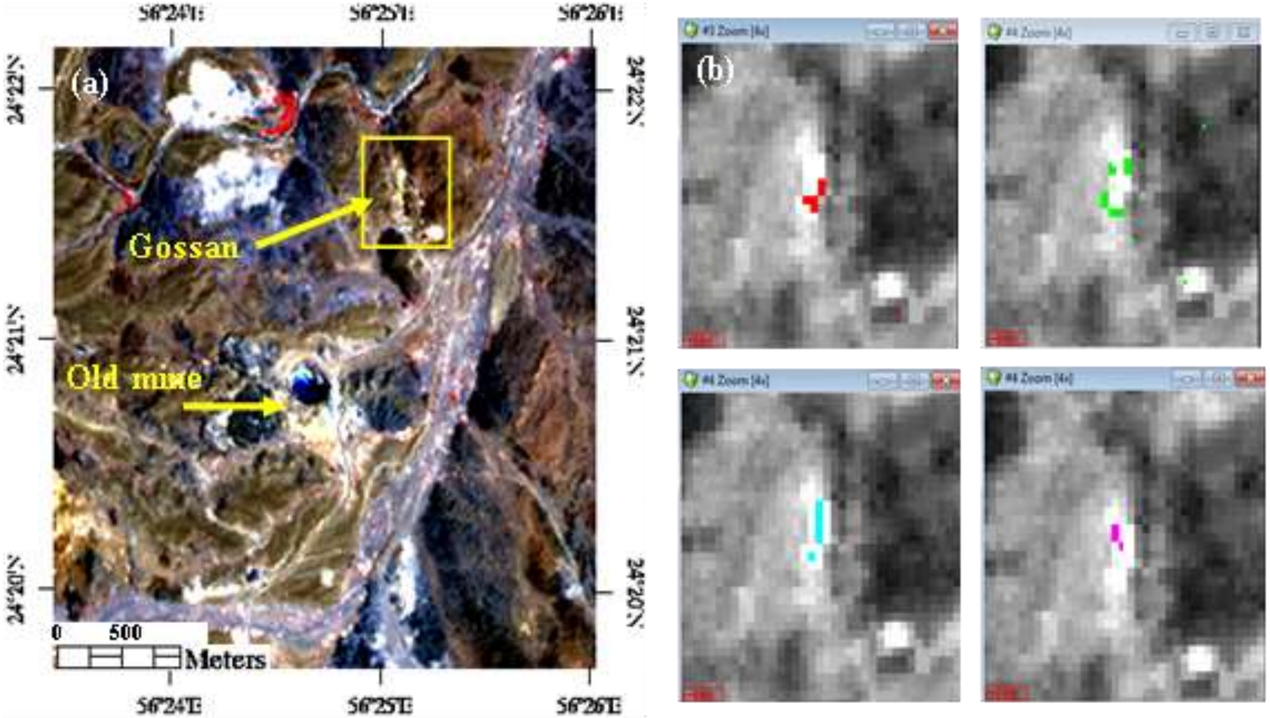

CASE STUY 3:

Mapping of manganese potential lithology in parts of the Sultanate of Oman

Rajendran and Nasir (2017) International Journal of Geosciences and Geomatics 1(2), 92-101.

Geology of study region occurred near Ras Al Hadd of Al-Batain basin of NE Oman margin (Ministry of Petroleum and Minerals 1993).

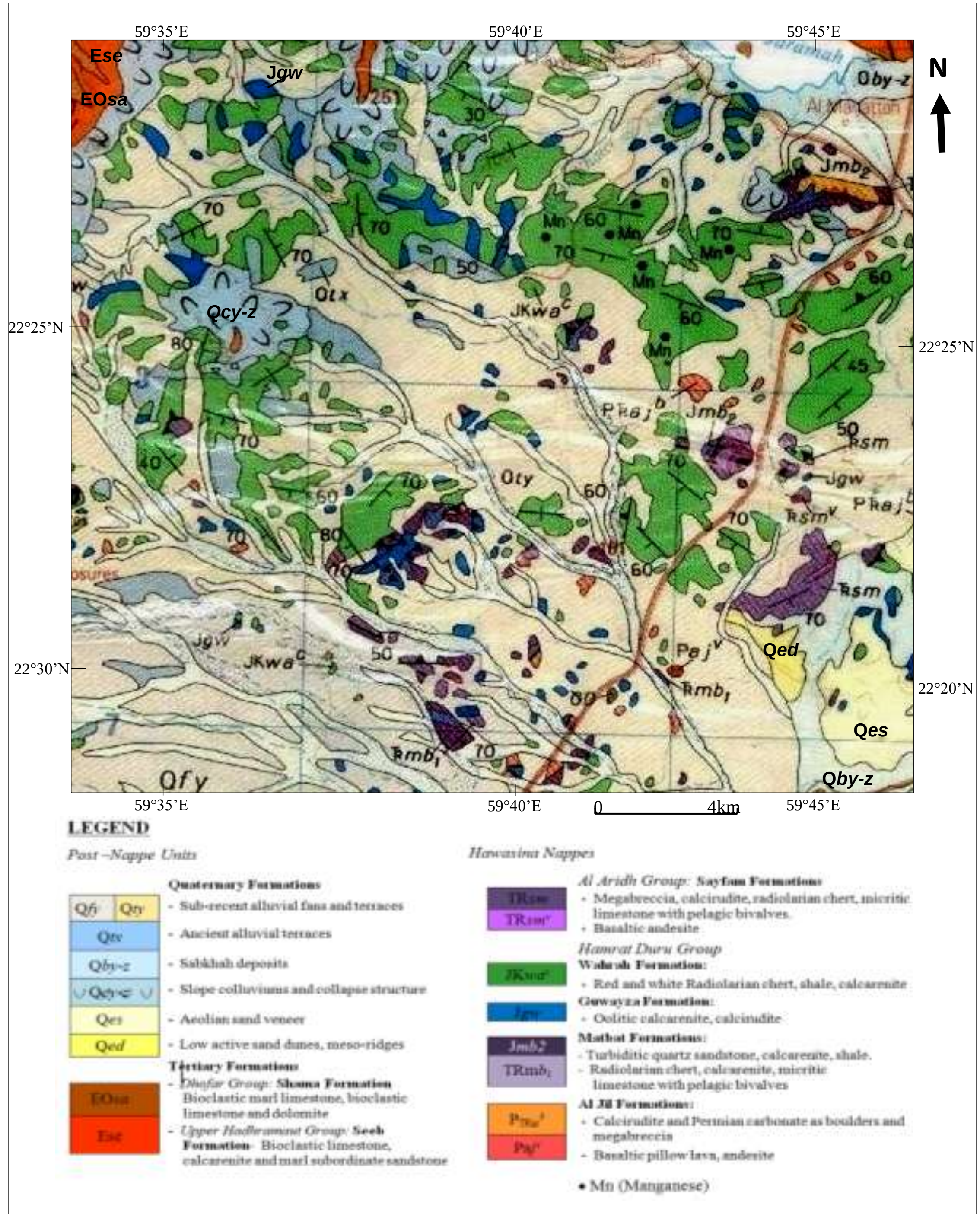

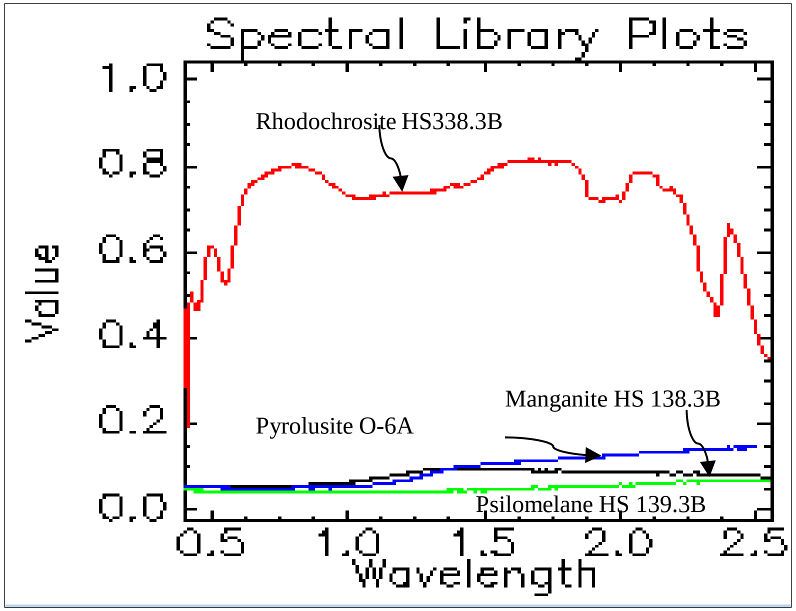

Spectral plot of manganese minerals stacked from USGS and JPL spectral libraries.

Pyrolusite (MnO_2), Psilomelane ($(Ba, H_2O)_2 Mn_5O_{10}$), Manganite ($MnO(OH)$) and Rhodochrosite ($MnCO_3$)

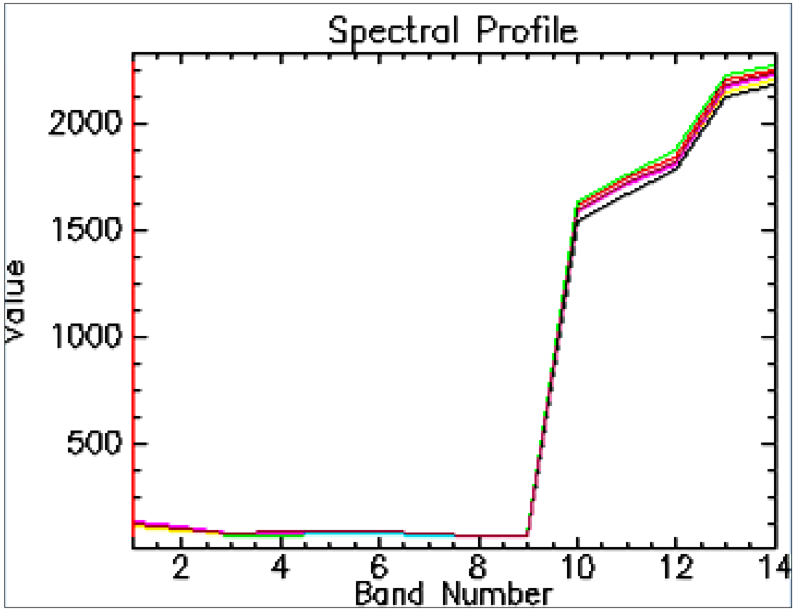

Image spectra of 14 ASTER spectral bands shows diagnostic absorption of manganese in VNIR and SWIR regions (1-9 spectral bands, low reflectance) and strong emission in TIR region (10-14 spectral bands).

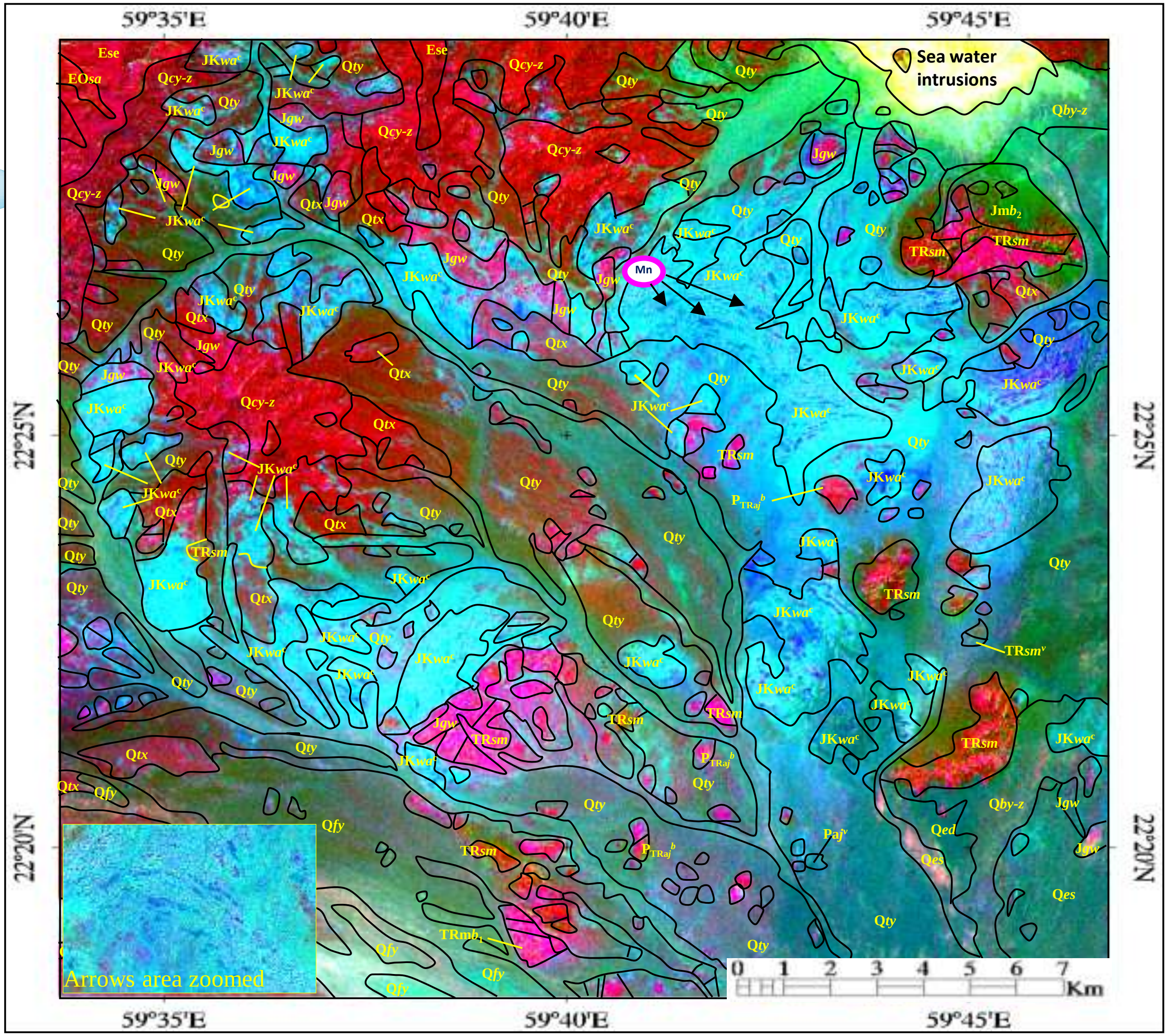

LEGEND

Post –Nappe Units

Qfy / Qty	**Quaternary Formations** -Sub-recent alluvial fans and terraces
Qtx	-Ancient alluvial terraces
Qby-z	- Sabkhah deposits
Qcy-z	- Slope colluviums and collapse structure
Qes	- Aeolian sand veneer
Qed	-Low active sand dunes, meso-ridges

Tertiary Formations

EOsa	- *Dhofar Group:* **Shama Formation** Bioclastic marl limestone, bioclastic limestone and dolomite
Ese	- *Upper Hadhramaut Group:* **Seeb Formation**- Bioclastic limestone, calcarenite and marl subordinate sandstone

Hawasina Nappes

TRsm / TRsm^v	*Al Aridh Group:* **Sayfam Formations** - Megabreccia, calcirudite, radiolarian chert, micritic limestone with pelagic bivalves. - Basaltic andesite
JKwa^c	*Hamrat Duru Group* **Wahrah Formation:** - Red and white Radiolarian chert, shale, calcarenite
Jgw	**Guwayza Formation:** - Oolitic calcarenite, calcirudite
Jmb2 / TRmb$_1$	**Matbat Formations:** - Turbiditic quartz sandstone, calcarenite, shale. - Radiolarian chert, calcarenite, micritic limestone with pelagic bivalves
P$_{TRaj}^b$ / Paj^v	**Al Jil Formations:** - Calcirudite and Permian carbonate as boulders and megabreccia - Basaltic pillow lava, andesite

• Mn (Manganese)

ASTER RGB image of band ratio (1+3)/2, (3+5)/4 and (5+7)6 of study region.

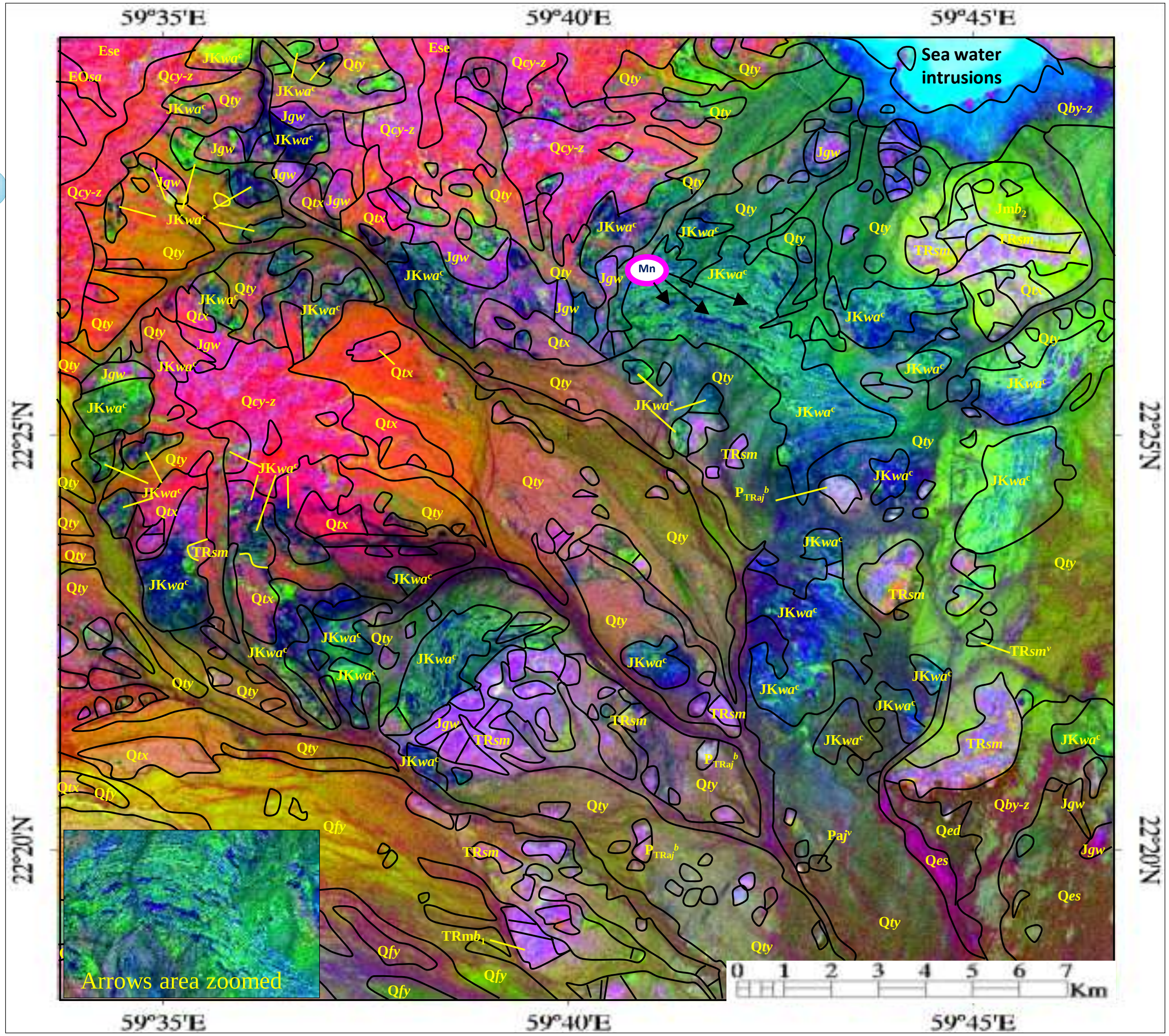

LEGEND

Post –Nappe Units

Qfy / Qty	**Quaternary Formations** -Sub-recent alluvial fans and terraces
Qtx	-Ancient alluvial terraces
Qby-z	- Sabkhah deposits
Qcy-z	- Slope colluviums and collapse structure
Qes	- Aeolian sand veneer
Qed	-Low active sand dunes, meso-ridges
EOsa	**Tertiary Formations** - *Dhofar Group:* **Shama Formation** Bioclastic marl limestone, bioclastic limestone and dolomite
Ese	- *Upper Hadhramaut Group:* **Seeb Formation**- Bioclastic limestone, calcarenite and marl subordinate sandstone

Hawasina Nappes

TRsm / TRsm^v	*Al Aridh Group:* **Sayfam Formations** - Megabreccia, calciruditе, radiolarian chert, micritic limestone with pelagic bivalves. - Basaltic andesite
JKwa^c	*Hamrat Duru Group* **Wahrah Formation:** - Red and white Radiolarian chert, shale, calcarenite
Jgw	**Guwayza Formation:** - Oolitic calcarenite, calcirudite
Jmb2 / TRmb$_1$	**Matbat Formations:** - Turbiditic quartz sandstone, calcarenite, shale. - Radiolarian chert, calcarenite, micritic limestone with pelagic bivalves
P$_{TRaj}$^{b} / Paj^v	**Al Jil Formations:** - Calcirudite and Permian carbonate as boulders and megabreccia - Basaltic pillow lava, andesite

• Mn (Manganese)

Principal Components RGB image (R: PC3, G: PC2 and B: PC1) of study region.

CASE STUY 4:

Mapping of limestone formations in parts of the Sultanate of Oman

Rajendran and Nasir (2013) Environ Earth Sci DOI 10.1007/s12665-013-2419-7.

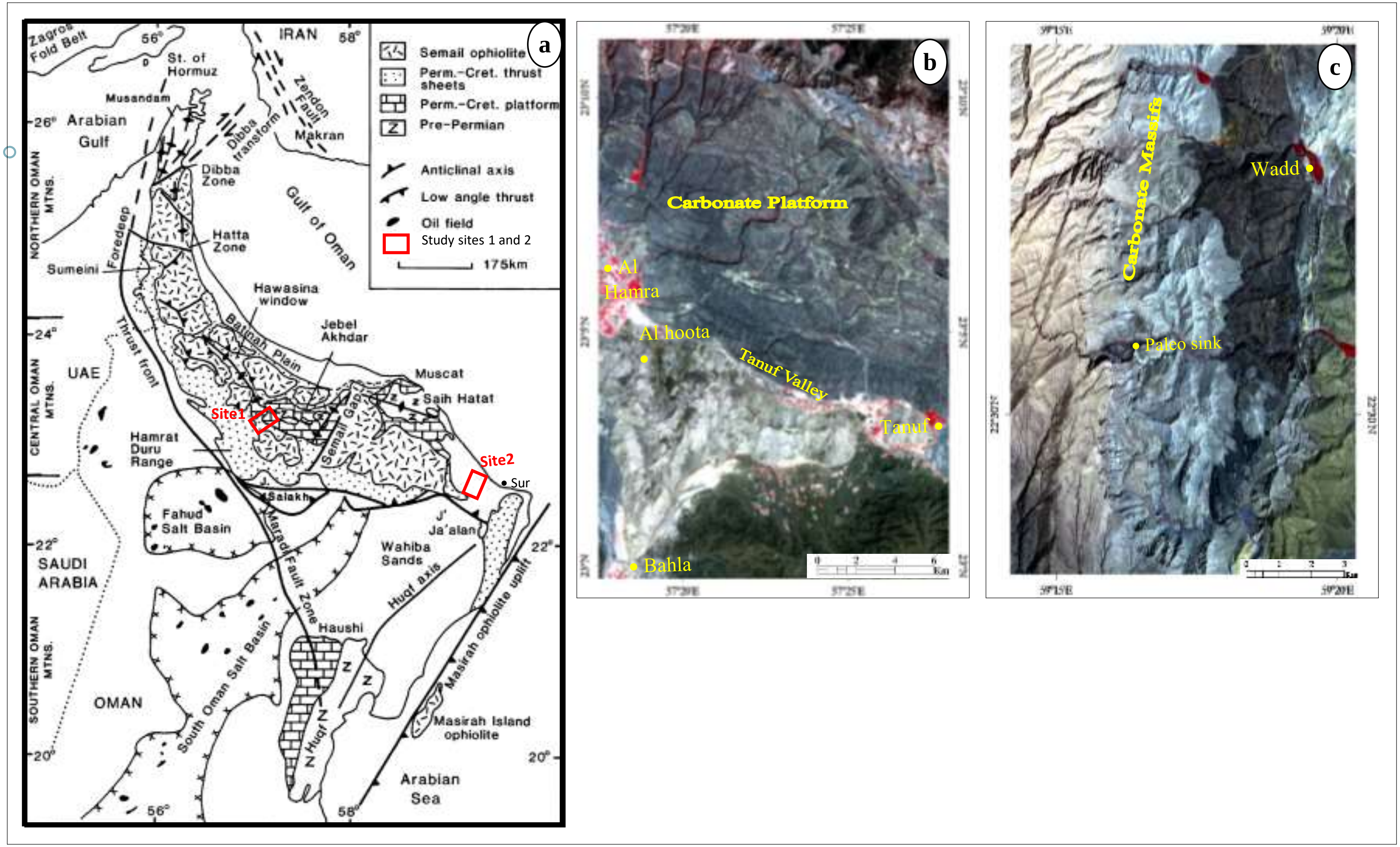

Regional geology and structural map of the Oman Mountain area (after Robertson and Searle, 1990), b and c the ASTER FCC image (RGB bands 3, 2 and 1) illustrates the carbonate massifs of Tanuf Valley (Site. 1) and the region near to Sur (Site. 2) respectively.

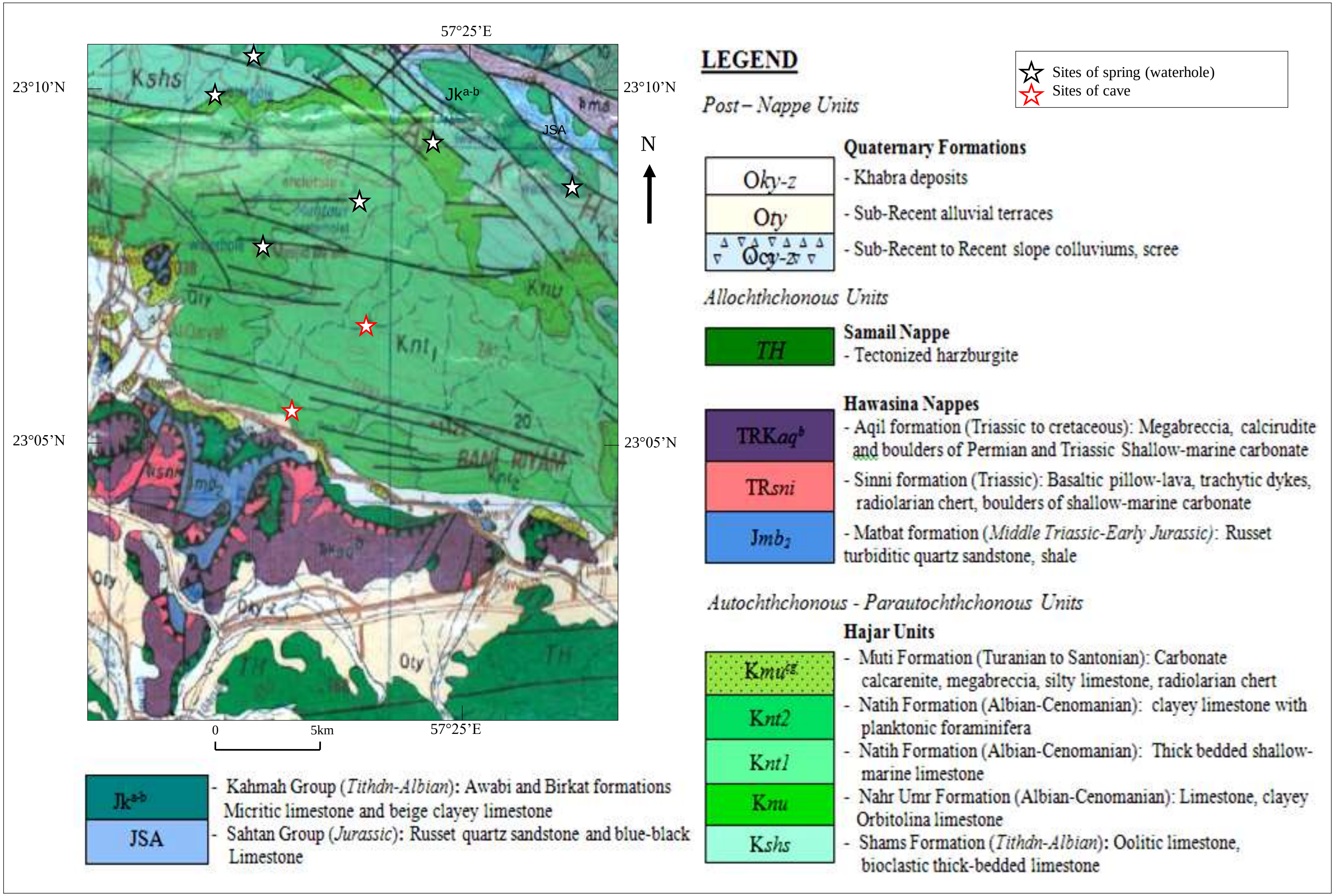

Geology of Site. 1 (Ministry of Petroleum and Minerals, 1992).

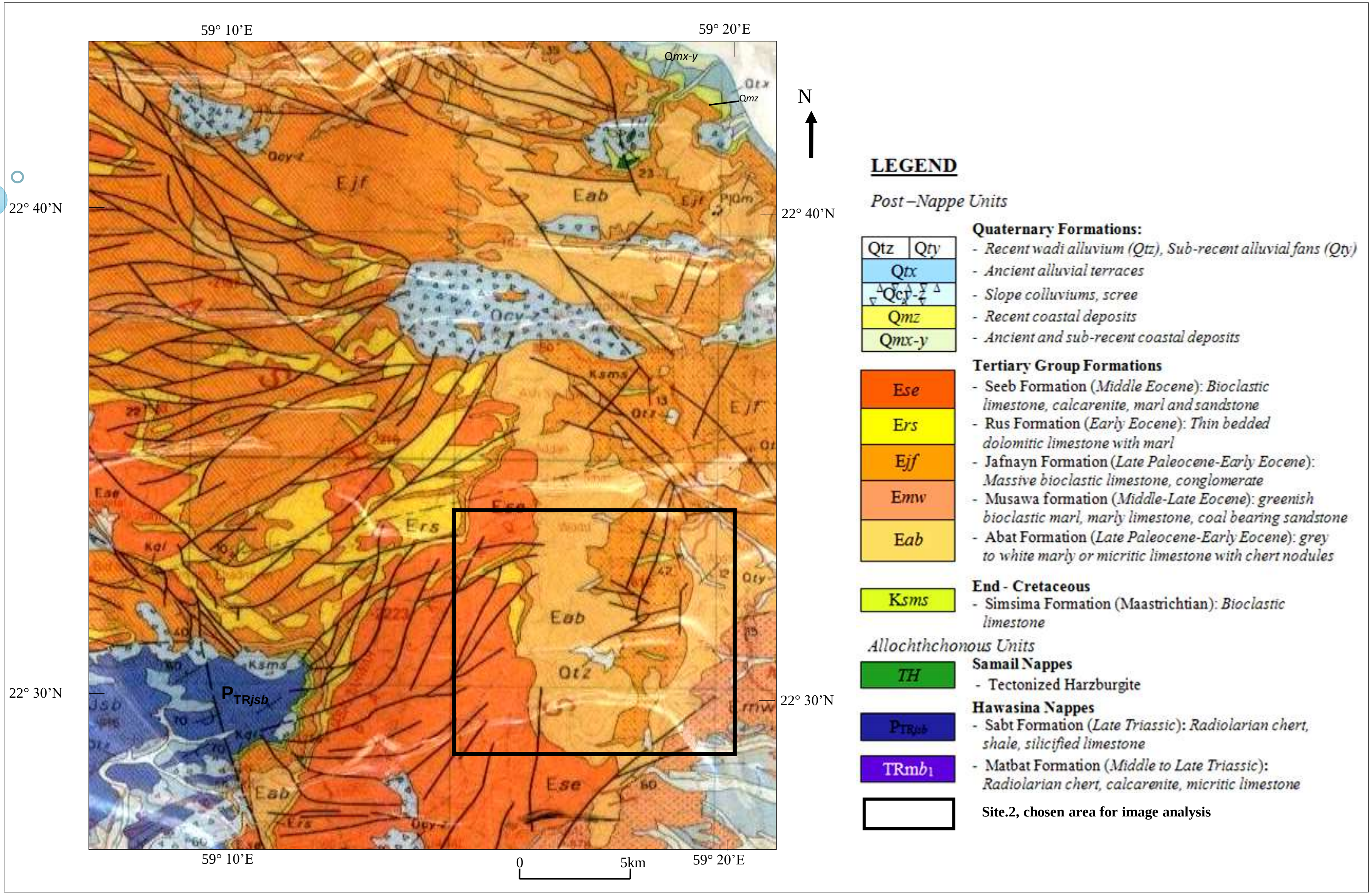

Regional geology of in and around of Site. 2 (Ministry of Petroleum and Minerals, 1992)

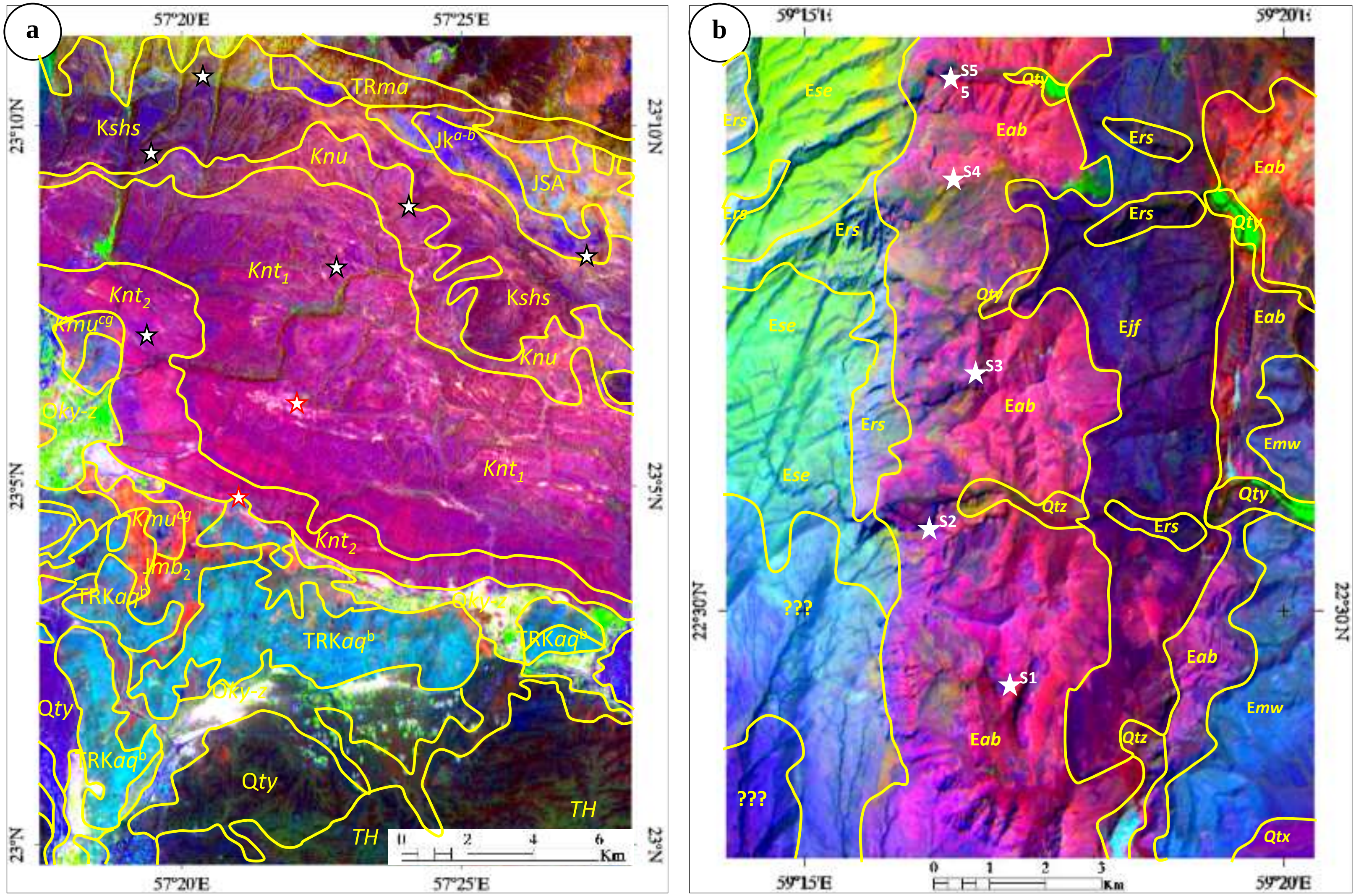

Decorrelated RGB images of ASTER spectral bands 8, 3, 1 of a Site. 1 and b Site. 2, shows the limestone formations in pink color. Decorrelated RGB images of ASTER spectral bands 8, 3, 1 of a Site. 1 and b Site. 2, shows the limestone formations in pink color (refer the legend of Figs. 3, 4)

CASE STUY 5:

Spectral analysis of ultramafic lamprophyres (carbonatite and aillikites) in Batain nappe, Northeastern margin of Oman

Rajendran and Nasir (2013) International Journal of Remote sensing, 34(8), 2763–2795.

Google Earth image shows the regional geology and structures of the northeastern Oman margin with allochthchonous and autochthchonous units as well as the locations of the UML in Batain nappes (modified from Nasir et al. 2011).

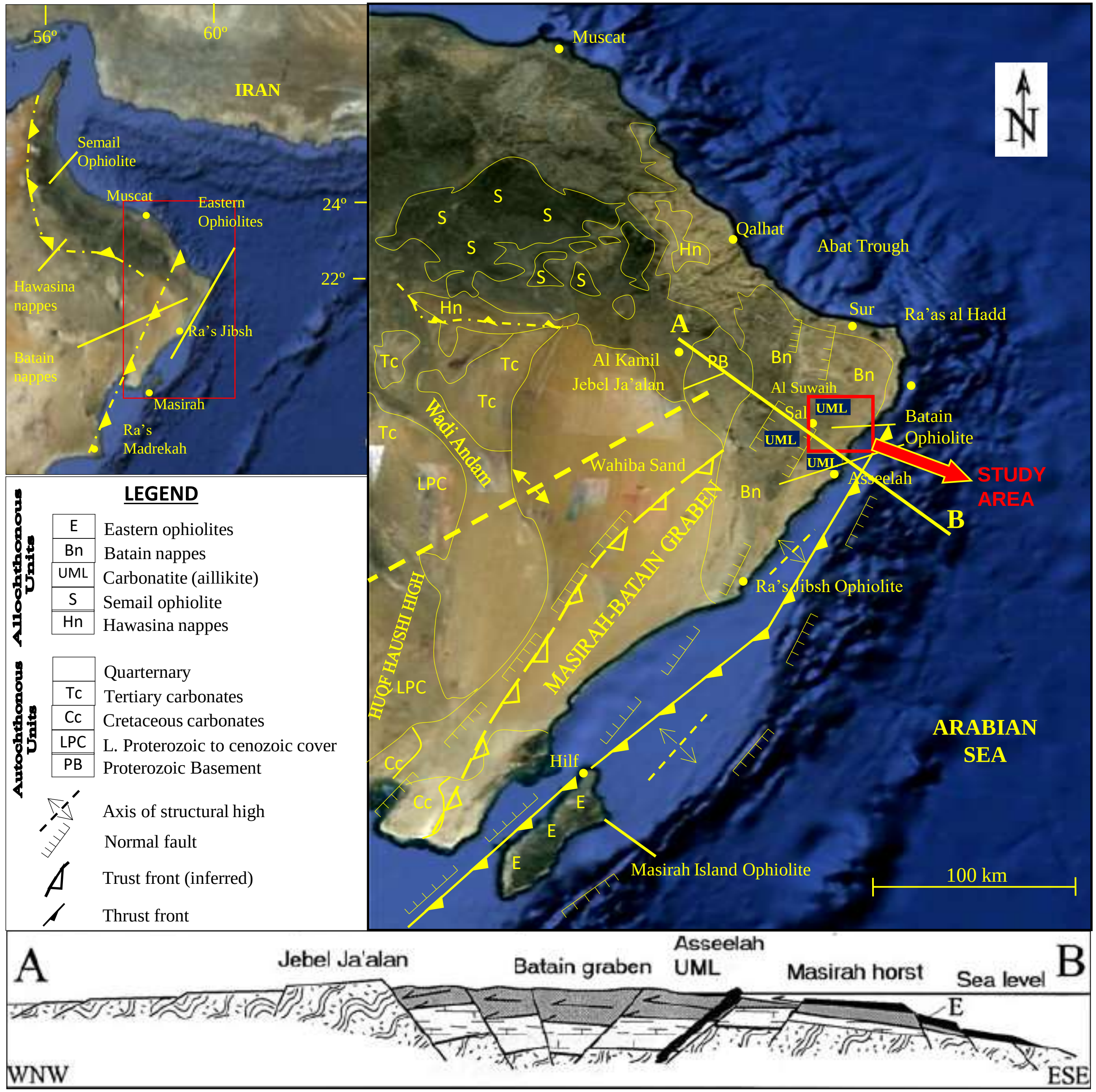

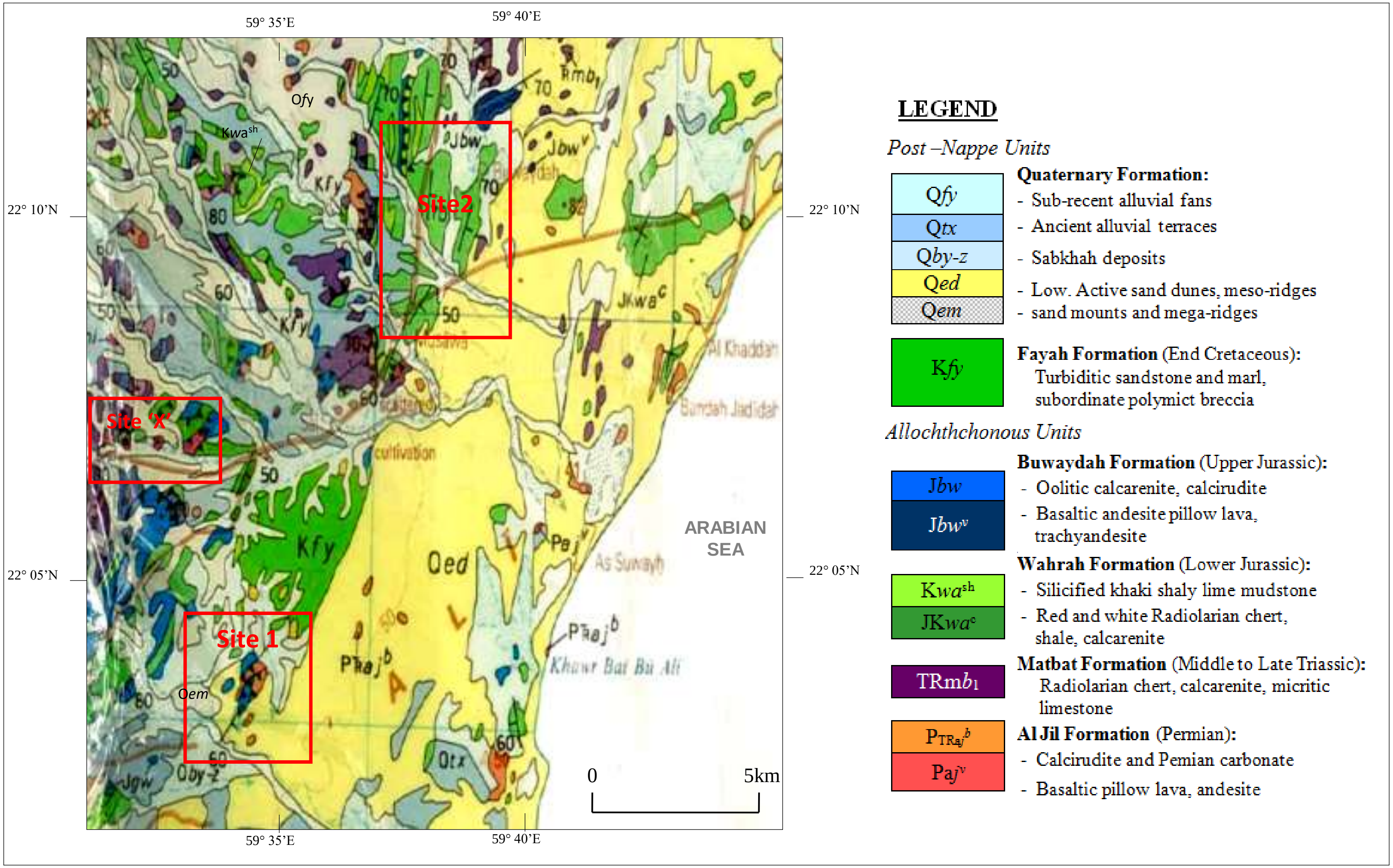

Regional geology of the study area (Ministry of Petroleum and Minerals, 1992; Scale 1:250,000)

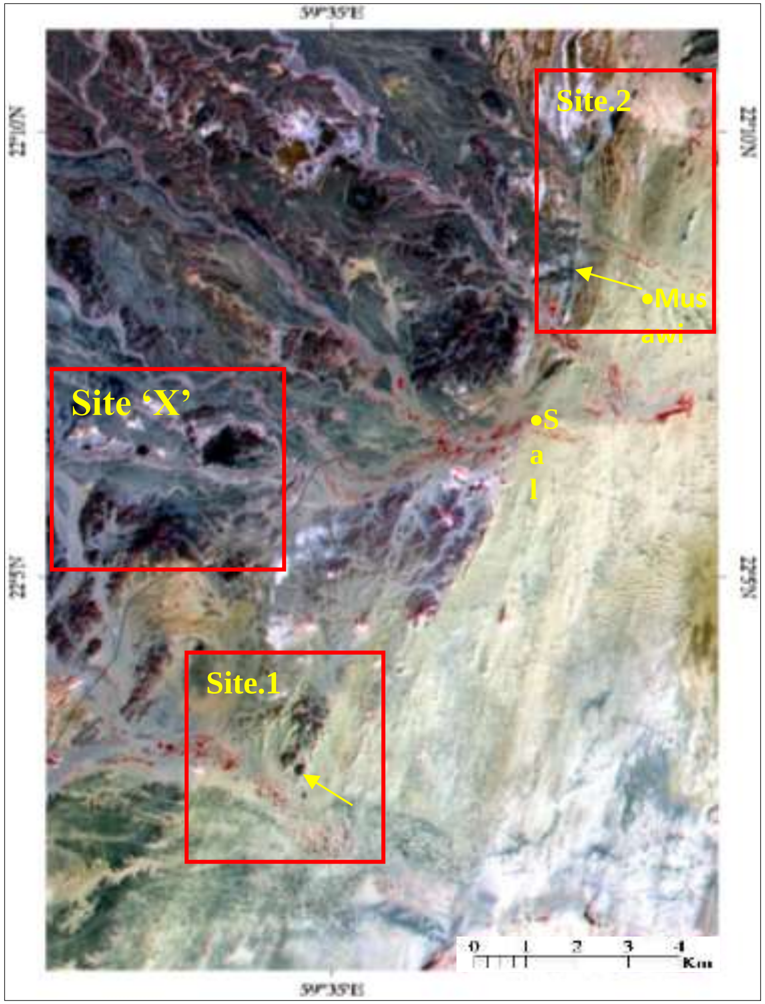

ASTER RGB (3, 2, 1) image shows the locations of carbonatite (Site.1, 7 km northwest to Sal) and aillikite (Site.2, at Musawi) dykes (yellow arrows marked). Site 'X' represents the occurrence of massive carbonatites.

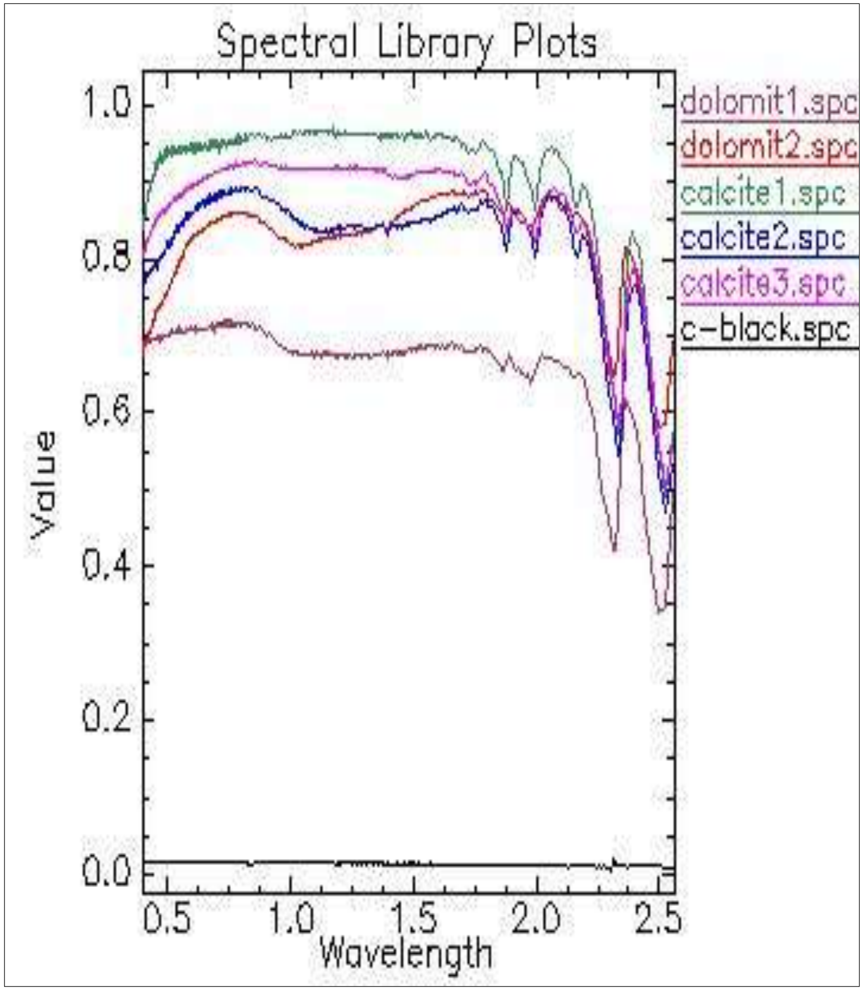

USGS Spectral Library plots for minerals shows absorption differences in the spectra of carbon (c-black) and the major carbonate minerals namely calcites and dolomites.

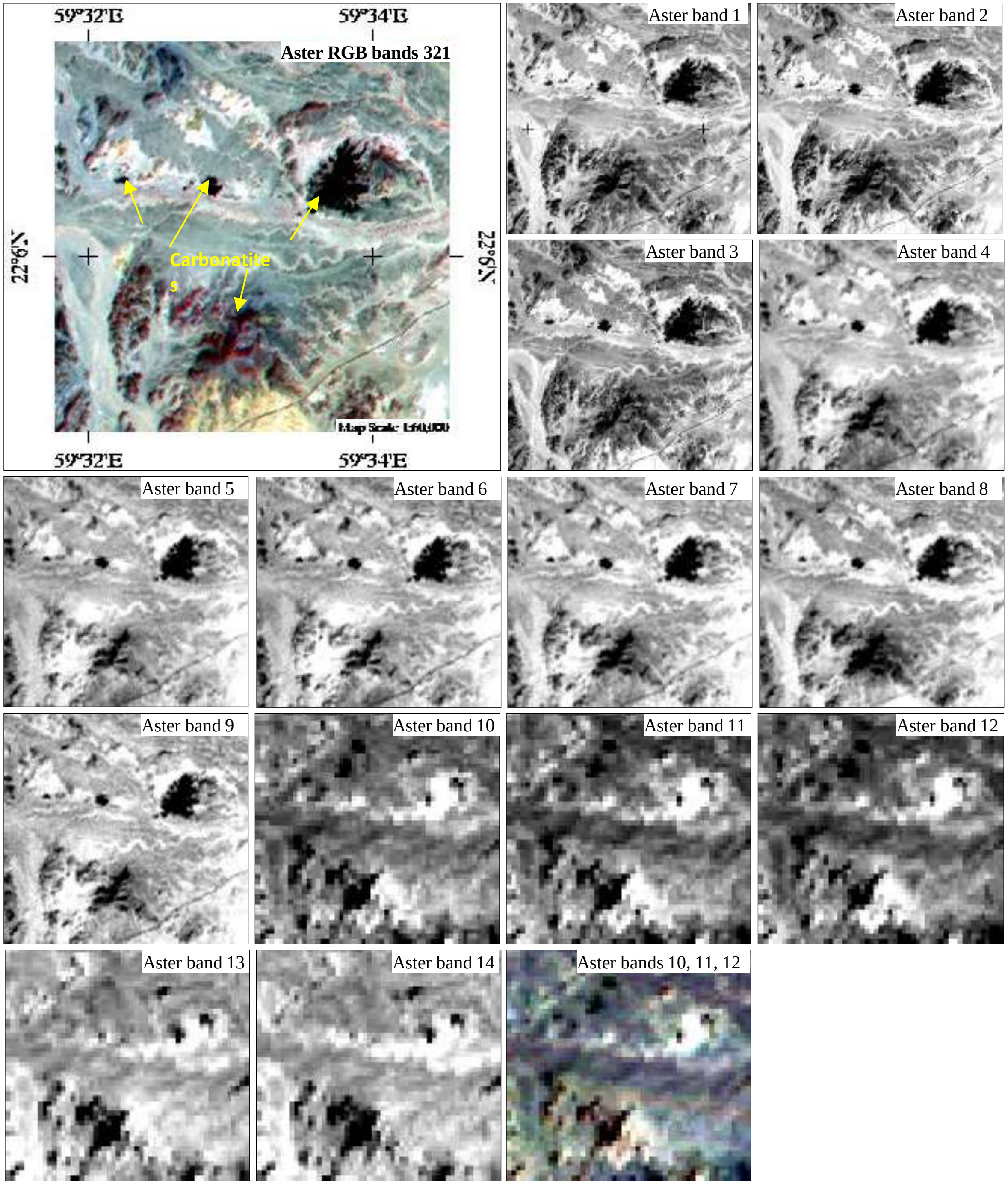

Occurrence of carbonatites in the area 5 km north to Sal, in Batain Nappe. The image of ASTER VNIR and SWIR spectral bands (band 1 to band 9) shows carbonatites in dark color and ASTER TIR bands (band 10 to band 14) shows carbonatites in white color.

Landsat TM images show the occurrence of carbonatites of the area 5 km north to Sal of Batain nappe in dark color in the visible and reflected infrared spectral bands (TM band 1 to TM band 5 and TM band 7) and by bright pixels in the TM band 6.

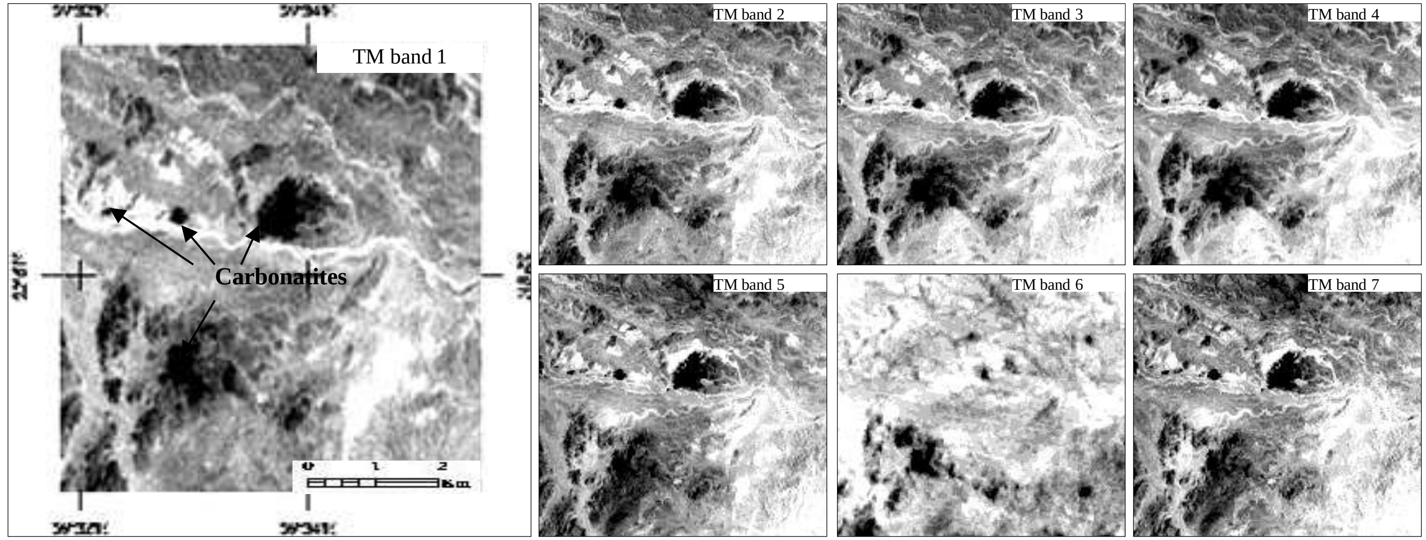

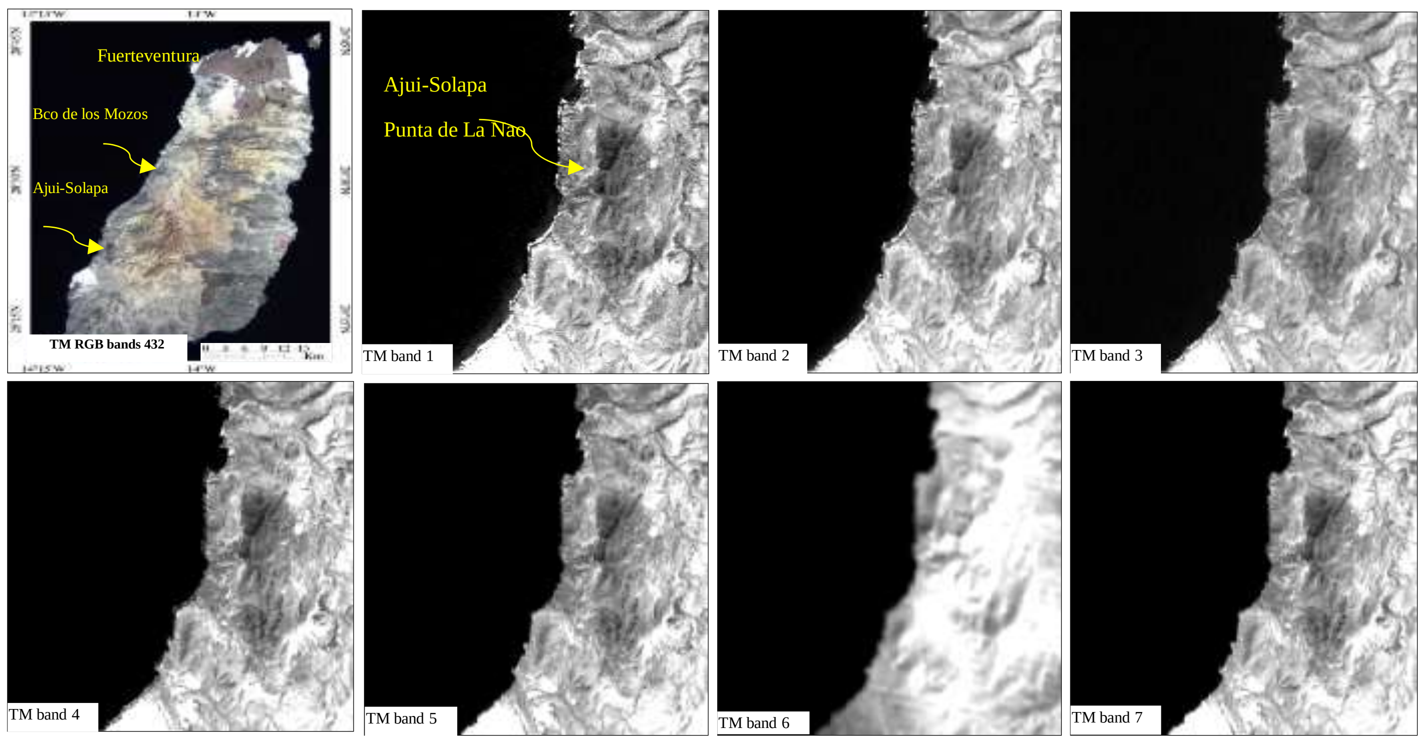

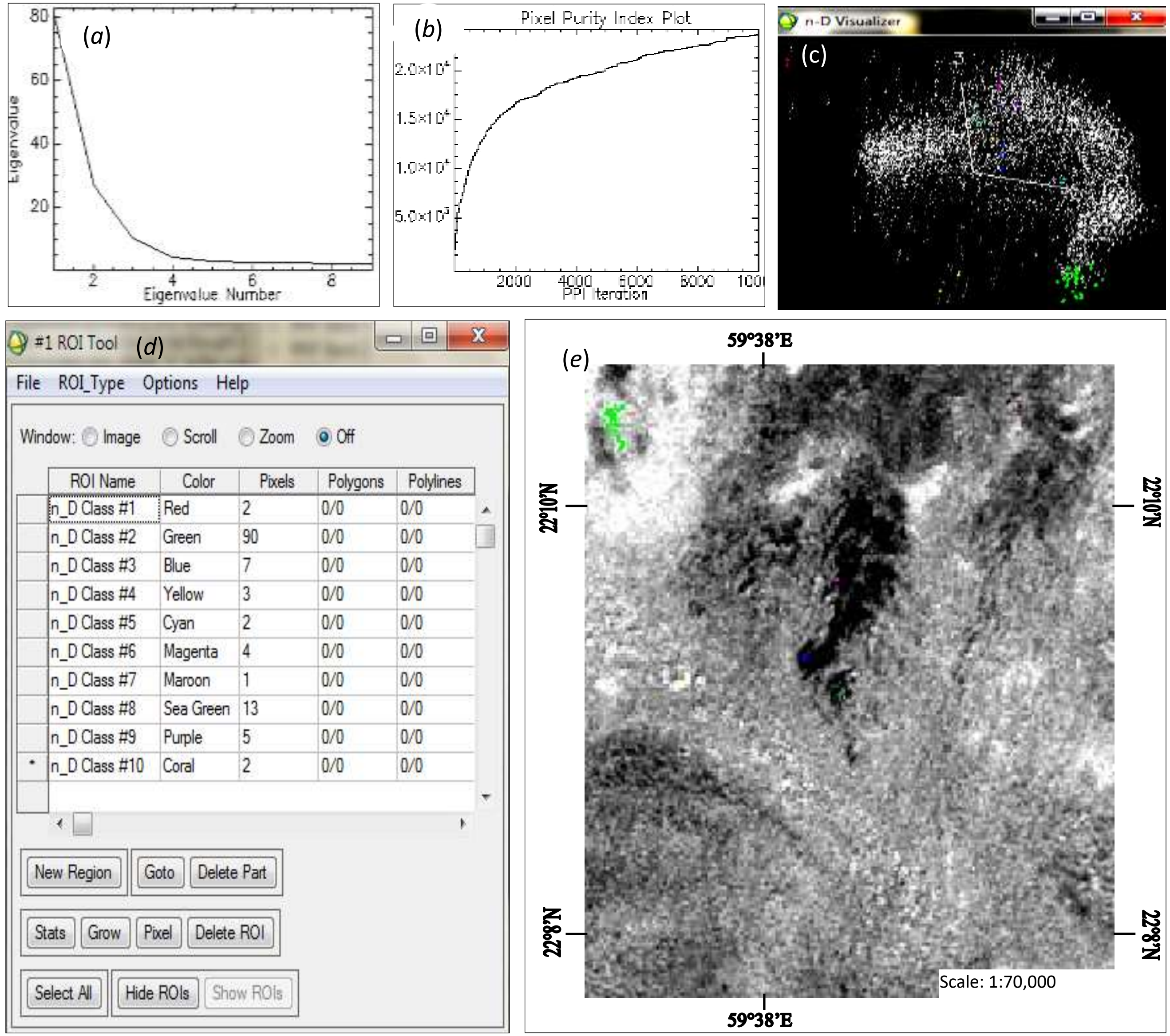

(*a*) MNF plot of Site.1, (*b*) plot of PPI, (*c*) groups of pure pixels in n-Dimensional visualizer, (*d*) the number of endmember pixels collected on selected colors and (*e*) spatial distribution of endmembers pixels on the image of MNF band 3.

The threshold images of SAM Target Detection wizard on the occurrences of (*a*) the carbonates (sea green color) and (*b*) the dolomite (blue color) minerals in the carbonatite dyke and (*c*) calcite (green color) minerals in ancient alluvial terraces in Site.1 and (*d*) the true color Google earth image showing the occurrences of carbonatites in dark or grey in color.

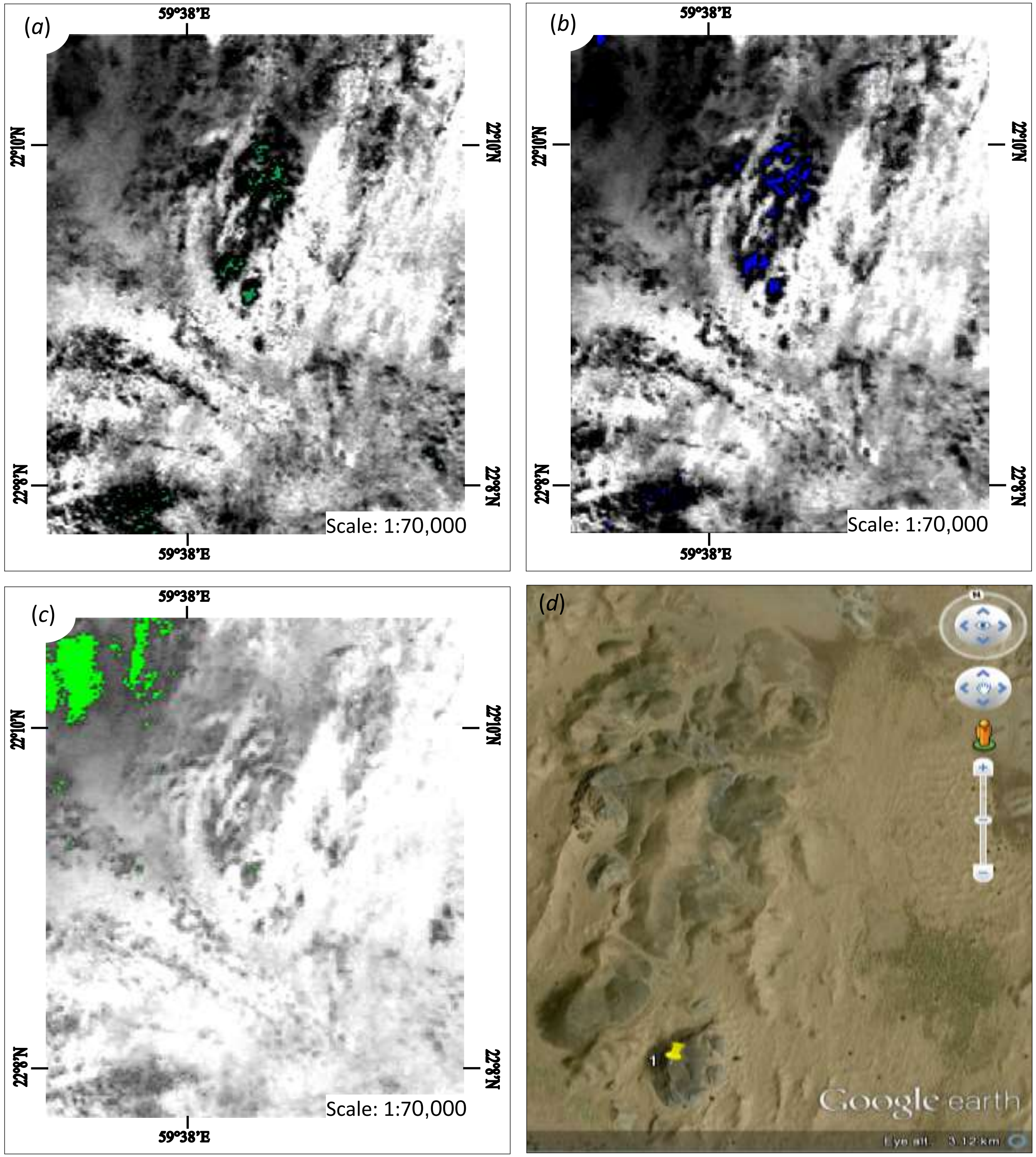

CASE STUY 6:

Mapping of Industrial rock: Marble – ‘The Oman Exotics’

Rajendran et al. (2017) Submitted to Ore Geology Reviews

Oman Exotics

Vast occurrences of exotics in the region of Oman Mountains found in the three major allochthonous units of Oman viz.

1. Hawasina Complex, Haybi Complex and Semail ophiolite;

2. the Haybi Complex comprises olistostromes, Haybi alkalic and tholeiitic basalts, exotics, sub-ophiolitic metamorphic rocks, and

3. a serpentinite melange (Searle and Malpas, 1980; Searle and Graham, 1982).

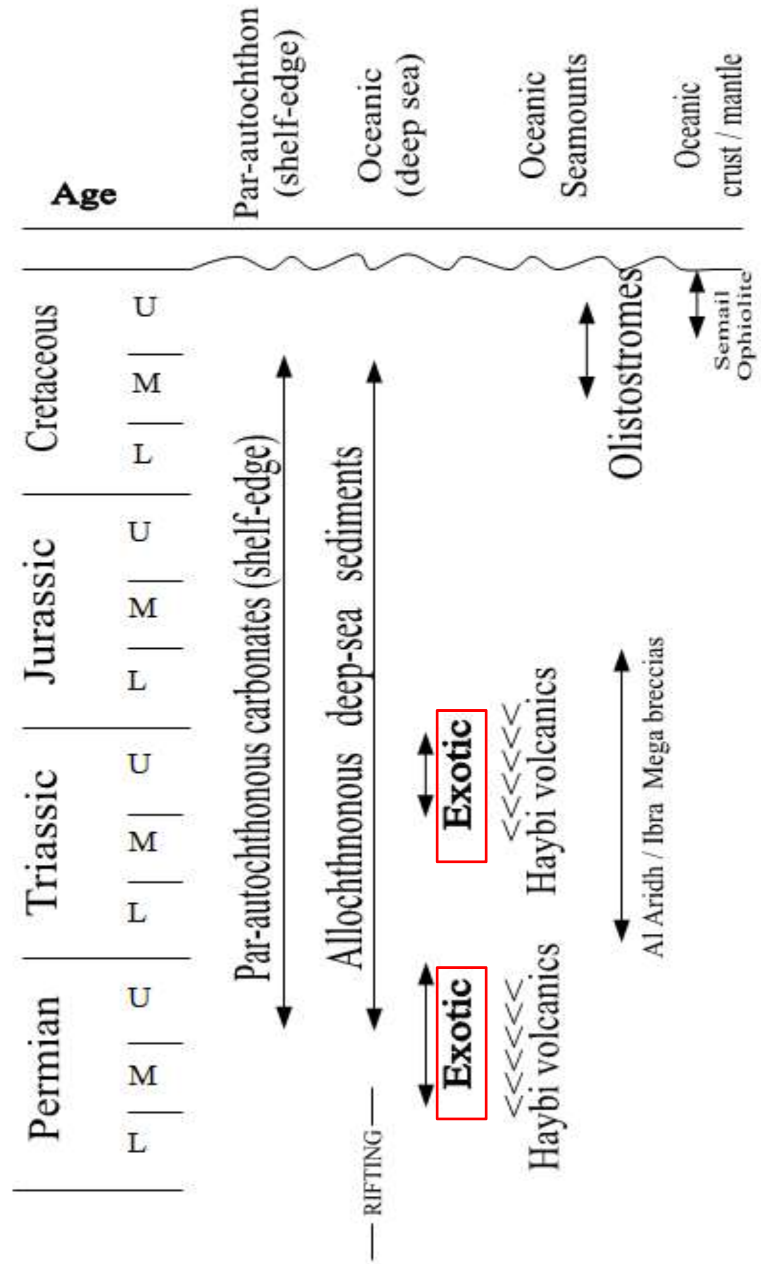

The stratigraphic position of Oman exotics:

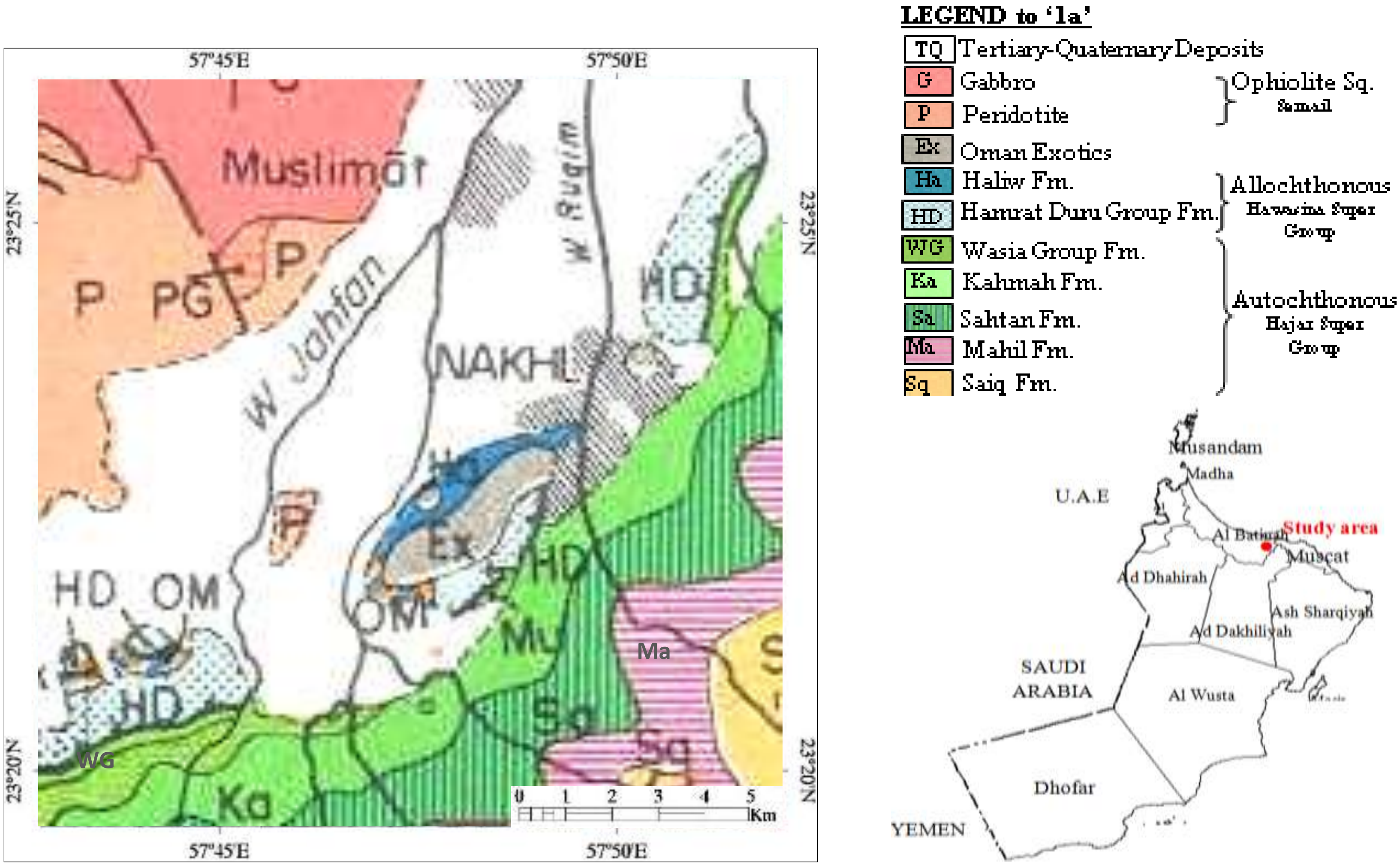

Figure. Shows the regional geology of the Nakhl region (Source: Geological map of the Oman Mountains, KSEPL, 1974).

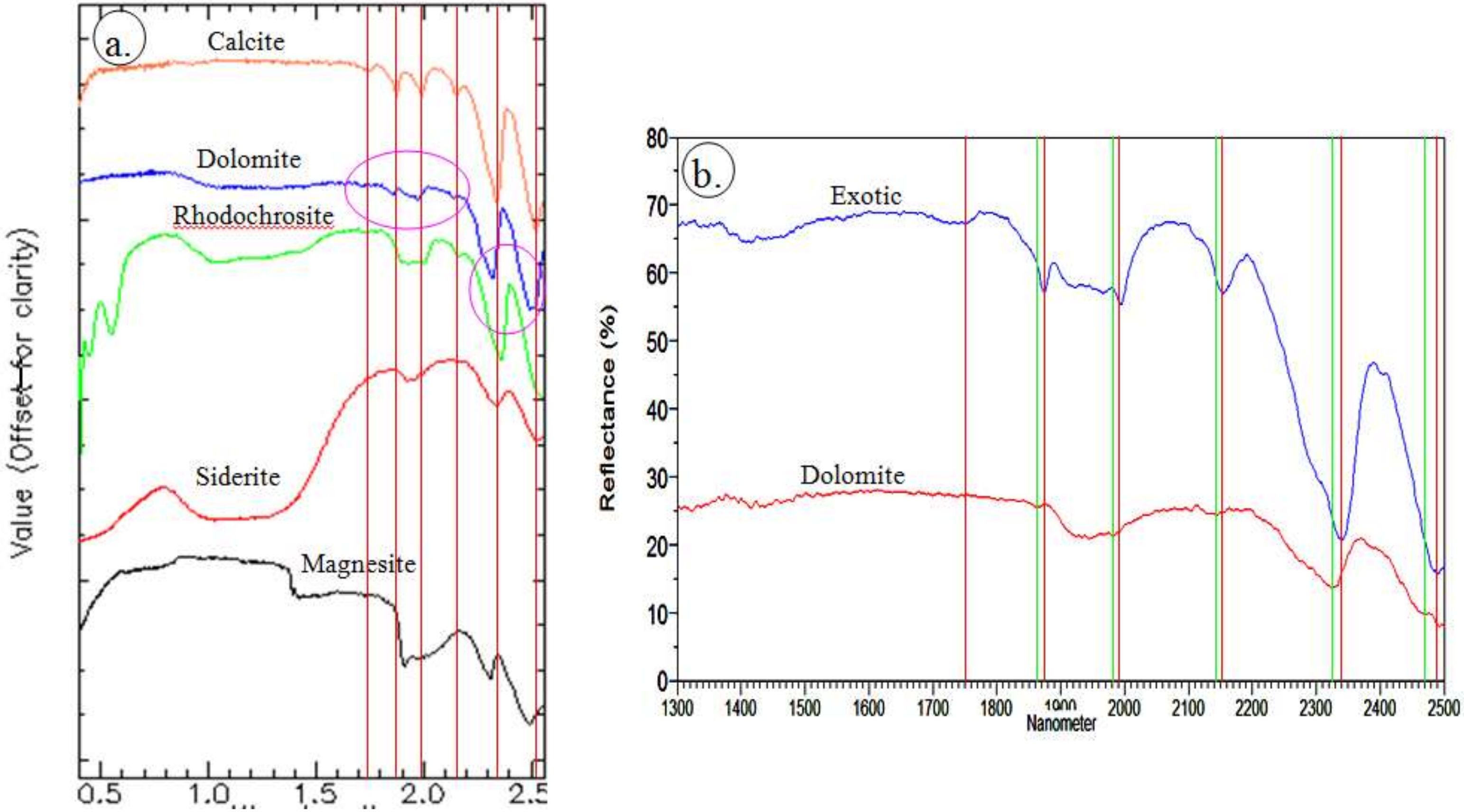

Figure. Spectral plot of carbonate minerals stacked from a. the USGS Spectral Library for minerals in the 0.3 to 2.5 µm and b. the exotic and dolomite rocks measured in 1.3 to 2.5 µm (1300 to 2500 nm) with the spectral resolution of 7 nm using PIMA spectrometer.

Results of Decorrelation of ASTER spectral bands

In the present study, we use the method of Rajendran and Nasir (2014) to delineate the exotics and discriminate them from associated rock types in the study region

1) the ASTER band 8 is chosen to show the occurrence of calcite rich exotics,
2) the band 3 is preferred to highlight the very low response of the ferro-magnesium silicate minerals associated with the rocks and
3) the band 1 is selected to characterise the iron rich ophiolites of the study region

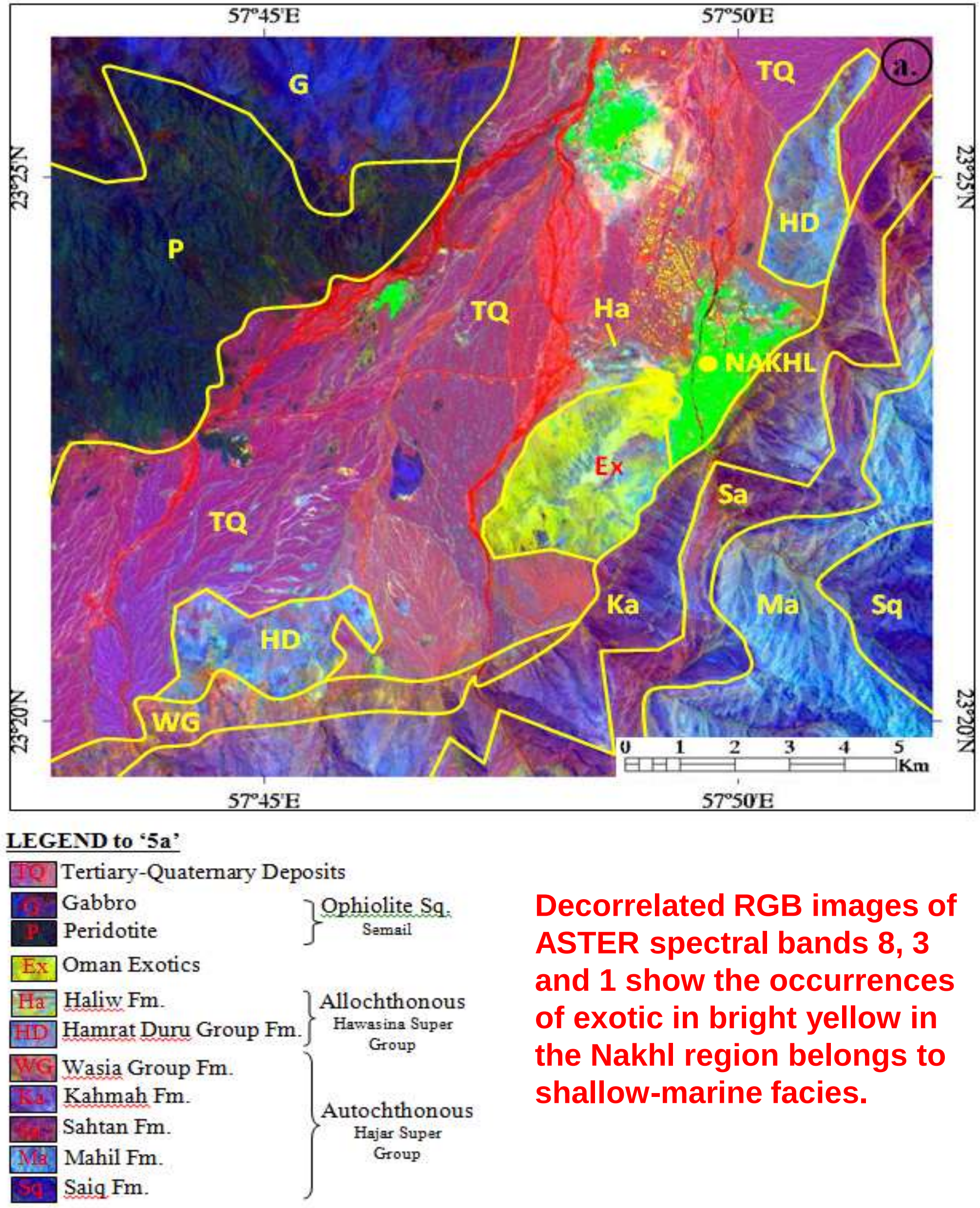

Decorrelated RGB images of ASTER spectral bands 8, 3 and 1 show the occurrences of exotic in bright yellow in the Nakhl region belongs to shallow-marine facies.

Results of Decorrelation of Landsat 7 ETM+ spectral bands

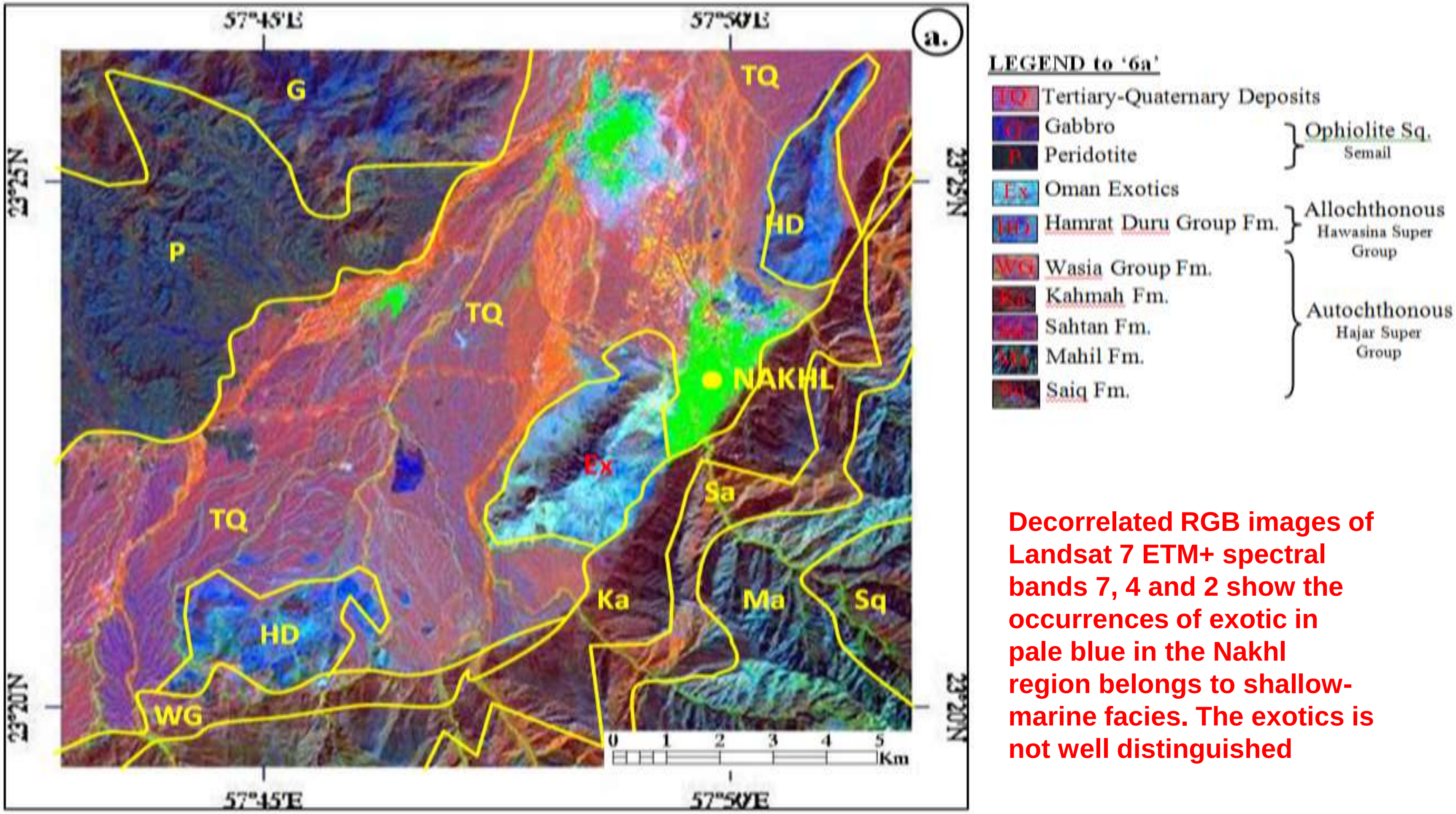

Decorrelated RGB images of Landsat 7 ETM+ spectral bands 7, 4 and 2 show the occurrences of exotic in pale blue in the Nakhl region belongs to shallow-marine facies. The exotics is not well distinguished

CASE STUY 7:

Detection of hydrothermal mineralized zones associated with listwaenites in the Central Oman

Rajendran et al. (2013) Ore Geology Reviews 53, 470–488.

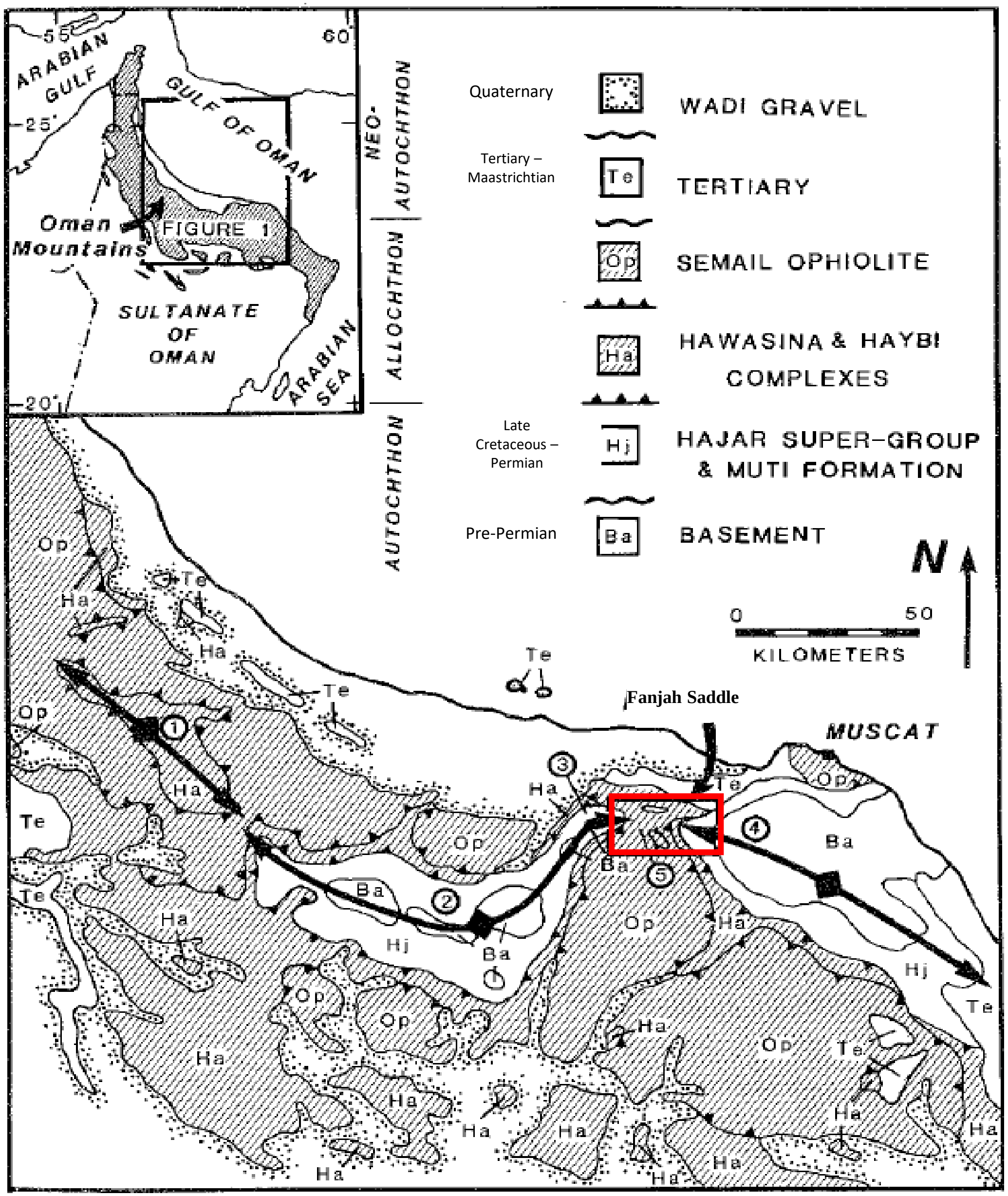

Location map shows simplified geology of the Oman Mountains with major culminations and the Fanjah Saddle indicated 1, Hawasina Window; 2, Jebel Akhdar culmination; 3, Jebel Nakhl culmination; 4, Saih Hatat culmination; and 5, Fanjah Saddle (after, Coffield, 1990).

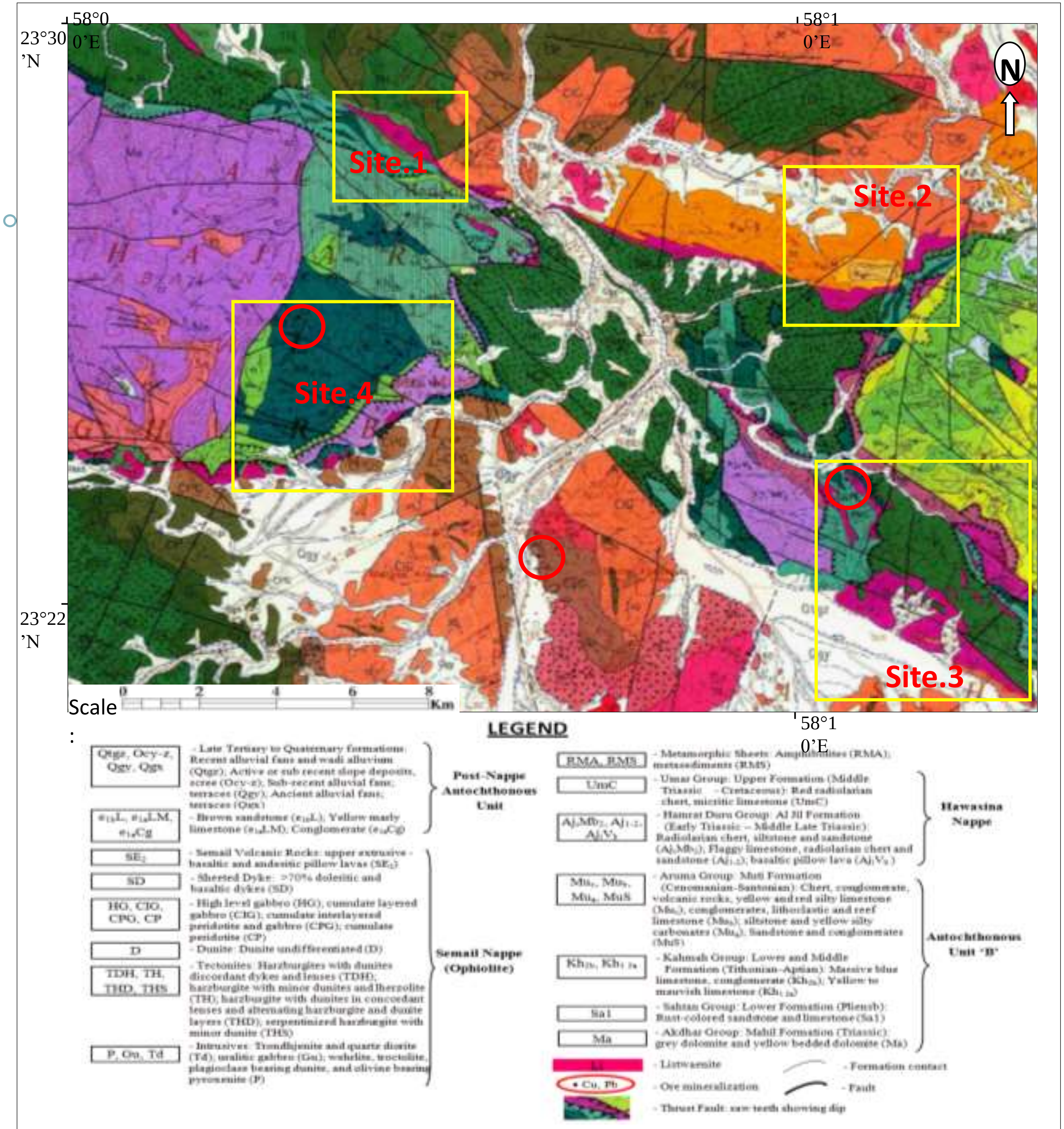

The geology in and around of Fanjah Saddle (Ministry of Petroleum and Minerals, Oman, 1986).

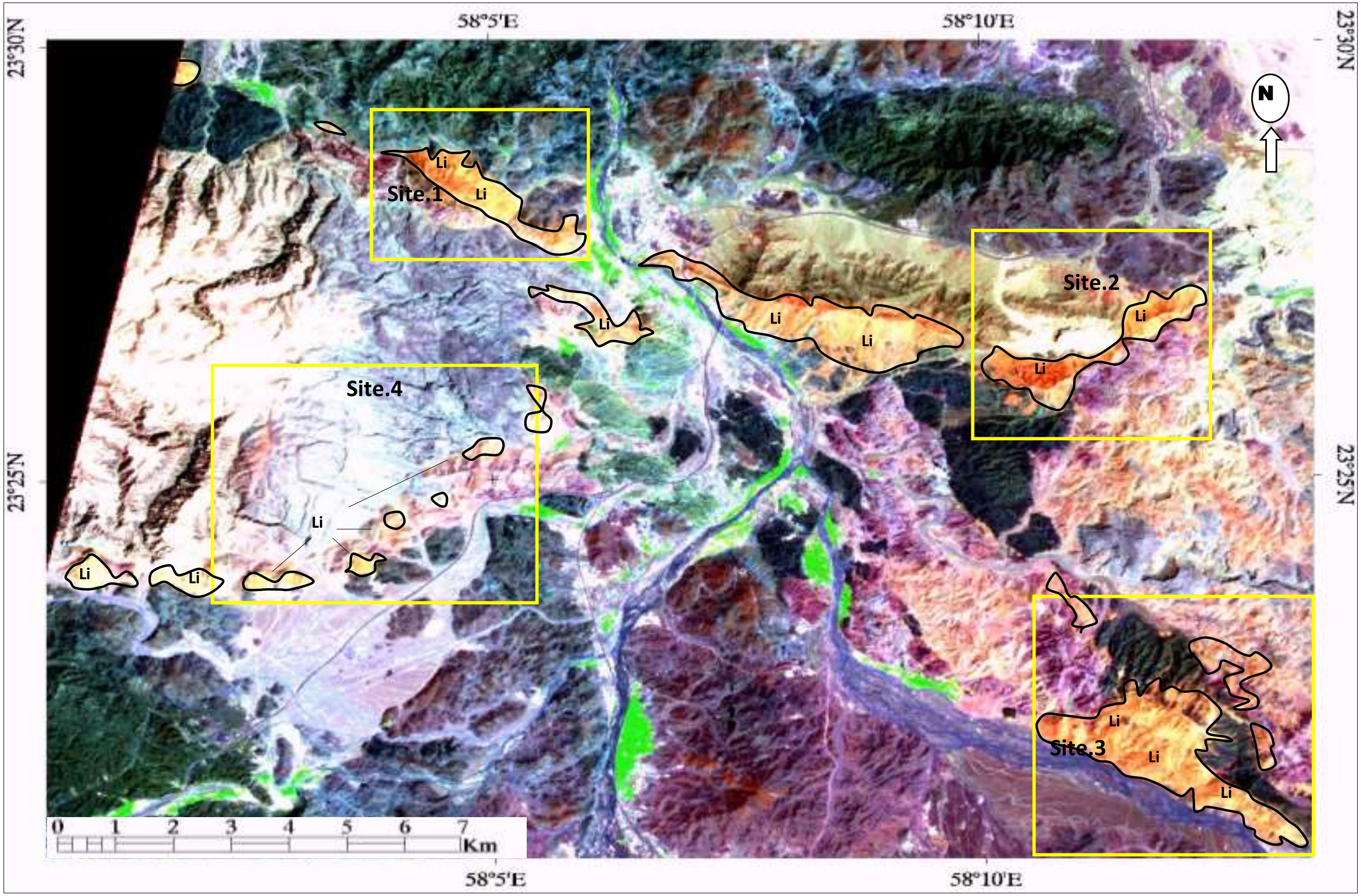

ASTER RGB (8, 3 and 1) image shows the occurrence and spatial distribution of listwaenites (golden yellow color marked as Li) and mantle sequences (dark green color) in Fanjah Saddle.

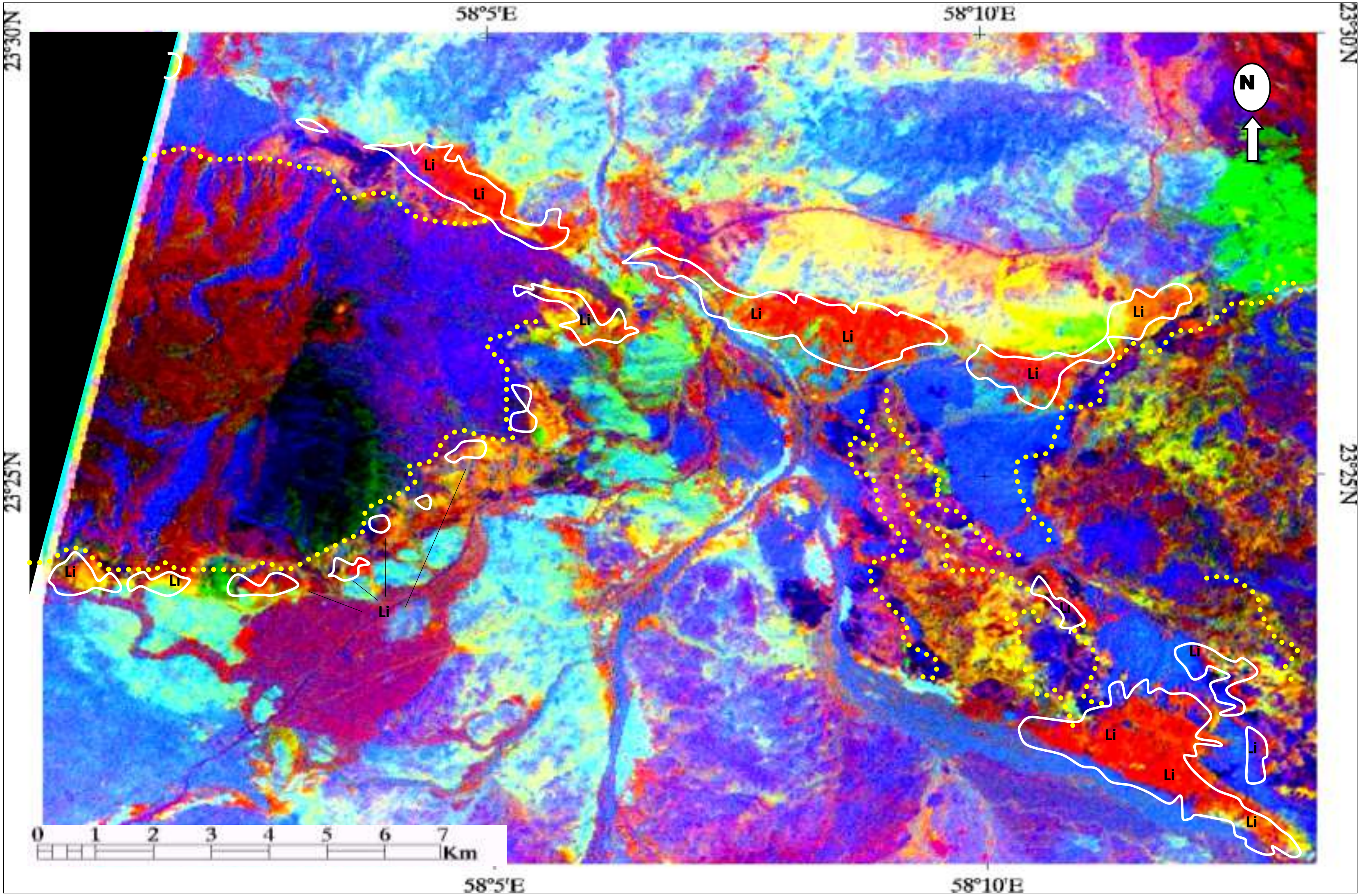

ASTER SWIR RGB (PC5, PC3 and PC1) image shows the presence of hydrothermal altered rock (listwaenite in dark red color marked as Li) and mineralized areas in range of colors interpreted along the thrust fault zones (dotted lines in yellow color) of the Fanjah Saddle.

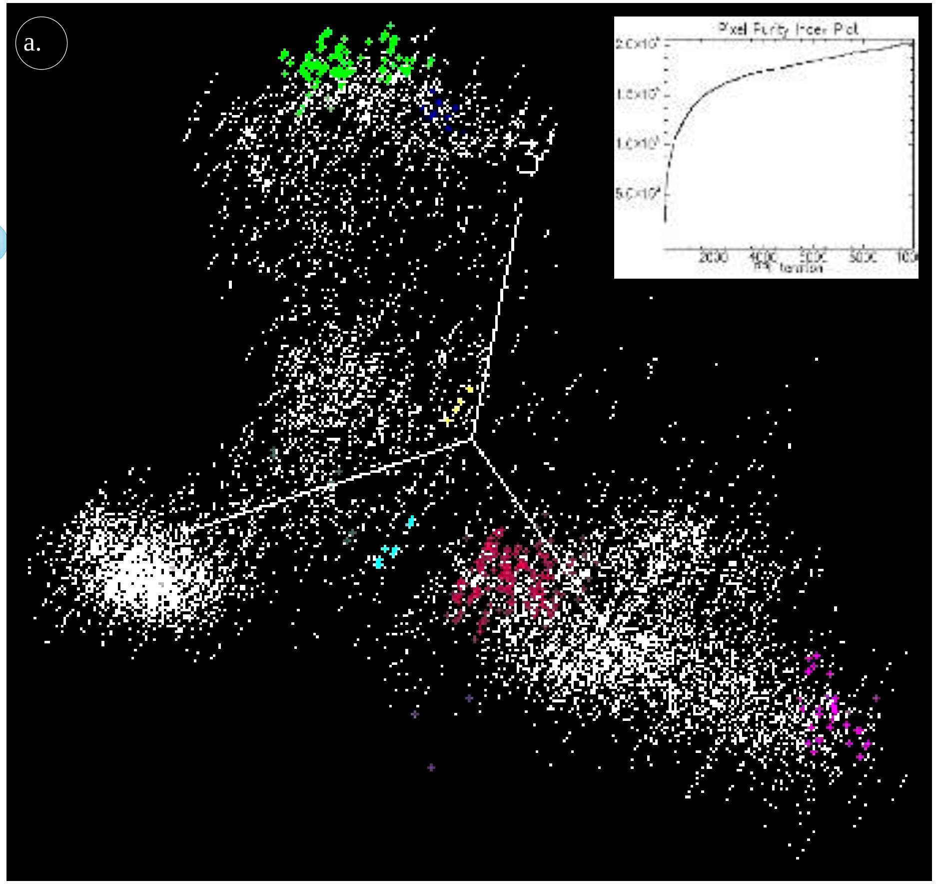

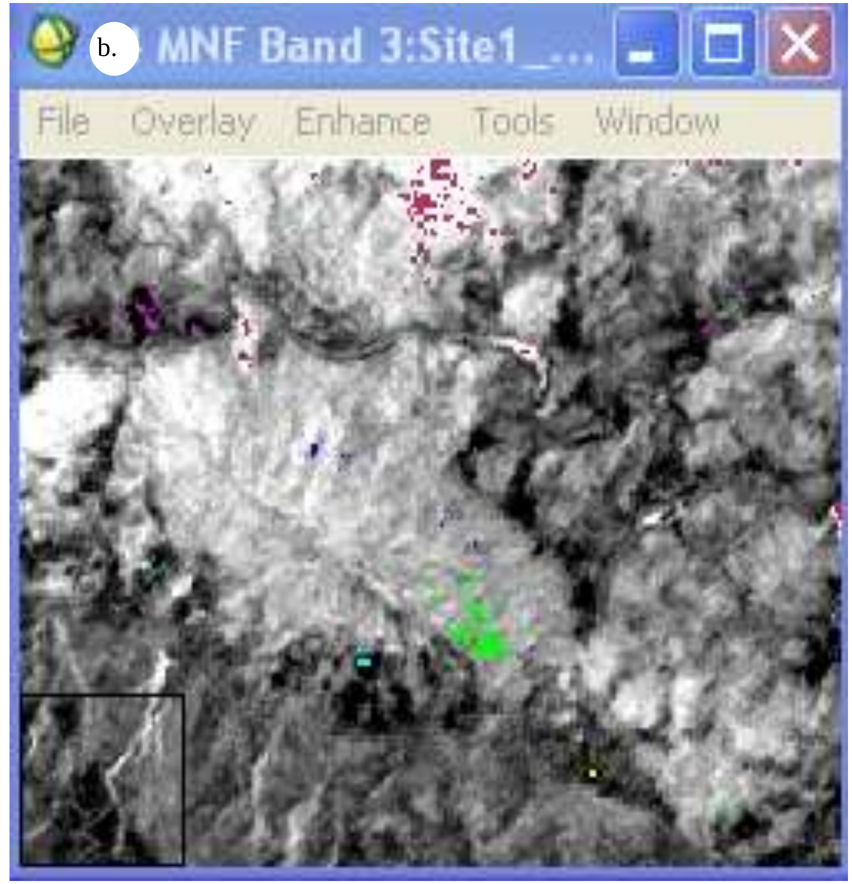

n-Dimensional visualizer plot of Site.1 shows the groups of pure pixels and endmembers (inset is the PPI plot of Site.1) and b. the spatial distribution of endmembers on the image of MNF band3.

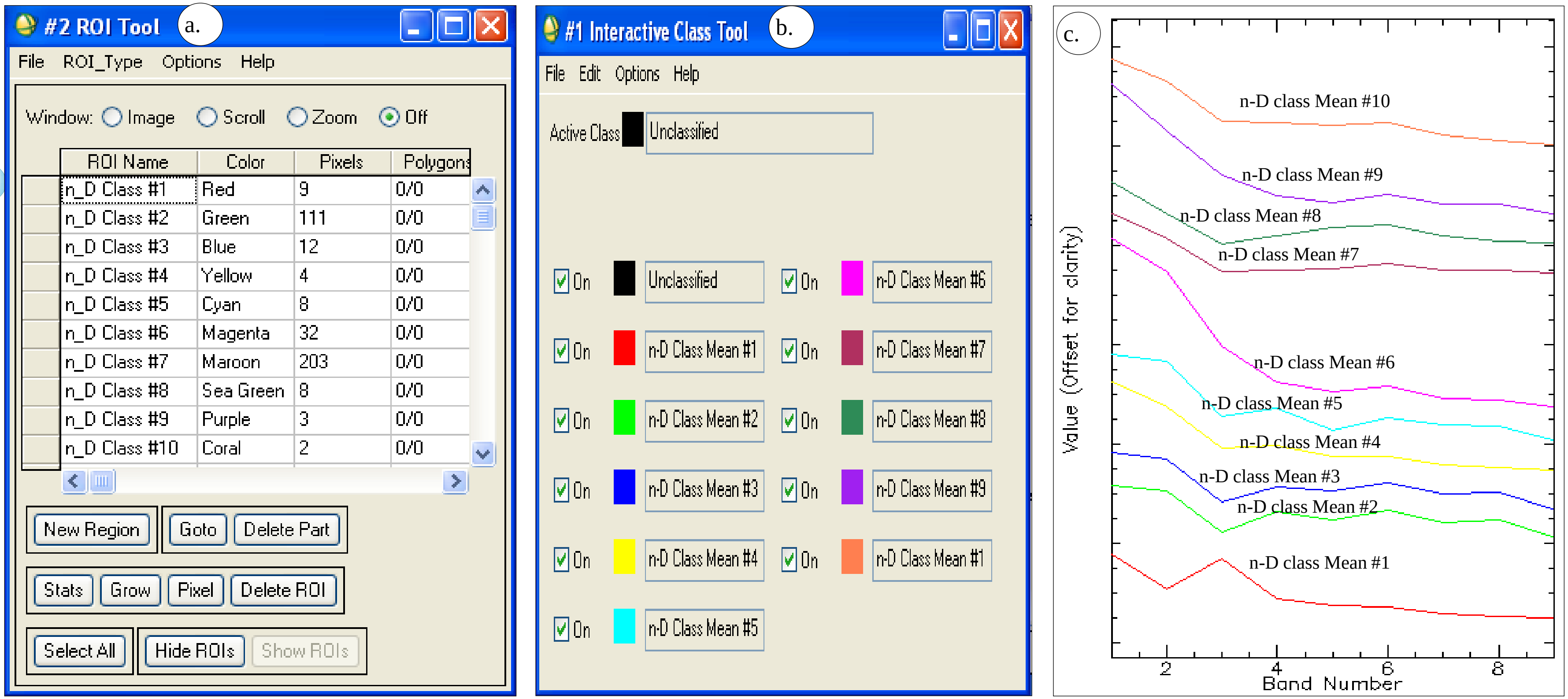

a. the number of pixels collected on the endmembers, b. selected colors to spectra and minerals and c. the plot of endmember spectra.

a. the SAM classified image shows the occurrence of minerals and mineralization and b. the ASTER SWIR PC5, PC3 and PC1 RGB image, c. the ASTER RGB (9/8, 4/3, and 2/1) band ratio image and the d. ASTER RGB (8, 3 and1) color composite image shows the rock types of Site.1. Li-listwaenite; TH-harzburgite; THS-serpentinised harzburgite; CP-cumulate peridotite; CIG-cumulate layered gabbro; RMS-metasediments; Mu_a-siltsone and silty carbonates; Kh_{2b}-massive limestone and conglomerate and Dashed Line - thrust fault zone.

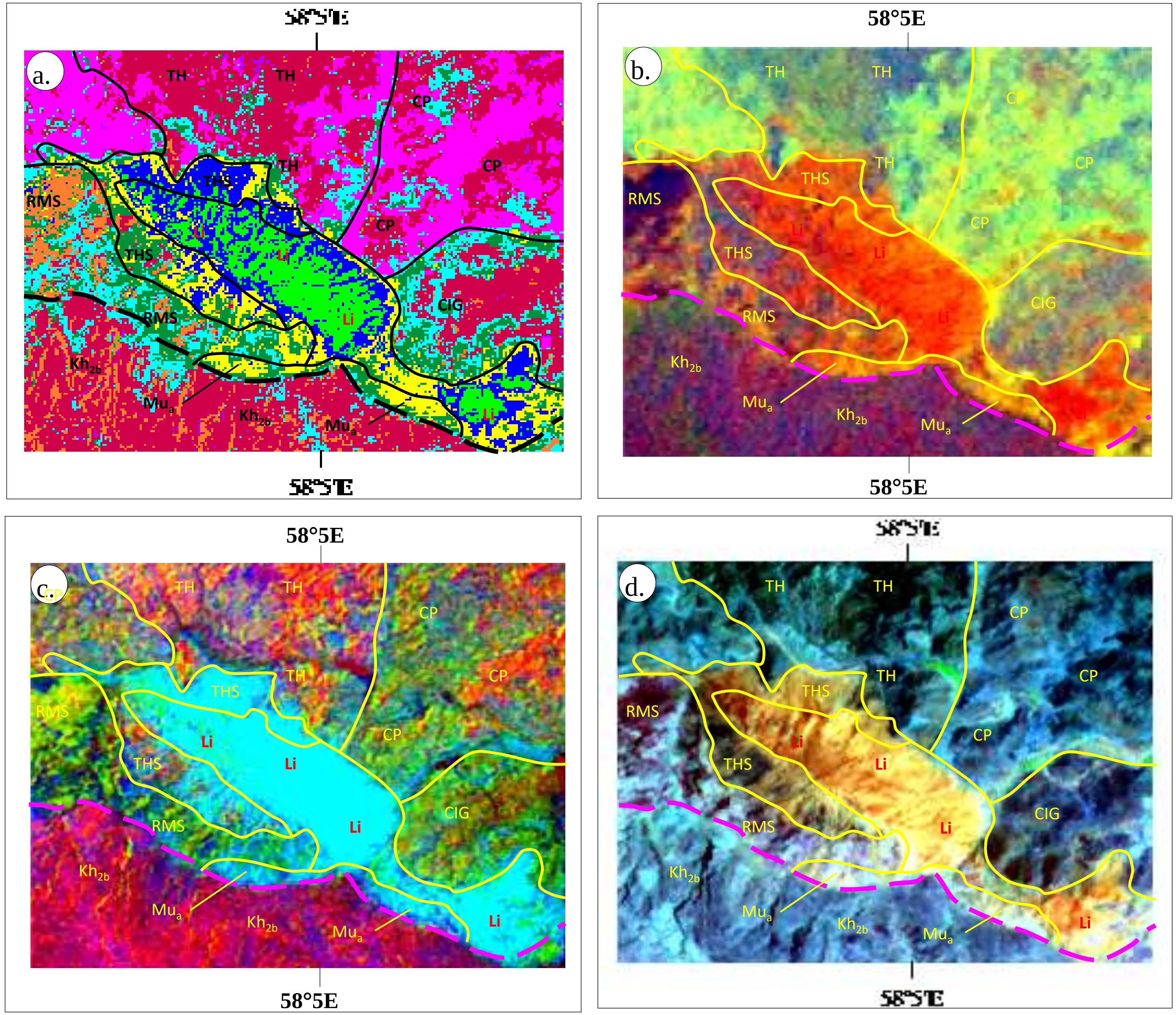

CASE STUY 8:

Mapping of CO2 sequestered region in Semail Ophiolite massifs of Oman

S. Rajendran et al. / Earth-Science Reviews 135 (2014) 122–140

About the study

- The removal of carbon dioxide from the atmosphere and ocean by the natural weathering processes of silicate rocks like peridotites is one of the long-term mechanisms.
- Peridotite is composed of > 40% of the mineral olivine (Le Maitre, 1989). The typical residual mantle peridotite exposed on the seafloor and in ophiolites is composed of 70 to 85% olivine, together with dunite with more than 95% olivine.
- During the weathering processes, the minerals such as olivine (particularly the Mg-rich end member), pyroxenes and serpentine in peridotite (ultramafic) rocks removes CO2 from the atmosphere (O'Connor et al., 2005; Gerdemann et al., 2007).
- In detail, the atmospheric CO2 reacts with rainwater to form carbonic acid.
- At the end, this carbonic acid chemically attacks the olivine on its surface and dissolves to produce hydrates and carbonates such as serpentine, talc, magnesite and dolomite and calcite.
- The reaction series of the predominant minerals can be expressed as

$$Mg_2SiO_4 \text{ [olivine]} + 2CO_2 \rightarrow 2MgCO_3 \text{ [magnesite]} + SiO_2 \text{ [silica]} \text{ ....1}$$

$$Mg_3SiO_3(OH)_4 \text{ [serpentine]} + 3CO_2 \rightarrow 3MgCO_3 \text{ [magnesite]} + SiO_2 \text{ [silica]} + 2H_2O \text{ .....2}$$

(A) MODIS image draped over digital elevation data showing the distribution of ophiolites (red in color) in parts of the Tethyan region (After Kahn and Mahmood, 2008), (B) the study area location in the Semail ophiolite massifs of Oman mountain region (After Robertson and Searle, 1990) and (C) the sequence of Oman ophiolites.

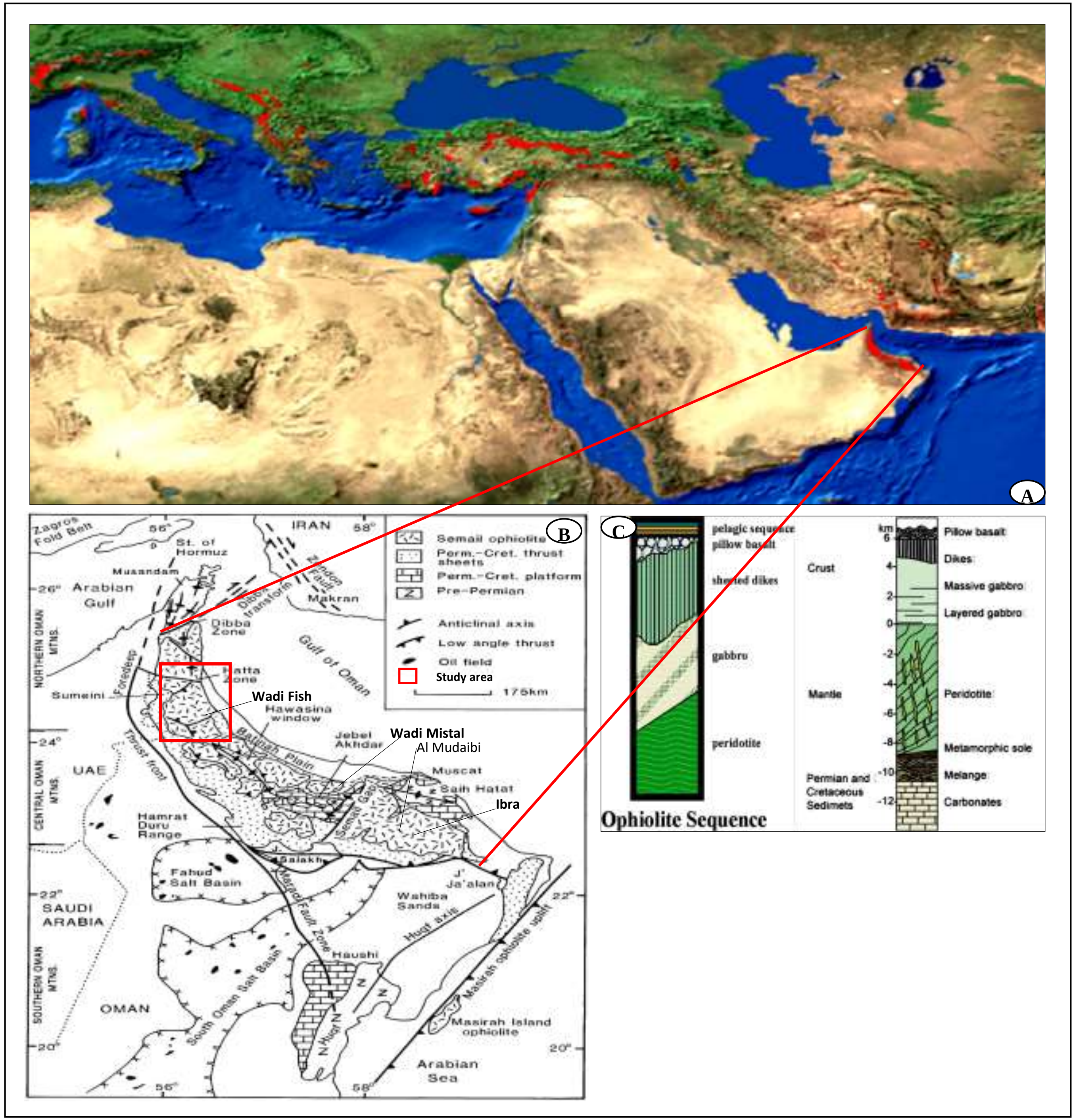

ASTER 8, 3, and 1 RGB image shows the discrimination of peridotites of Semail ophiolite massifs.

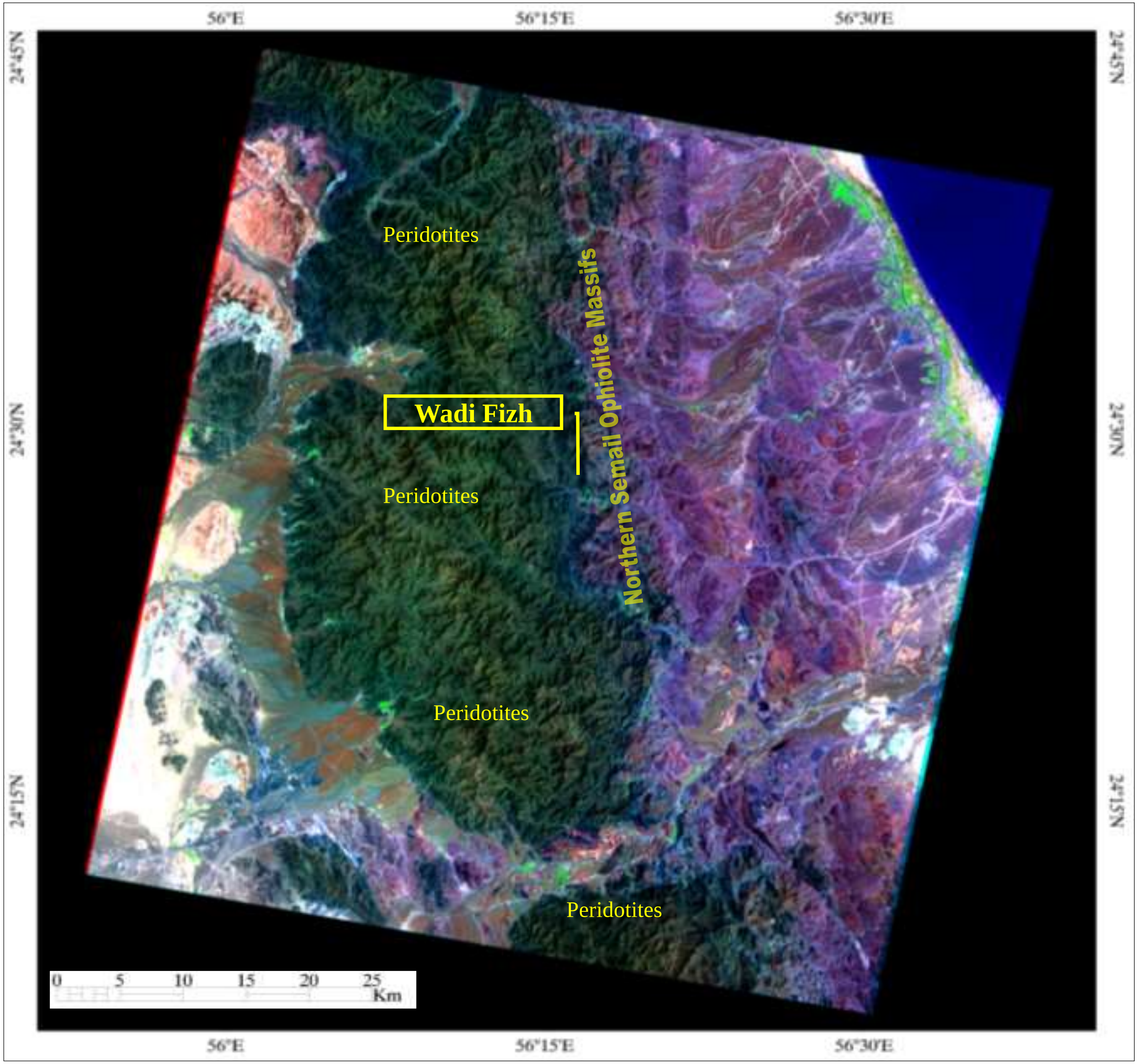

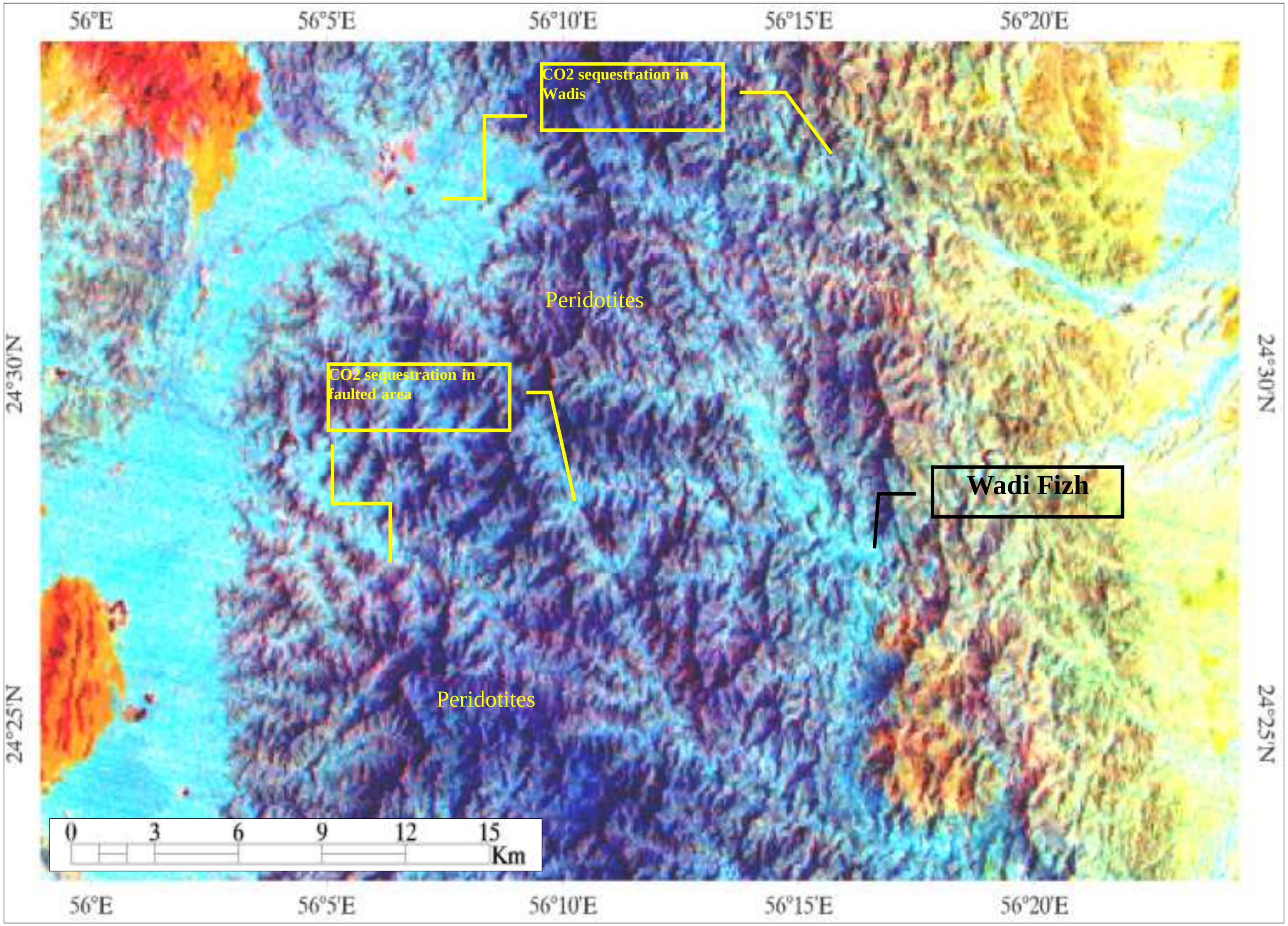

Mineral Indices RGB image (R: CI; G: QI; B: MI) shows the distribution of the CO_2 sequestered minerals in cyan color along the wadis (drainages) and structural zones (the regions better exposed and have interaction with atmosphere and water), altered serpentinites associated peridotites in purple color and the associated rocks layered gabbro, dykes, basalts and pelagic sequences in yellow brown to light yellow colors (based on the presence of silica contents).

ASTER RGB image shows the regional distribution of the CO_2 sequestered minerals in parts of the Semail ophiolite massifs.

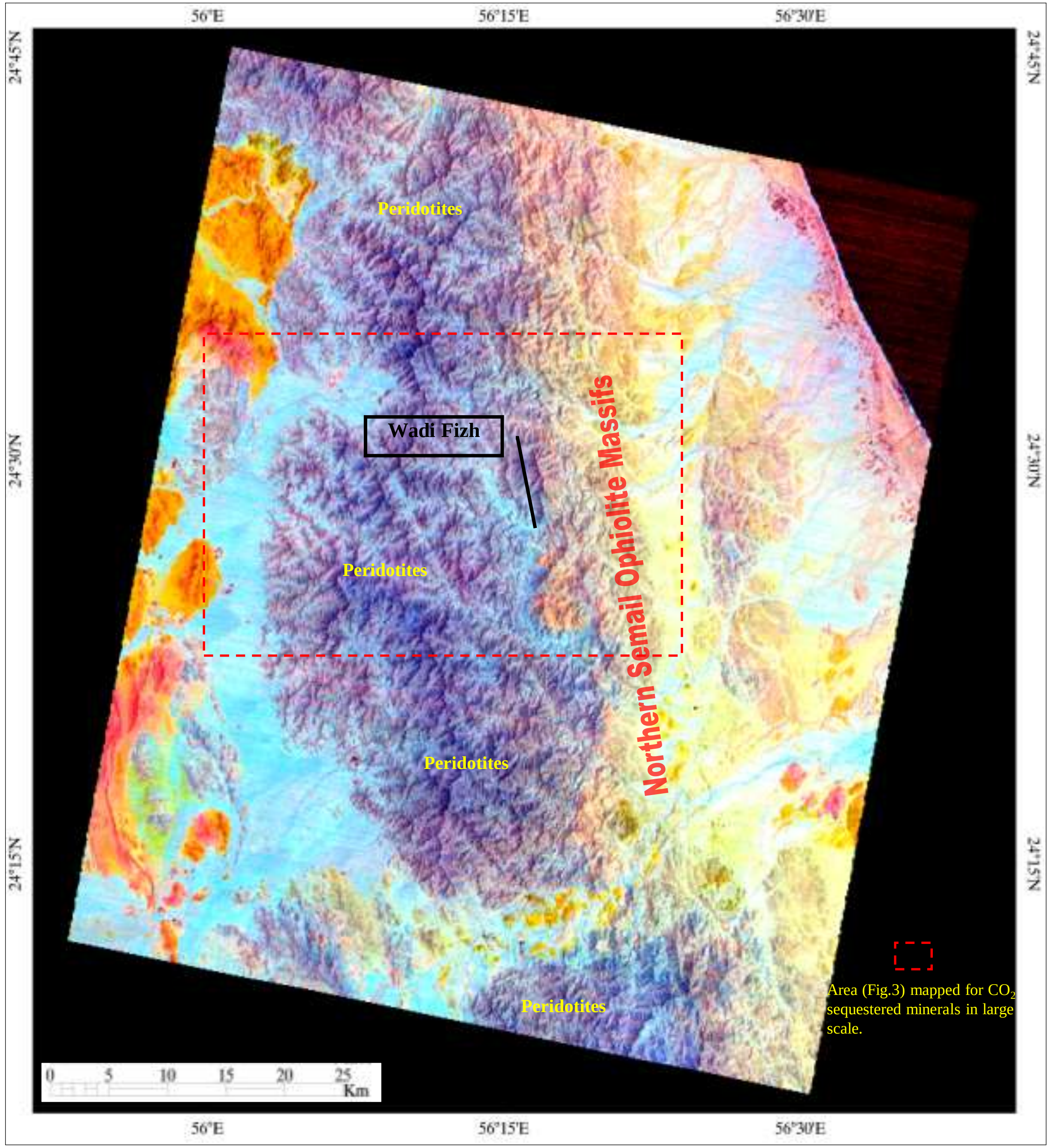

CASE STUY 9:

Mapping of Moho and Moho Tranisition Zone (MTZ) in Samail ophiolites of Sultanate of Oman using remote sensing technique

S. Rajendran, S. Nasir / Tectonophysics 657, (2015) 63–80.

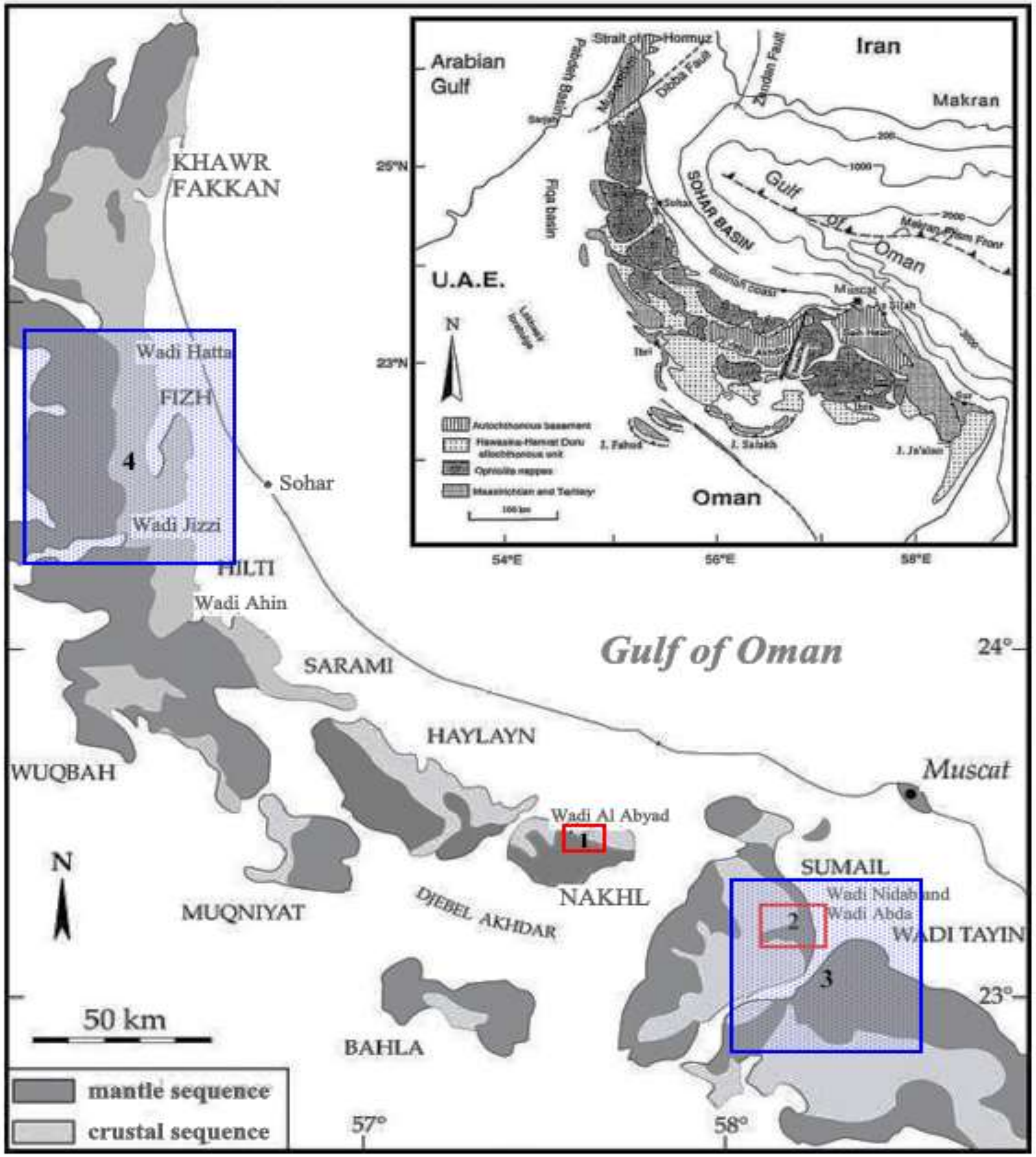

Fig. 1. Map showing the distributions of the mantle and crustal sequence in the northern Samail ophiolites (adapted from Nicolas et al., 1988; Yaouancq and MacLeod, 2000). Inset shows the geodynamic framework of the northern Oman (adopted from Ravaut et al. (1997) and Coleman (1981)). Sites 1 and 2 (boxes in red) are chosen for detailed study and sites 3, and 4 (boxes shaded in blue) are chosen for regional study on ASTER satellite data.

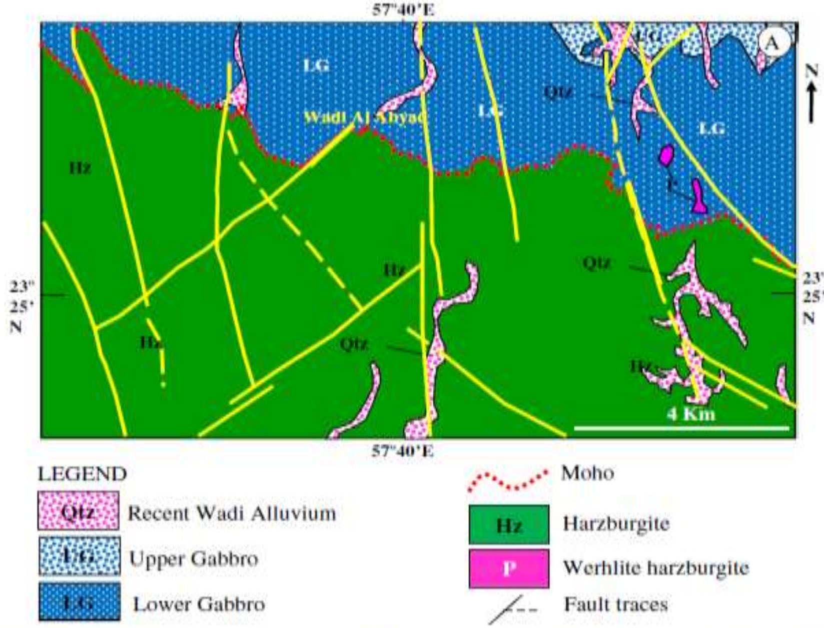

Fig. 2. Geological map of Wadi Al Abyad region of the Nakhl massif shows the Moho (dashed line) in between the mantle (harzburgites) and crustal (gabbros) rocks (Nicolas and Boudier, 1995; P – werhlite harzburgite, Hz – harzburgite, LG – lower gabbro, UG – upper gabbro, Qtz – recent Wadi alluvium).

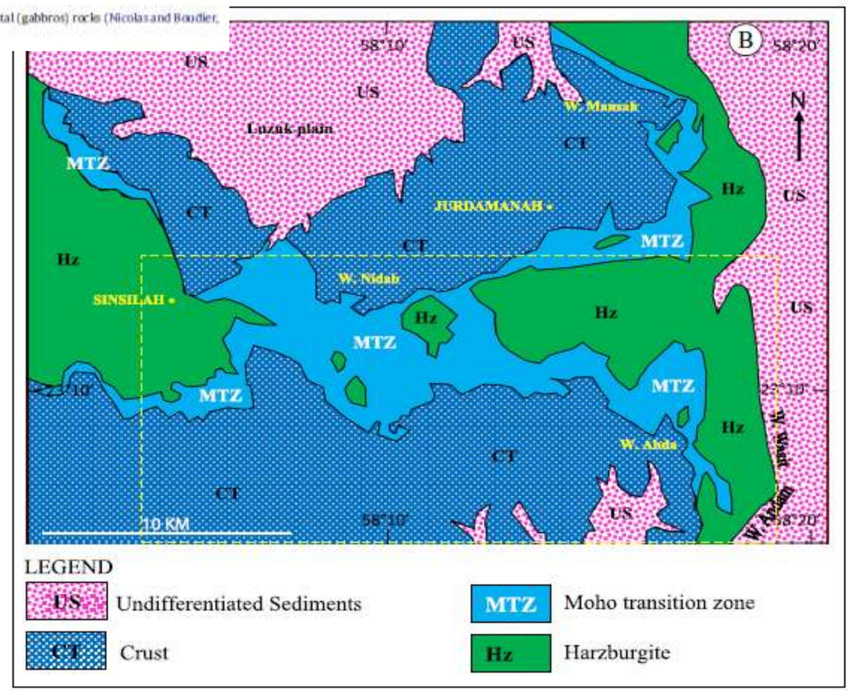

Fig. 3. Geological map around of Wadi Nidab and Wadi Abda of the Sumail massif shows the presence of thick MTZ (extracted from Jousselin and Nicolas, 2000b; Hz – harzburgite, MTZ – Moho Transition Zone, CT – crust, US – undifferentiated sediments).

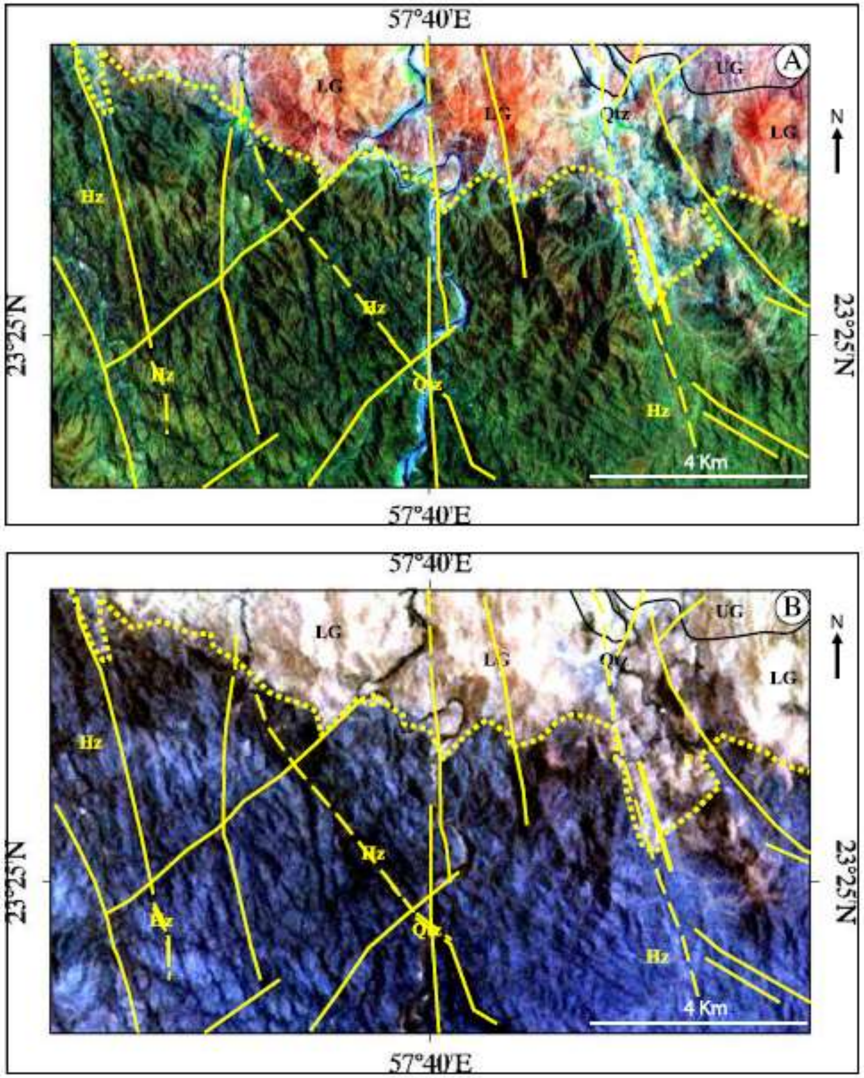

ASTER RGB color composite A) 8, 3, and 1 and B) 8, 7, and 4 ofWadi Al Abyad region of the Nakhlmassif shows the thin Moho (dashed line) in between themantle (harzburgite) and crustal (gabbro) rocks (Hz – harzburgite, LG – lower gabbro, UG – upper gabbro, Qtz – recentWadi alluvium).

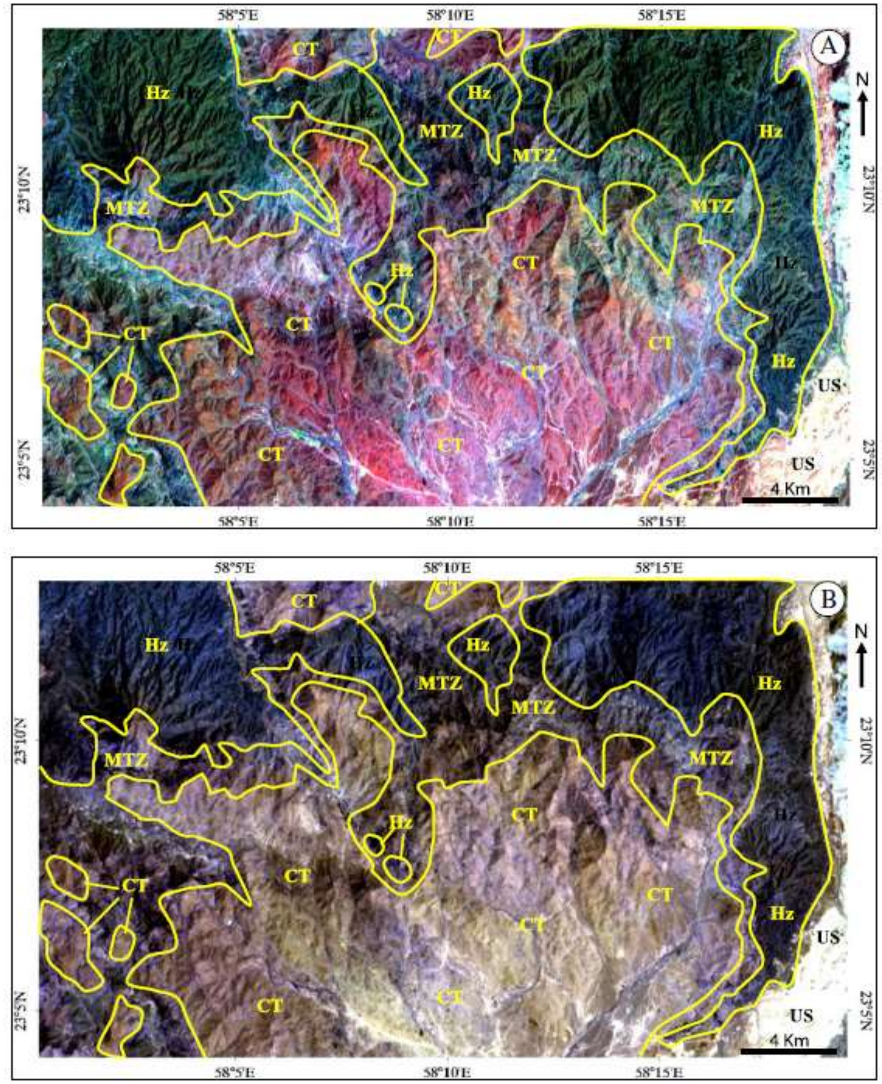

ASTER RGB color composite A) 8, 3, and 1, and B) 8, 7, and 4 ofWadi Nidab andWadi Abda of the Sumailmassif shows the occurrence of thickMoho Transition Zone (Hz – harzburgite, MTZ – Moho Transition Zone, CT – crust, US – undifferentiated sediments).

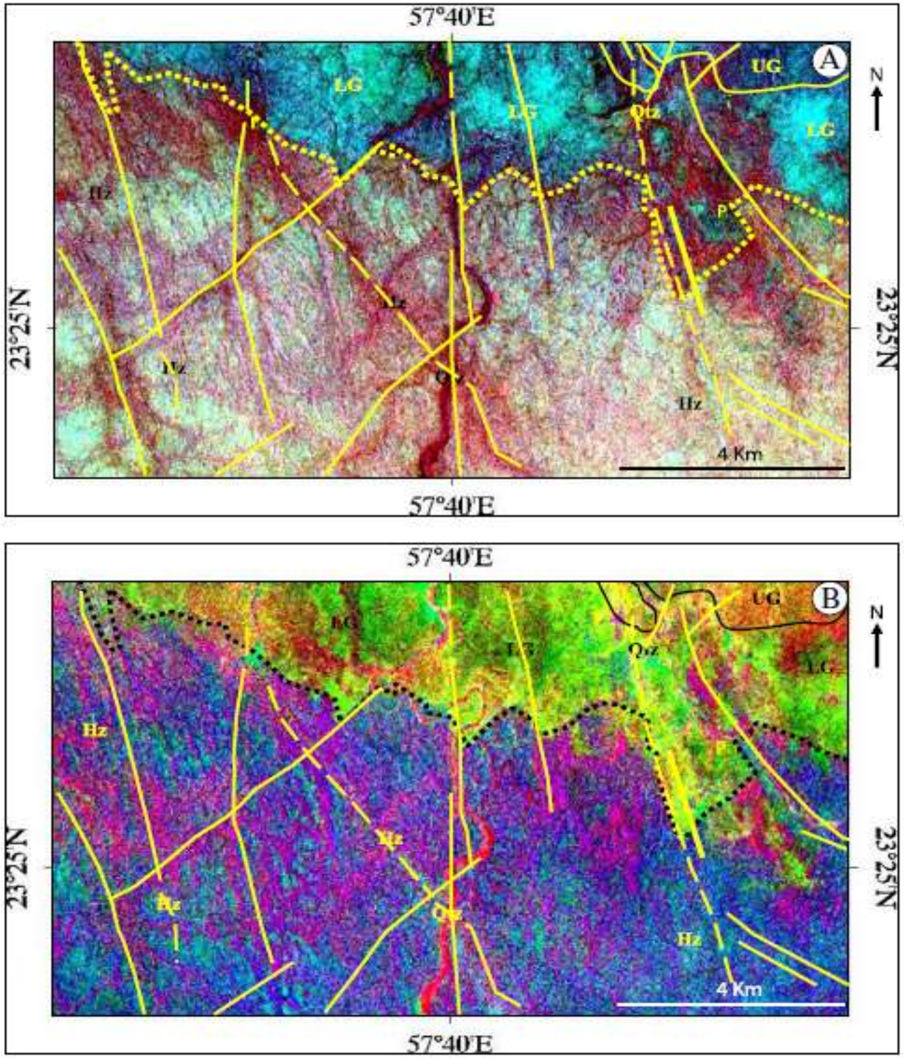

ASTER RGB images of band ratios A) (4/8, 4/1, 3/2 * 4/3)) and B) ((1+3)/2, (4+6)/5, (7+9)/8) ofWadi Al Abyad region of the Nakhlmassif showthe thinMoho (dashed line) inbetween the mantle (harzburgite) and crustal (gabbro) rocks (Hz – harzburgite, LG – lower gabbro, UG – upper gabbro, Qtz – recentWadi alluvium).

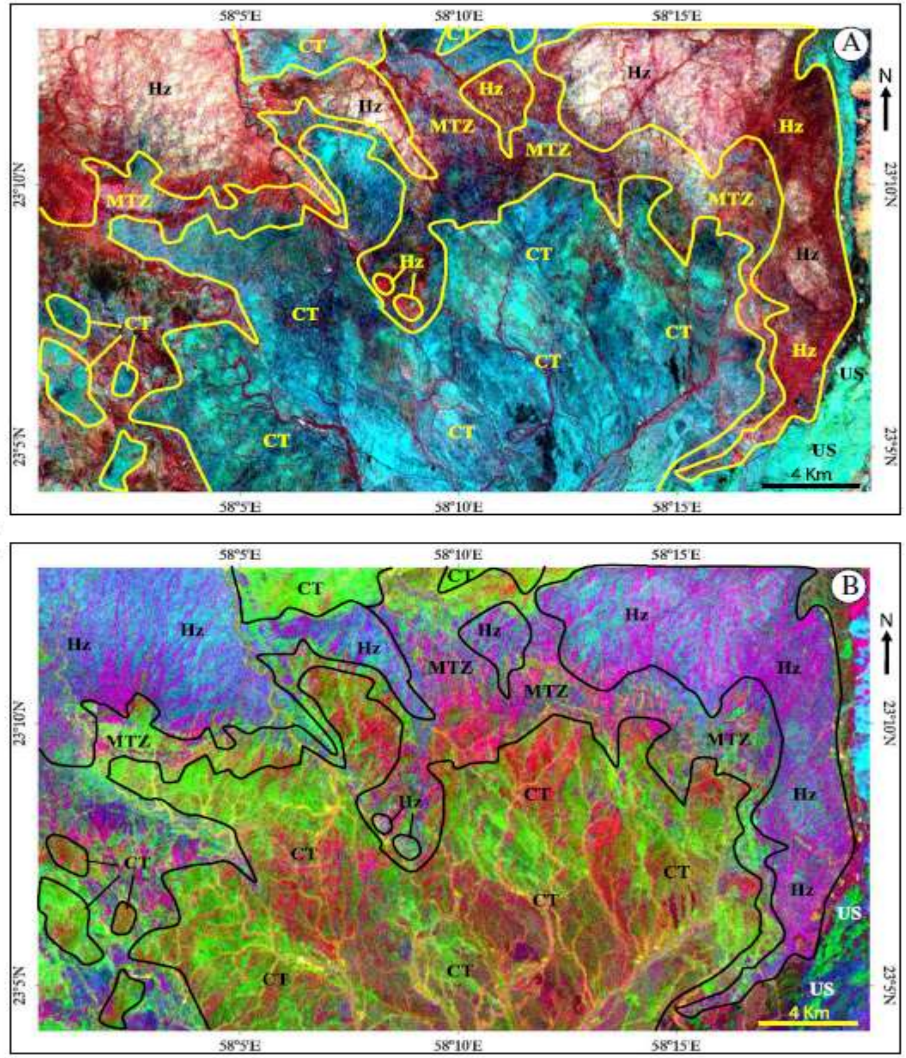

ASTER RGB images of band ratios A) 4/8, 4/1, 3/2 * 4/3 and B) (1+3)/2, (4+6)/5, (7+9)/8 ofWadi Nidab andWadi Abda of the Sumailmassif showthe occurrence of thick Moho Transition Zone (Hz – harzburgite, MTZ – Moho Transition Zone, CT – crust, US – undifferentiated sediments).

Field photographs show A) the presence of Moho in between the harzburgites and gabbros (comparable to the image of Geoeye-1, Fig. 10), B) the thin Moho traced at the Wadi section and C) the fresh typical mantle materials and crustal rocks in the Wadi Al Abyad. Dashed lines are the transition zone.

CASE STUY 10:

Mapping of high pressure metamorphics in the As Sifah region, NE Oman using ASTER data

Rajendran and Nasir (2015) Advances in Space Research, 55, 1134–1157

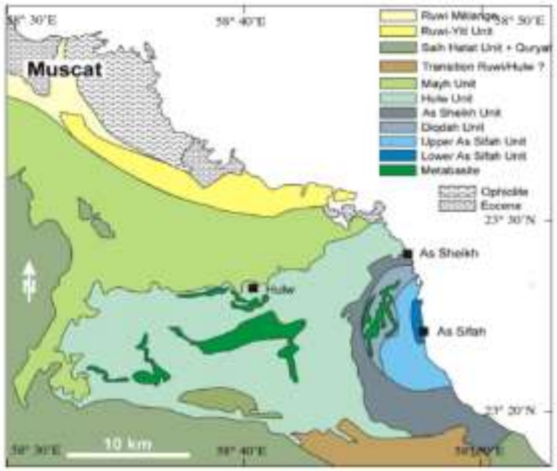

Geological map showing the Mesozoic–Tertiary rock units, southeast of Muscat, Oman. (Source: Massonne et al. (2013); this map was simplified on the basis of a map presented by Yamato et al. (2007)).

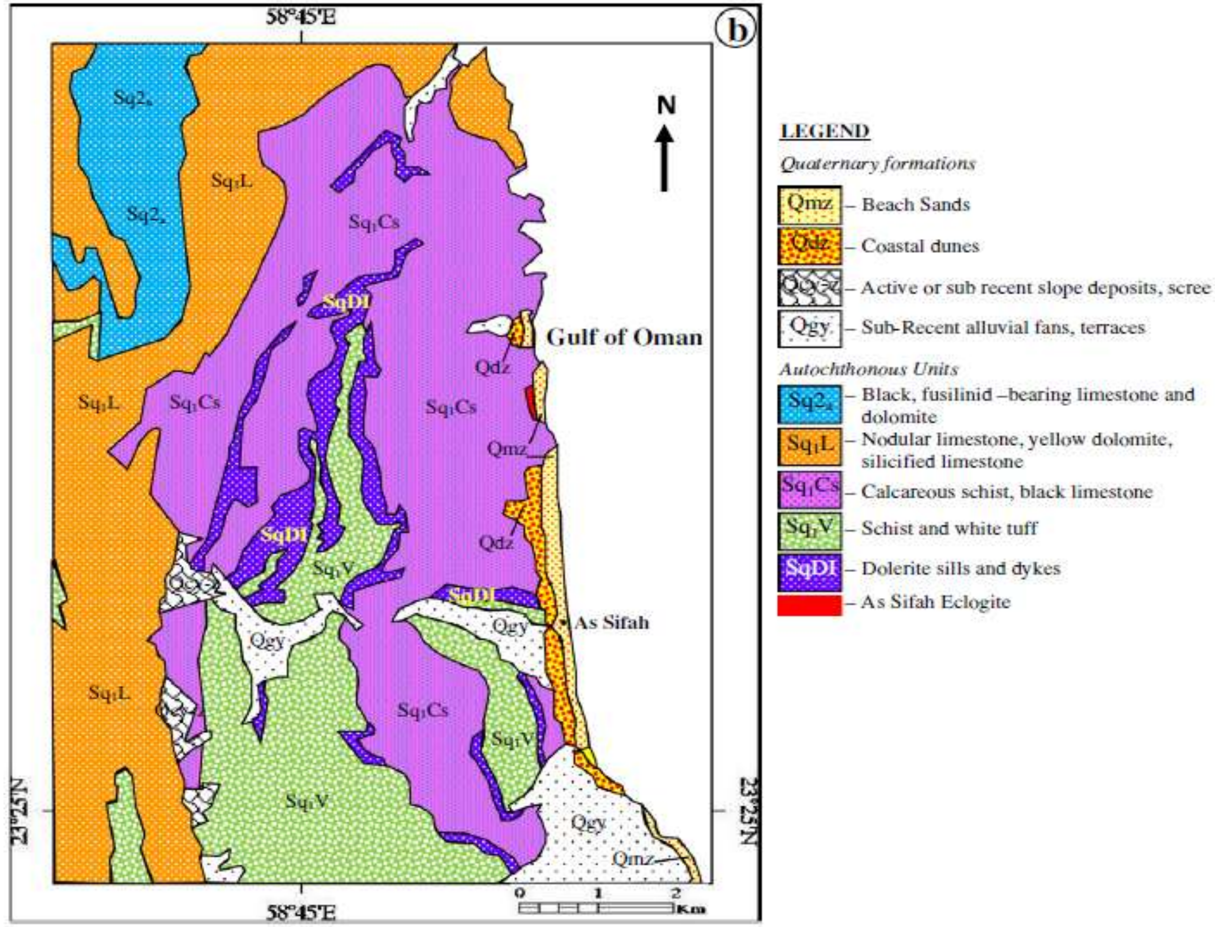

Geology around of As Sifah region (modified from Ministry of Petroleum and Minerals, 1986).

Decorrelated image of ASTER spectral bands 5, 6 and 8 shows the high pressure metamorphic zone in the As Sifah region.

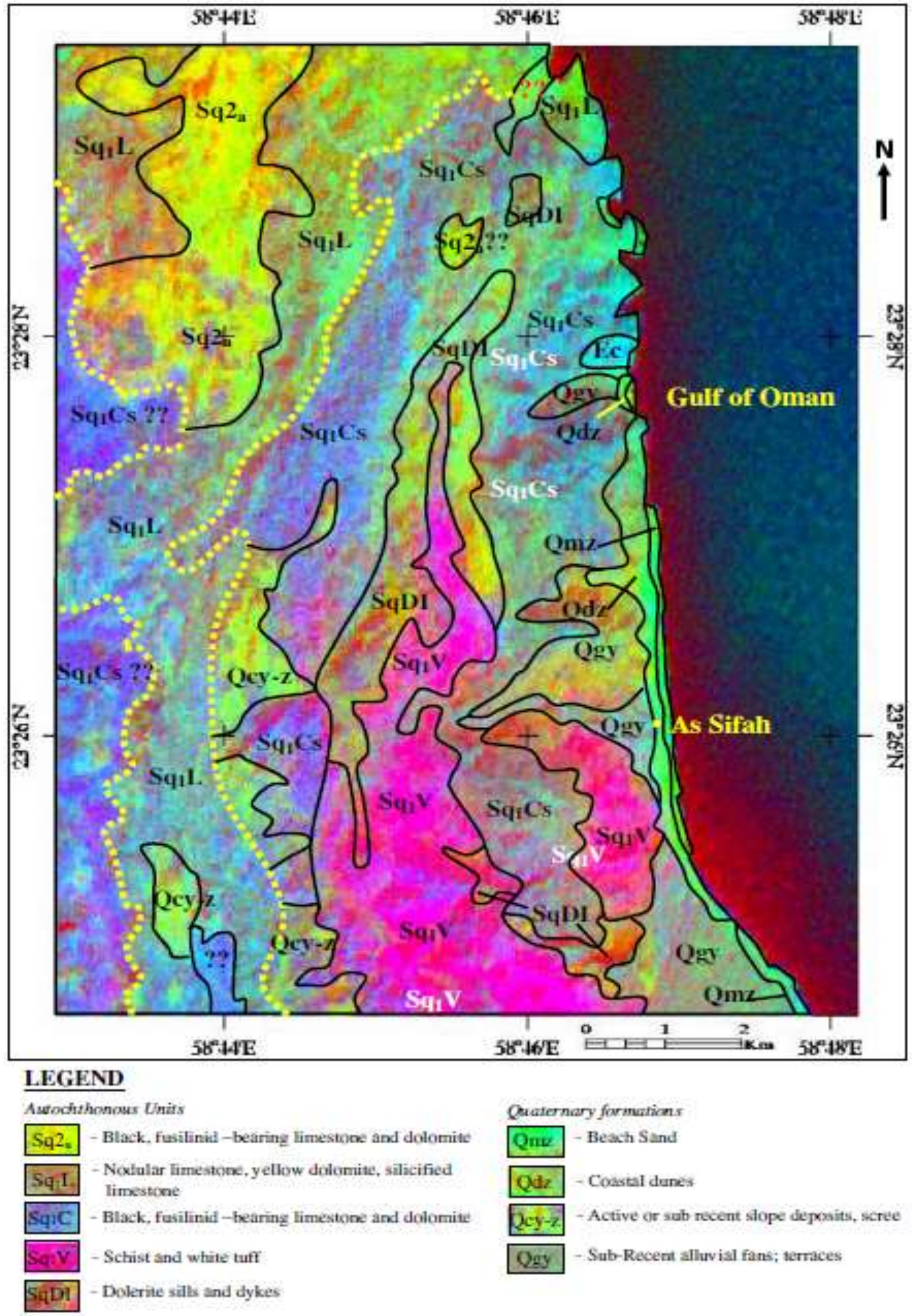

The ASTER RGB image of principal components PC4, PC3 and PC2 shows the occurrence and spatial distribution of hydroxyl bearing metamorphic rocks and carbonate formations in the As Sifah region

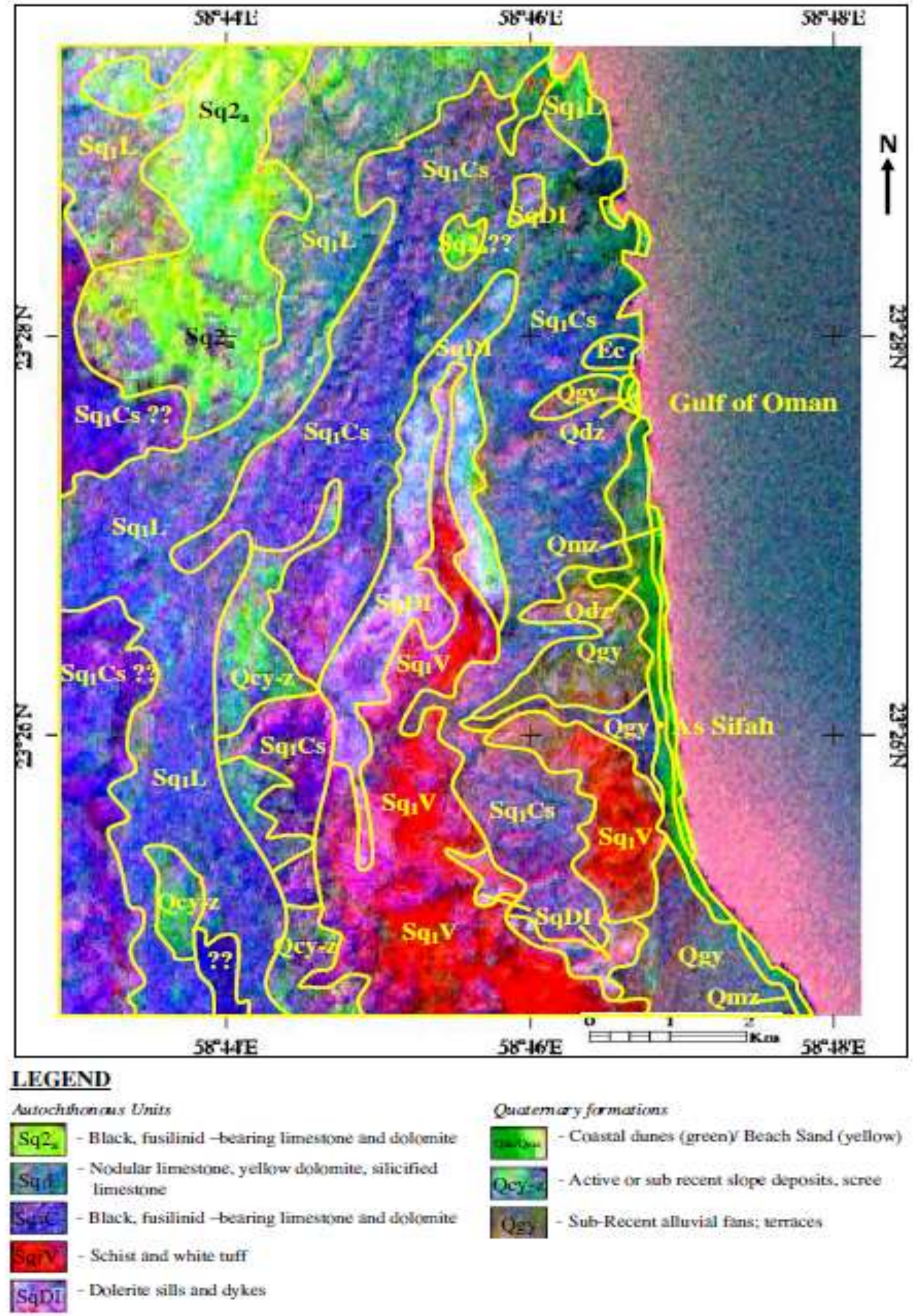

CASE STUY 11:

Discrimination of Carbonates and associated rocks and Mineral Identification of Eastern Mountain region (Saih Hatat Window) of the Sultanate of Oman

Rajendran et al (2011) Carbonates and Evaporites 26,351-364

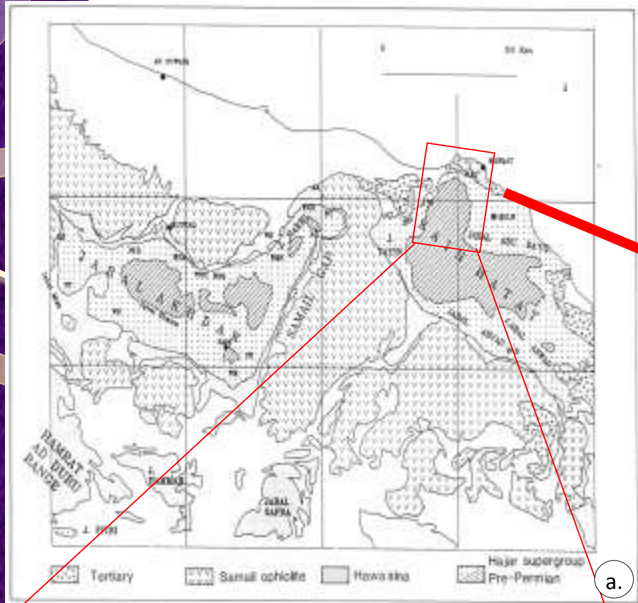

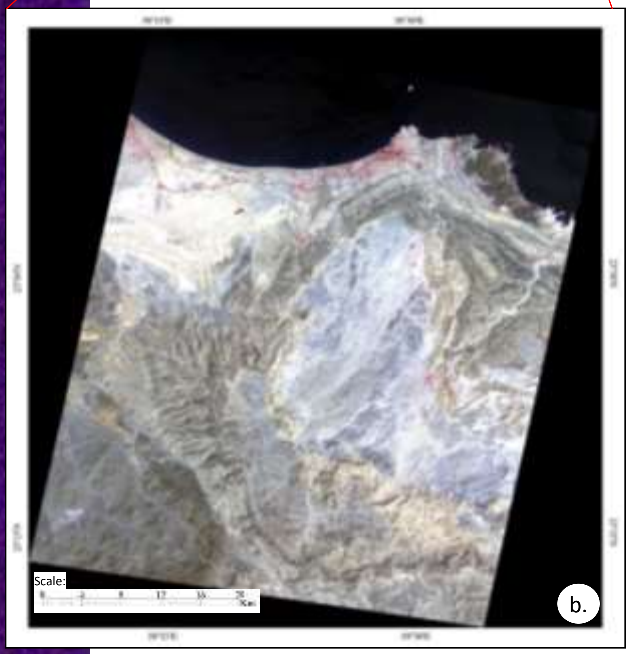

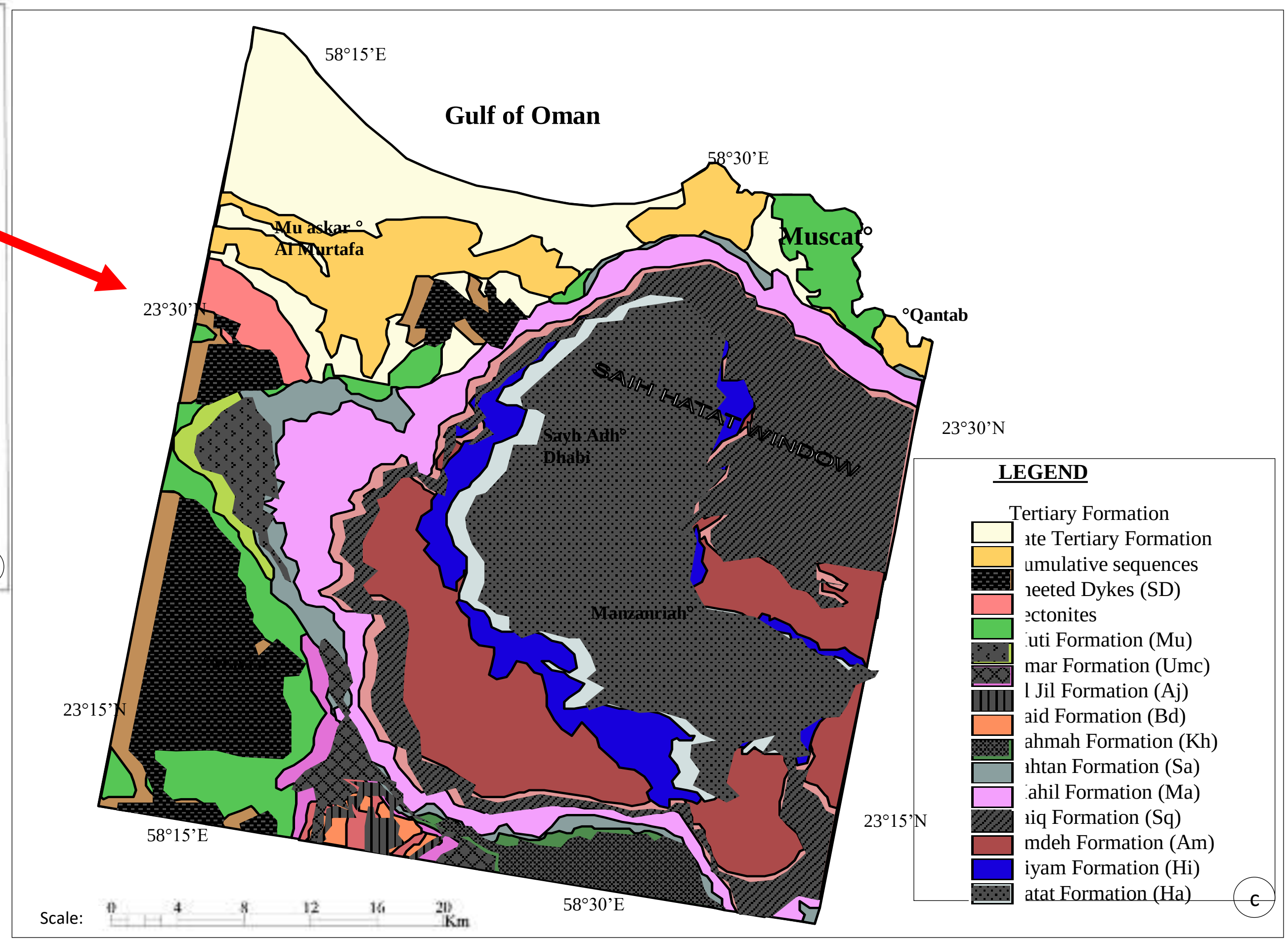

Figure shows the location of study area (red marked) in the regional geology of part of eastern mountain region of Oman (after Rabu et al., 1990; *AA, A1* Ajal; AB, A1 Bir; BT, Barut; BS, Bani Shahum; JBS, Jabal Bawshar; JM, Jabal Muraydah; SR, Saiq Road; WAD, Wadi Aday; WBA, Wadi Bani Awf; WBK, Wadi Bani Kharus; WD, Wadi Dayqah; WH, Wadi Hedeck; WKH, Wadi Khubrah; WM, Wadi Mu'aydin; WMS, Wadi Misin; WN, Wadi Nakhr; WS, Wadi Sahtan; WSQ, Wadi Saqla; WT, Wadi Taww). **b.** the study area in RGB (bands 321) subset of ASTER image showing Saih Hitat window **c.** the geology of study area (from Geological Map of Directorate General of Minerals, 1986).

RGB Band Ratio (9/7=R; 6/8=G; and 1/2=B) shows the discrimination of major quartz-rich silicates (blue; Sc), carbonates (purple; Cs and CsD), mafic-rich ophiolite (light green; Mc), Layered Gabbro (Gb), Sheeted dykes (SD) and biocalst and limestone rich sands (Ty) and minerals bearing rock formations.

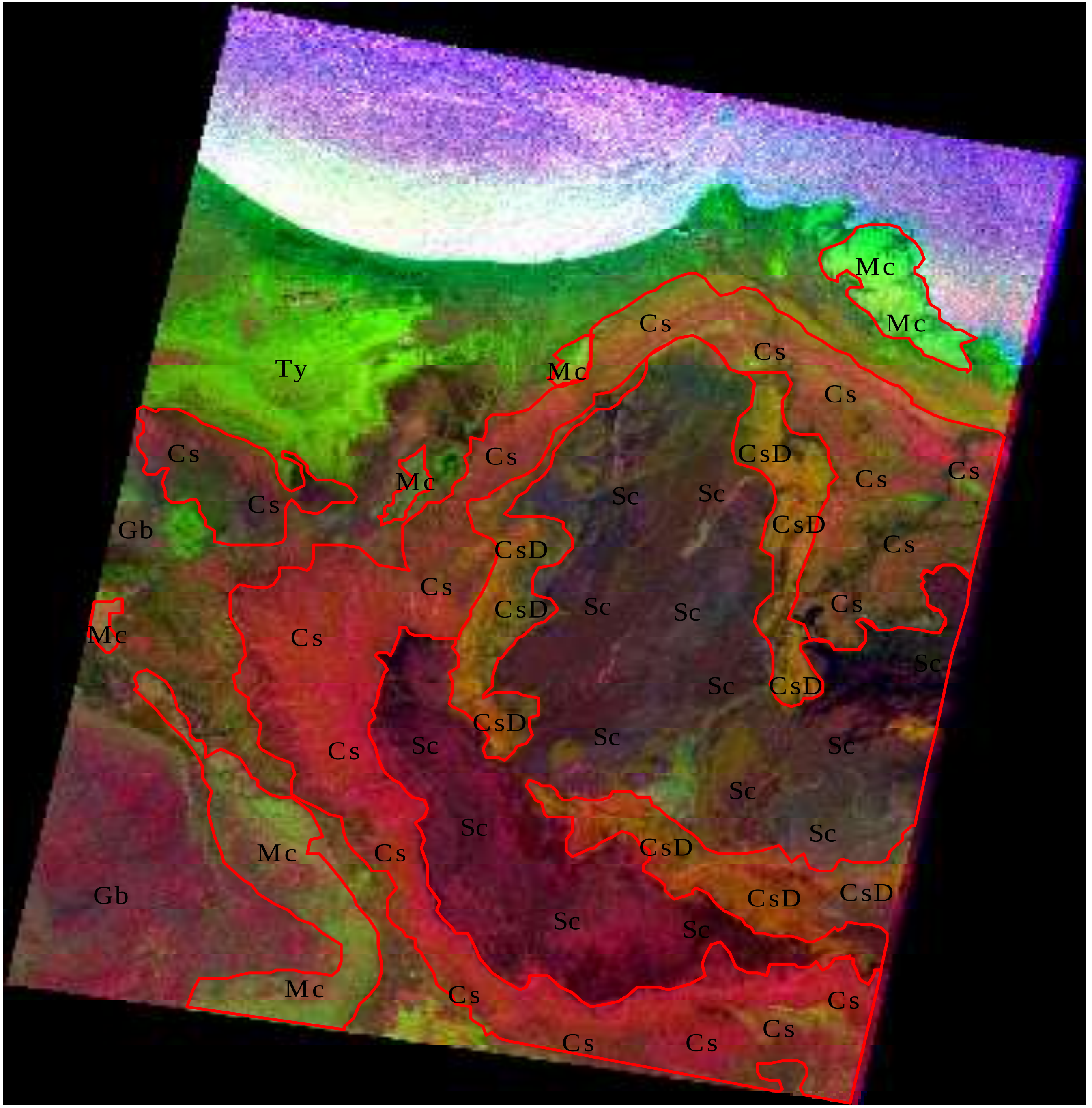

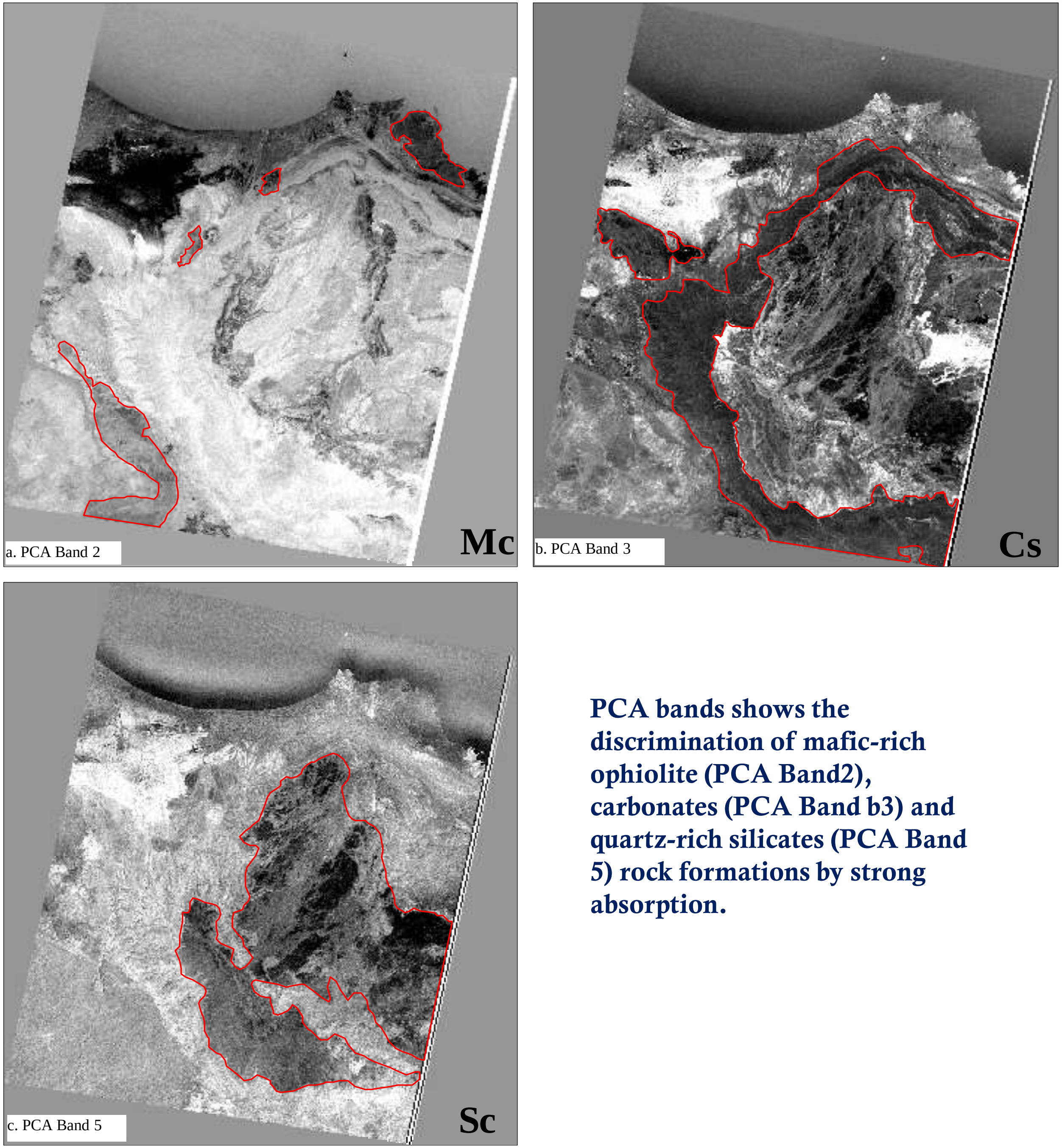

PCA bands shows the discrimination of mafic-rich ophiolite (PCA Band2), carbonates (PCA Band b3) and quartz-rich silicates (PCA Band 5) rock formations by strong absorption.

RGB color composite (R = PC5, G = PC3, B = PC2) shows the discrimination of quartz-rich silicates (as blue), carbonates (as purple) and mafic-rich ophiolite (as light green) rock formations.

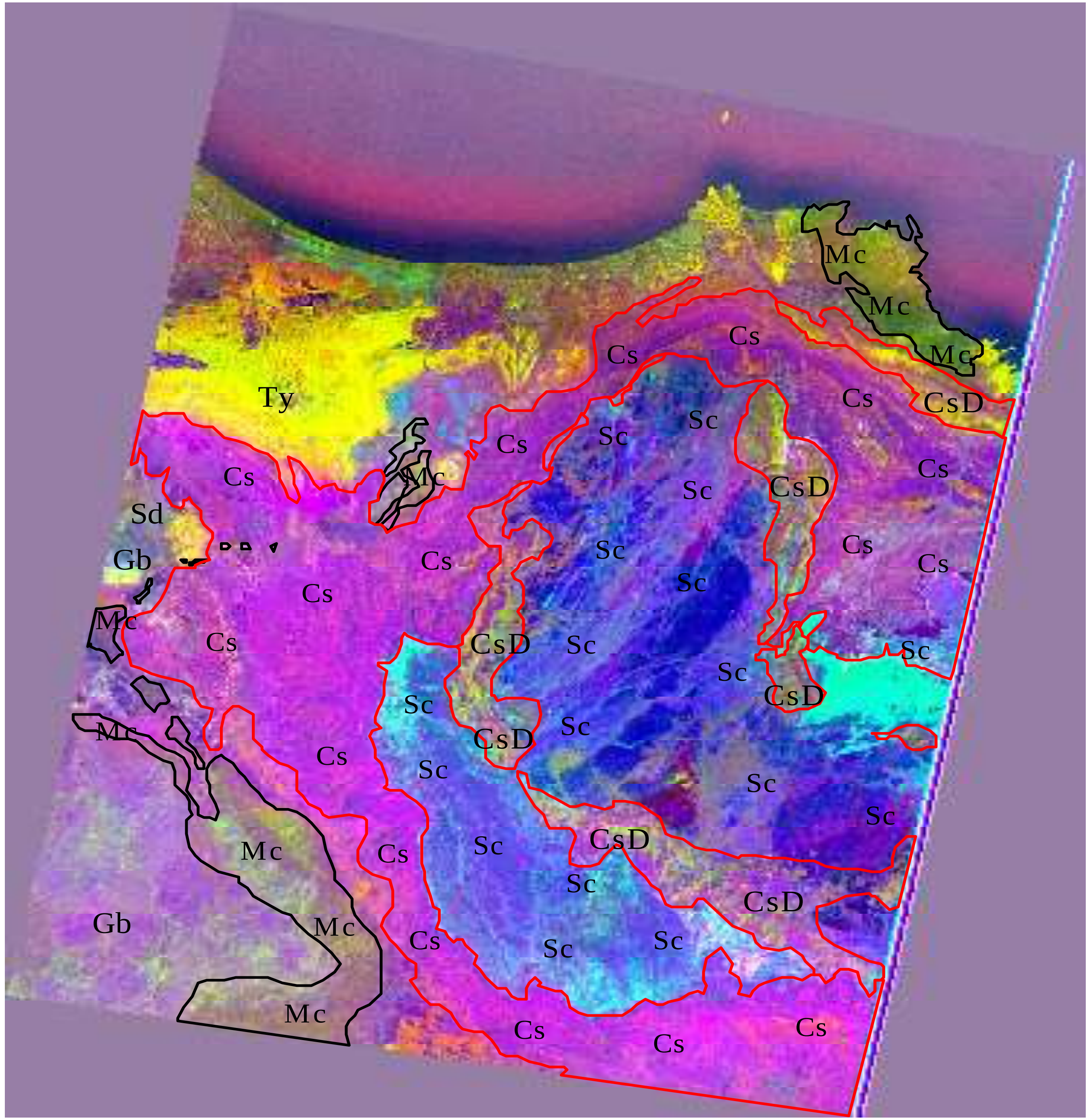

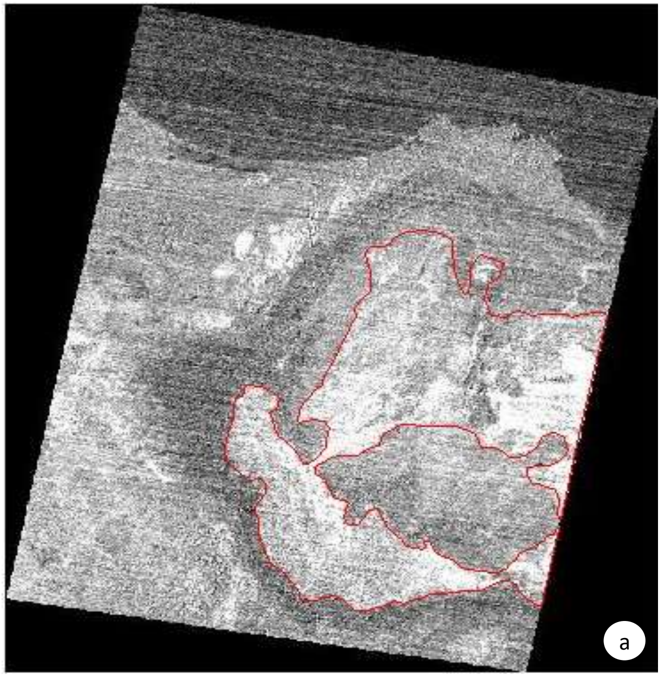

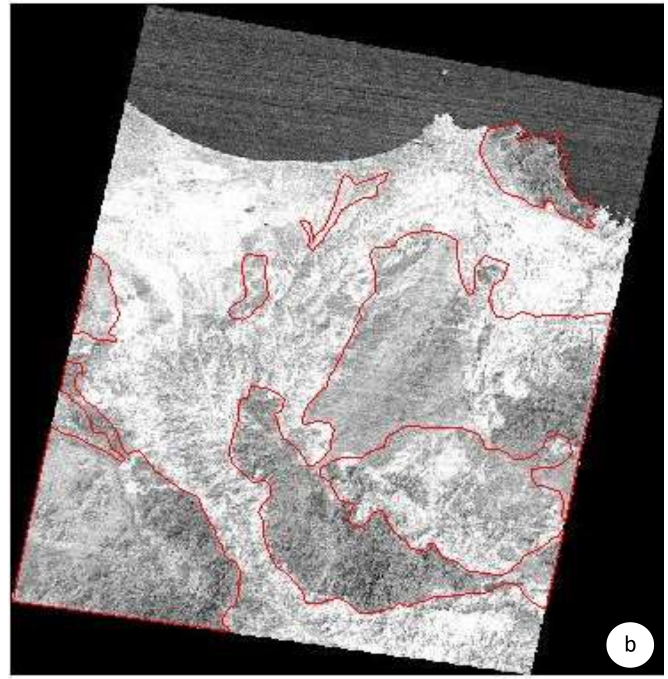

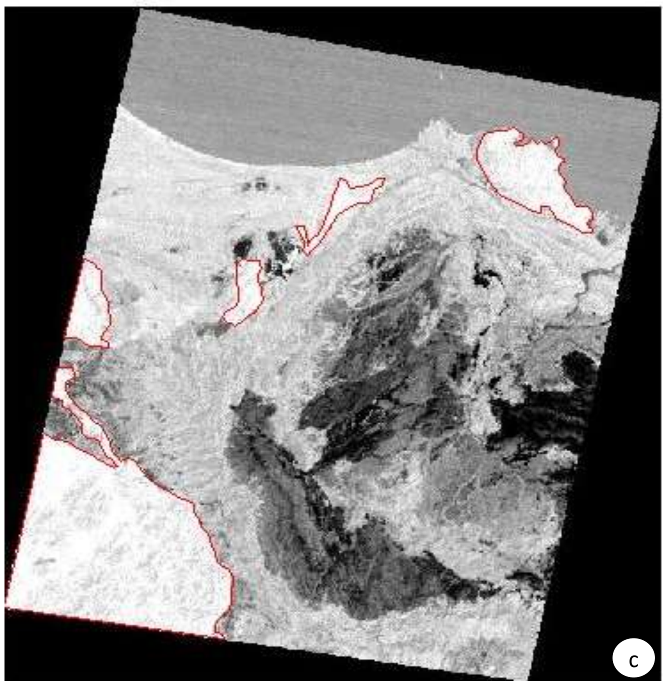

$CI = \frac{\text{Band } 13}{\text{Band } 14}$

$MI = \frac{\text{Band } 12}{\text{Band } 13}$

$QI = \frac{\text{Band } 11 \times \text{Band } 11}{\text{Band } 10 \times \text{Band } 12}$

Grayscale images a. Quartz Index (QI), b. Carbonate Index (CI), and c. Mafic Index (MI) Ninomiya et al. 2005, Corrie et al. 2010) identifies the bright pixels of minerals of quartz-rich silicates, carbonates and mafic-rich ophiolite rock formations comparable to RGB image of PCA.

RGB Colour composite image (R=QI, G=CI, and B=MI) identifies the major minerals of quartz-rich silicates (quartz, feldspar, chlorite as in the range of orange), carbonates (calcite and dolomite as in the range of blue) and mafic-rich ophiolite (calcic-plagioclase, pyroxene, olivine as in the range of purple) rock formations.

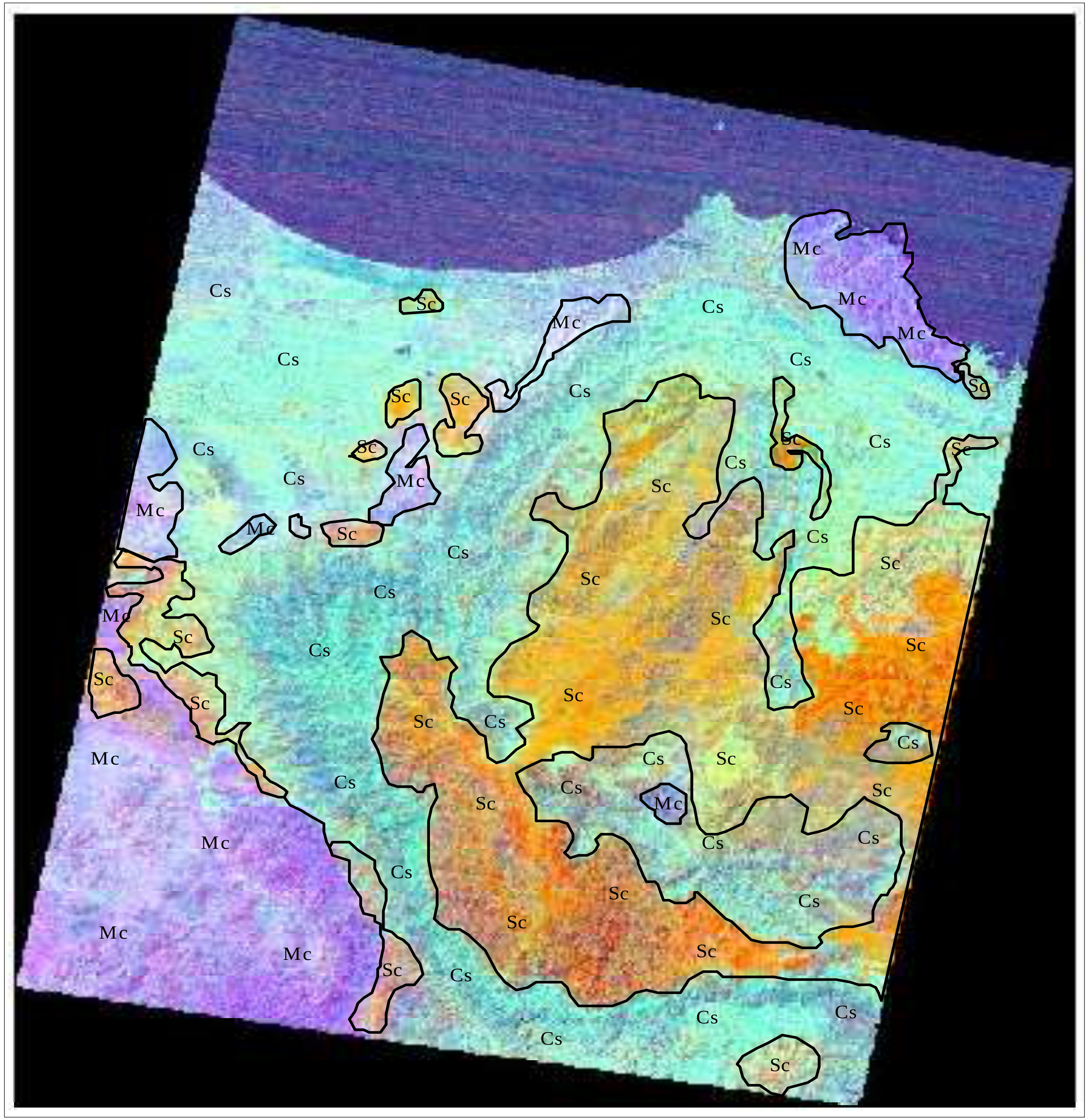

Remote sensing plays vital role in Mineral Exploration

Case studies for mapping of economic minerals and mineralized zones of the Sultanate of Oman.

The case study discussed here are about the

1. **the mapping of carbonates, silicates and mafic rocks;**
2. **the mapping of carbonate lithology;**
3. **the delineation of mineralized zones;**
4. **the mapping of lithology that consists the REE concentrations;**
5. **the mapping hydrothermal mineralised listwaenite zone and detection of minerals and etc…**

Conclusion:

- The ASTER spectral bands processed by different image processing methods based on the study of the spectral absorptions are able to show the occurrence and spatial distribution of the minerals and rock types of parts of the Sultanate of Oman.

- The review of applications of remote sensing applicaitons show that the satellite sensor has potential to mapping of minerals and mineralized zone in arid region.

References

Amer, R., Kusky, T.M., Ghulam, A., 2010. Lithological mapping in the central eastern desert of Egypt using ASTER data. J. Afr. Earth Sci. 56 (2–3), 75–82.

Eslami. A, Ghaderi. M, Rajendran. S Pour. A. B, and Hashim. M., (2015b). Integration of ASTER and landsat TM remote sensing data for chromite prospecting and lithological mapping in neyriz ophiolite zone, south Iran. Resource Geology 65(4), 375-388.

Gealey, W. K., 1977. Ophiolite obduction and geologic evolution of the Oman Mountains and adjacent areas: Geological Society of America Bulletin 88, 1183-1191.

Glennie, K. W., Boeuf, M.G.A., Hughes-Clarke, M. W., Moody-Stuart, M., Pilaar, W.F.H., Reinhardt, B. M., 1973. Late Cretaceous nappes in the Oman Mountains and their geologic evolution: American Association of Petroleum Geologists Bulletin 57, 5-27.

Glennie, K. W., Boeuf, M.G.A., Hughes-Clarke, M. W,, Moody-Stuart, M., Pilaar, W.F.H., Reinhardt, B. M., 1974. Geology of the Oman Mountains: Transactions of the Royal Dutch Geological and Mining Society of the Netherlands. 31(2), 423.

Harding, D.J., Wirth, K.R., Bird, J.M., 1989. Spectral mapping of Alaskan ophiolites using landsat thematic mapper data. Remote Sens. Environ. 28, 219–232.

Mwaniki, M.W., Moeller, M. S., Schellmann, G., 2015. A comparison of Landsat 8 (OLI) and Landsat 7 (ETM+) in mapping geology and visualising lineaments: A case study of central region Kenya. Archives of the Photogrammetry, Remote Sensing and Spatial Information Sciences XL-7/W3, 897-903.

Ninomiya, Y., Fu, B., Cudahy, T.J., 2005. Detecting lithology with advanced spaceborne thermal emission and reflection radiometer (ASTER) multispectral thermal infrared ‘‘radiance-at-sensor’’ data. Remote Sens. Environ. 99, 127–139.

Rajendran, S., Nasir, S., 2015b. Mapping of Moho and Moho Transition Zone (MTZ) in Samail ophiolites of Sultanate of Oman using remote sensing technique. Tectonophysics 657, 63-80.

Rajendran, S., Nasir, S., 2015a. Mapping of high pressure metamorphics in the As Sifah region, NE Oman using ASTER data. Advances in Space Research 55(4), 1134-1157.

Rajendran, S., Nasir, S., Kusky, T.M., Al-Khirbash, S., 2014. Remote sensing based approach for mapping of CO2 sequestered regions in Semail ophiolite massifs of the Sultanate of Oman. Earth Science Review, 135, 122–140.

Rajendran, S., Nasir, S., Kusky, T.M., Ghulam, A., Gabr, S., ElGhali, M., 2013. Detection of hydrothermal mineralized zones associated with Listwaenites rocks in the Central Oman using ASTER data. Ore Geology Reviews 53, 470–488.

Searle, M.P., Graham, G.M., 1982. "Oman Exotics"—Oceanic carbonate build-ups associated with the early stages of continental rifting. Geology 10, 43-49.

Searle, M. P., Malpas, J., 1980. Structure and metamorphism of rocks beneath the Semail ophiolite of Oman and their significance in ophiolite obduction: Royal Society of Edinburgh Transactions 71, 213-228

Sultan, M., Arvidson, R.E., Sturchio, N.C., Guinness, E.A., 1987. Lithologic mapping in arid regions with landsat thematic mapper data: Meatiq dome, Egypt. Geol. Soc. Am. Bull. 99, 748–762.

Van der Meer, F.D.M., Van der Werff, F.D.H., Van Ruitenbeek, F.J.A., Hecker, C.A., Bakker, W.H., Noomen, M.F., Van der Meijde, M., Carranza, E.J.M., De Smeth, J.B., Woldai,t., 2012. Multi- and hyperspectral geologic remote sensing: A review. International Journal of Applied Earth Observation and Geoinformation 14, 112–128.

Welland, M. J., Mitchell, A. H,, 1977. Emplacement of the Oman ophiolite: A mechanism related to subduction and collision: Geological Society of America Bulletin 88, 1081-1088.

Wilson, H. H., 1969, Late Cretaceous eugeosynclinal sedimentation, gravity tectonics and ophiolite emplacement in Oman Mountains, southeast Arabia: American Association of Petroleum Geologists Bulletin 53, 626-671.

THANK YOU

more @ **‘Sankaran Rajendran’ – Research Gate**